Zeolite MFI Membranes Towards Industrial Applications

A Dissertation
SUBMITTED TO THE FACULTY OF
UNIVERSITY OF MINNESOTA
BY

Xuekui Duan

IN PARTIAL FULFILLMENT OF THE REQUIREMENTS
FOR THE DEGREE OF
DOCTOR OF PHILOSOPHY

Advisor

Prof. Michael Tsapatsis

Nov 2020

Acknowledgements

First, I would like to sincerely thank my advisor, Prof. Michael Tsapatsis, for his continuous supports and guidance along my Ph.D. journey. Being a part of the Tsapatsis group has taught me how to conduct independent research with a scientific mindset and a perfection-oriented attitude. All his help and mentorship make this thesis possible and make who I am today.

I am also very thankful to be able to work with my colleagues in the Tsapatsis group. Dr. Han Zhang has taught me multilamellar MFI synthesis and exfoliation, polymer hollow fiber spinning, and MFI membrane fabrication. Dr. Donghun Kim has guided me on the dc-5 nanosheet synthesis, purification, and seeding. Dr. Neel Rangnekar has helped me a lot with MFI membrane separation tests. Dr. Garrett Swindlehurst has guided me on the NaA water vapor separation project and provided me with valuable feedback. Dr. Xiaoli Ma, Dr. Qiang Guo, Dr. Kiwon Eum, Dr. Deawoo Kim, Dr. Feng Xue, and Dr. Sabrina Conrad have had valuable discussions with me.

I would also like to thank my family and friends for supporting me through my doctoral studies. My mother Yuqun Li and sisters Xinyao Duan and Xuelin Duan have given me a lot of encouragements. My wife Meng Xi has always been my supporter. My host family Mr. Van Nixon and Mrs. Kathy Nixon have made me feel at home in the US.

Finally, I would like to express my gratitude to Prof. Alon McCormick, Prof. Paul Dauenhauer and Prof. Andreas Stein for agreeing to serve in my committee and the CEMS staff Julie Prince, Teresa Bredahl, Daniel Williams, Susan Wermager for their kind help.

Dedication

To my family and friends

Abstract

Zeolite membranes have been the interest of research for decades due to their potentials in various separation applications including gas separation, water purification, pervaporation, etc. Among the zeolite materials studied, MFI zeolite (Silicalite-1 and ZSM-5) is one of the major subjects of research, mainly because of its suitability for the separation of hydrocarbons, such as *n*-butane from *iso*-butane and *para*-xylene from its isomers. Besides, all-silica Silicalite-1 and high-silica ZSM-5 have been explored for organic/water pervaporation as well by utilizing their high hydrophobicity. Despite years of research efforts on these applications, the industrialization of MFI membranes has not been achieved. One reason is that the cost associated with the fabrication of these membranes is too high to be commercially attractive. The high-cost, specially engineered silica membrane supports account for a major share of the total cost. Alternative supports such as polymeric supports and low-cost and commercially available alumina supports are possible substitutes to explore. Another problem is the lack of demonstration of high membrane separation performance at industrially relevant conditions (high temperature and high pressure). It is thus the goal of this thesis to address these problems and make progress towards the commercialization of MFI membranes. First, the recent advances of MFI zeolite membranes were reviewed. Then, the fabrication of high-performance MFI membranes using aqueous dispersions of open-pore, two-dimensional MFI zeolite nanosheets on low-cost polymeric substrates was demonstrated. Next, progress towards making MFI membranes on alumina supports has been made. Despite these efforts to use other supports, we failed to make high-performance membranes as comparable to the silica supported ones. Besides these efforts, ultra-thin MFI membranes fabricated using dc-5 nanosheets as seeds were showed to have high xylene isomer separation performance at industrial conditions and high performance for H_2/hydrocarbons separation and ammonia/H_2/N_2 separation. These works demonstrated the potential of high-performance MFI membranes for energy-efficient separation processes in industrial conditions.

Table of Contents

List of Tables

List of Figures

List of Abbreviations

1. MFI: Zeolite Framework Type MFI.

   See detailed structure at

   https://america.iza-structure.org/IZA-SC/framework.php?STC=MFI

2. LTA: Zeolite Framework Type LTA. NaA zeolite has this type of topology.

   See detailed structure at:

   https://america.iza-structure.org/IZA-SC/framework.php?STC=LTA

3. PBI: Polybenzimidazole. The PBI material used in this research is poly[2,2'-(m-phenylen)-5,5'-bisbenzimidazole]. The chemical structure is shown below.

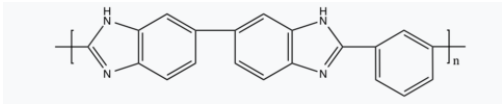

4. PVDF: Polyvinylidene fluoride.

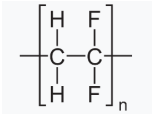

5. PI: Polyimide. Several types of polyimide are commercially available. The polyimide material used in this work is Matrimid ® 5218. The chemical structure is shown below.

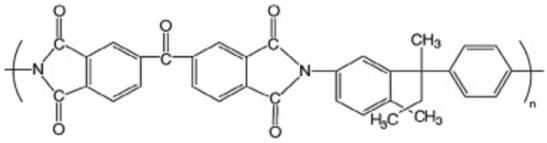

6. PES: Polyethersulfone. The PES material used in this work is Ultrason® PES. The chemical structure is shown below.

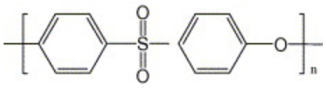

7. PDMS: Polydimethylsiloxane.

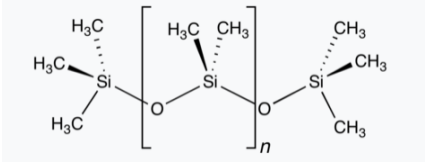

(Note: All the chemical structures are taken from Wikipedia)

8. MWCO: Molecular weight cut-off. MWCO of a membrane refers to the molecular weight of a tracing solute (in Daltons) when 90% of the solute is retained by the membrane during a separation test. The molecular weight of the tracing solute can be translated to molecular size using rheology data. Therefore, the pore size of a membrane can be represented by using this MWCO concept.

9. OSDA: Organic structure directing agent. OSDA is used to guide the structure of zeolite.

10. dC5: bis-1,5(tripropyl ammonium) pentamethylene ion. This is the OSDA used to template the bottom-up synthesis of MFI zeolite nanosheet.

11. TEAOH: Tetraethylammonium-hydroxide.

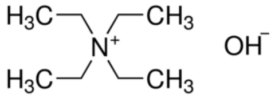

12. TPAOH: Tetrapropylammonium-hydroxide.

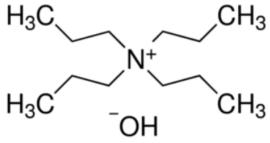

13. TEOS: Tetraethyl orthosilicate.

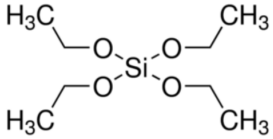

14. S.F.: Membrane Separation Factor. Membrane Separation Factor is defined as the composition ratio of components A and B in the permeate mixture relative to the composition ratio of A and B in the retentate mixture, i.e. $SF(AB) = [X_A/ X_B]_{permeate} / [X_A/ X_B]_{retentate}$. It is usually applied to characterize selectivity performance of a membrane after a mixture gas permeation test.

15. Ideal selectivity: Membrane ideal selectivity is defined as the ratio of the permeability or permeance of the two individual species. It is usually applied to characterize selectivity performance of a membrane after a single gas permeation test. For two species of A and B, the ideal selectivity is described by: $\alpha_{A/B}=P_A/P_B$.

16. Permeance: Membrane permeance is defined as a transport flux normalized by transmembrane driving force. Permeance = P_i/l. (l is membrane thickness). For pressure driven membrane separation process, commonly used units for permeance include [$kmol \cdot m^{-2} \cdot s^{-1} \cdot kPa^{-1}$], [$m^3 \cdot m^{-2} \cdot s^{-1} \cdot kPa^{-1}$] or [$kg \cdot m^{-2} \cdot s^{-1} \cdot kPa^{-1}$]. Another commonly used unit in gas separation community is GPU:

$$1GPU = 10^{-6}\ cm^3(STP)/(cm^2 \cdot s \cdot cmHg) = 7.6 \times 10^{-9}\ m^3(STP)/(m^2 \cdot s \cdot kPa) = 3.35 \times 10^{-10}\ kmol/(m^2 \cdot s \cdot kPa)$$

(Note: for mixture, the pressure refers to partial pressure.)

Chapter 1. Introduction

Zeolites are a family of silica-based microporous materials. They are inorganic, crystalline, and have well-defined pore systems. Studies on zeolites began with the discovery of the first member of the zeolite family [1], stilbite, which is a naturally occurred zeolite material, in 1765. And since the late 1940s and the early 1950s, the availability of synthetic zeolite crystals [2] promoted the growing research interests on zeolite materials, with specific applications including catalysis [3-5], membrane separations [6-10], energy storage [11-12], chemical sensors [13-14] as well as electronic [15-17] and optical materials [18].

Among all the zeolite materials studied, MFI-type zeolite (ZSM-5 and silicalite-1 (pure silica)) is one of the major subjects of research because of their interesting pore system. The pore system of MFI zeolite is shown in ***Figure 1.1***. It contains two intersecting channel systems: one straight channel system running parallel to its *b*-axis with an estimated pore aperture of 0.56 nm × 0.54 nm and the other zig-zag channel system running parallel to its a-axis with an estimated pore aperture of 0.51 nm × 0.55 nm. This unique pore system makes MFI zeolite very attractive for membrane separation applications, including the separation of hydrocarbon isomers [19-27], organic/water pervaporation [28-32] as well as the removal of ions from aqueous solutions (water desalination) [33-40].

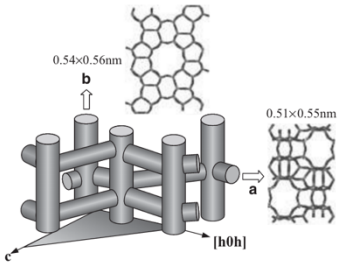

Figure 1.1: Pore system of the MFI zeolite. Picture taken from [41].

For hydrocarbons separation, MFI-type zeolites have been proven to be suitable for the separation of several industrially important hydrocarbons. One of the promising applications is separating *n*-butane from *iso*-butane [19-23] and another application is separating *para*-xylene from its isomers [24-27]. These hydrocarbons are crucial for the petrochemical industry. *n*-butane can be used as a fuel gas in the form of LPG (liquefied petroleum gas) and as a key ingredient for the production of ethylene and butadiene which are two major components for the manufacturing of synthetic rubber. Data showed that the global demand for *n*-butane was anticipated to reach as high as 240 million tons by 2018 [42] and increase to about $203 billion by 2020 [43]. *para*-xylene is an important feedstock for the large scale synthesis of teraphthalic acid (TPA), which is a component for the production of polyethylene terephthalate (PET), an important and ubiquitous plastic used in our daily life (e.g. beverage bottles). The demand for *para*-xylene is growing annually in the range of 6-8% per year [44]. Statistics showed that the world annual demand for *para*-xylene was about 18 million tonnes in 2003 [45] and increased to more than 30 million tonnes in 2010 [44]. Currently, the production of these raw materials employs energy-intensive technologies, such as distillation and fractional crystallization.

Hydrocarbon separation using membrane technology could replace some of these currently employed energy-intensive processes. The possibility of replacing the butane isomers' distillation process by a hybrid membrane-distillation process has been explored by colleagues in our group [42]. The simulation concluded that a 10-fold improvement in the MFI membrane permeance can be achieved by reducing pore blockages or equivalently, by reducing the membrane thickness from the currently achieved ~500 nm to ~50 nm or less. With a 10-fold improvement in the permeance as compared to that in the current state-of-the-art ceramic supported ~500 nm thick MFI membranes [46], a payback period of 3 years can be achieved with installed membrane cost of up to $5000/m^2. Alternatively, a payback period of 3 years can be achieved by reducing the membrane installation cost to $500/m^2 with the current membrane performance. This implies two approaches in advancing the industrial application of MFI membranes: (1) the development of even-higher-performance MFI membranes to make it highly competitive in industrial applications; (2) reducing the cost of the MFI membrane fabrication without significantly compromising the membrane performance.

In order to prepare high-performance membranes suitable to be employed in industrial hydrocarbon separation processes, it is desirable that the membrane should simultaneously exhibit high flux and high selectivity. This requires the zeolite film to be as thin as possible (high flux) and free of defects (high selectivity). Currently, the state-of-the-art zeolite membrane preparation is based on the secondary seeded growth technique to make the zeolite film well inter-grown and defect-free. This usually compromises the flux of the membrane because a relatively thick layer of zeolite is formed. To make ultra-thin, high-

performance MFI membranes, major advancements were achieved in the past 20 years. Early efforts were made to grow the membranes in a preferred orientation [25]. The *b*-oriented membranes had their straight channels aligned perpendicular to the support. Molecular transport through the membranes will have minimum resistance as the straight channels run down the membrane thickness. Later in 2013, a gel-free secondary growth method was developed by Yoon and coworkers [47] to grow *b*-oriented MFI membranes on silica supports. This method is environmentally friendly as it prevents the wastage of chemicals associated with fabricating membranes in the secondary growth process. The aforementioned membranes were made by the secondary growing of large and thick MFI crystals. The membranes were inevitably thick. To further increase the permeation flux of MFI zeolite molecular sieve membranes, the preparation of an ultra-thin film of zeolite is needed. Ultra-thin zeolite membranes can be obtained if zeolite nanosheets are employed as seeds for secondary growth. Our group has dedicated a lot of efforts to develop MFI nanosheets and has used them as seeds for the fabrication of MFI membranes. These efforts succeeded in making ultra-thin MFI membranes with record-high separation performance. The first generation of MFI nanosheets was based on a top-down exfoliation method. These MFI zeolite nanosheets were obtained from a multilamellar MFI precursor, which consists of ~3 nm-thick MFI layers stacked along their *b*-axis [48]. Single-layer MFI zeolite nanosheets can be generated from this multilamellar precursor by using a polymer-melt-blending exfoliation method [49]. After extensive purification processes to remove the polymer material and un-exfoliated particles [50], high purity nanosheet suspension could be obtained. These nanosheets were coated on silica supports and the gel-less

secondary growth method was performed to the seeded supports to make *b*-oriented MFI membranes with thickness ~100 nm, resulting in ultra-thin membranes with record-high selectivities and permeances for hydrocarbons separation [51].

Despite these inspiring achievements, the commercialization of MFI zeolite-based membranes has not been realized. This is due to the high capital cost associated with the manufacturing of these high-performance membranes. In order to grow mechanically and thermally robust membranes, inorganic supports were used. This is inevitable as the micropores of the nanosheets are blocked by the organic structure-directing agent (OSDA) used to template the multilamellar MFI precursor and membrane secondary growth. High temperature calcination is needed to activate the seeding layer and the final membrane. This requires the supports for the zeolite membranes to be mechanically and thermally robust. To cut down the manufacturing cost of zeolite membranes, it is desirable that polymer substrates can be used to replace the high-cost inorganic supports, which contribute to the major share (up to several thousand dollars per square meter) of the total cost of the membranes ($5000/m^2 to $10,000/m^2 for an assembled module) [52]. In 2016, a breakthrough has been achieved by Zhang et.al [53]. They used a piranha solution treatment method to effectively remove the OSDA in the micropores of the nanosheets. The resulted nanosheets were open-pore and hydrophilic (can be dispersed in water). This enabled the fabrication of high-performance zeolite membranes on low-cost polymer substrates using easily controllable and environmentally friendly solution processing techniques. Deposition of these zeolite nanosheets on flat porous polymer substrates by simple filtration (without secondary growth or other treatment) yielded membranes that

exhibit moderate selectivity (~5.4) of *n*-butane over *iso*-butane with a high *n*-butane permeance (~3.5×10^{-7} mol/(m^2-Pa-s)). In chapter 2, following work on the preparation of MFI nanosheets based membranes on polymer hollow fibers as substrates is discussed. Hollow fiber membrane modules are self-supporting (without the need of a backing material) and have a much higher surface area to volume ratio (7,000-13,000 m^2/m^3 for hollow fiber modules compared to 300-1,000 m^2/m^3 for spiral wounded modules [54]). The assembled membrane modules from hollow fiber substrates are more compact and cost-effective.

Recently, the second generation of MFI zeolite nanosheets was developed from a bottom-up synthesis method [55]. These nanosheets were directly synthesized using seeded growth of nano-sized MFI particles templated by a specially designed structure-directing agent (SDA): bis-1,5(tripropyl ammonium) pentamethylene diiodide (dC5). These nanosheets have a higher aspect ratio compared to the first generation and the production process is much easier with a much higher yield. By employing the directly synthesized MFI nanosheets and a floating-particle coating method to form a dense and uniform nanosheet seeding layer on specially engineered silica supports, ultra-selective MFI membranes were achieved after secondary growth with unprecedented permeances and separation factors for *para*-xylene/*ortho*-xylene separation [56]. This is a great achievement in terms of membrane fabrication. However, the fabrication cost is still high as the silica supports employed in the manufacturing process is very expensive and commercially unavailable. Preparing high-performance membranes using alternative supports such as commercially available alumina supports is desirable. In chapter 3, protocols for the

preparation of high-performance MFI membranes on low-cost alumina supports are discussed. The process avoids the need for tedious surface treatment of silica supports and allows the production of high-performance MFI membranes at a lower cost. Another problem presented is that the permeation tests were done at low temperatures (<200 °C) and very low xylene pressure (~500 Pa particial pressure). A solid demonstration of the separation performance at industrial conditions (high temperature and pressure) is needed. Thus, the ultimate success of commercialization is still elusive. In chapter 4, membranes were made from bottom-up synthesized nanosheets and permeation data at industrially relevant conditions were obtained. The results showed record-high *para*-xylene fluxes at high feed pressures and high temperatures. This is very exciting and proves the high potential of MFI membranes for industrial xylene separation application.

Besides butane isomers separation and xylene isomers separation, MFI membranes can also be used for other applications. One potential application is the separation of hydrocarbons from hydrogen. In 1999, L. J. P. van denBroeke [57] reported the permeation of binary gaseous mixtures through a silicalite-1 membrane. It was shown that at room temperature, *n*-butane flux was ~5×10^{-3} mol/(m^2-s) with separation factor ~40. Later in 2000, J. Dong et al. [58] showed that all-silica MFI membranes can separate multicomponent hydrogen/hydrocarbon mixtures in wide temperature and feed pressure ranges. At room temperature and atmospheric pressure on both feed and permeate sides, the total hydrocarbon permeation rate was measured to be 2-4×10^{-4} mol/(m^2-s). The thinner and easier diffusion path in nanosheet based membranes should allow a much higher permeation rate for the hydrogen/hydrocarbons separation. In chapter 5, the ultra-

thin nanosheet based MFI membranes were evaluated for the separation of H_2 and hydrocarbons mixtures. The results showed the high promise of these ultra-thin nanosheet based MFI membranes for industrial H_2/hydrocarbons separation applications. The adsorptive separation mechanism also works for the ammonia/hydrogen/nitrogen system. A screening program was carried at the University of Bath [59] to find suitable membranes for the effective recovery of ammonia. Tubular MFI zeolite membranes were reported to have moderate permeances but quite low selectivities. The highest selectivity obtained for ammonia/H_2 separation was 10, with an ammonia permeance of 2.1×10^{-7} mol/(m^2·s·Pa) at 80 °C. The permeance and selectivity were not very satisfactory for industrial application. In chapter 6, the ultra-thin, highly selective MFI nanosheet membranes were evaluated for the separation of ammonia and hydrogen or nitrogen. The membranes had very high permeances and selectivities. These results showed the possibility of the high-performance MFI membranes for industrial ammonia/H_2/N_2 separation application.

In summary, the objective of this thesis work is to make progress towards the commercialization of MFI membranes. Chapter 1 describes the recent advances of MFI zeolite membranes. To make cheaper and more scalable MFI membranes, different supports are used to replace the expensive silica supports. Chapter 2 discusses the fabrication of MFI membranes using aqueous dispersions of open-pore, two-dimensional MFI zeolite nanosheets on low-cost polymeric substrates. Chapter 3 studies the preparation of MFI membranes on alumina supports. Despite these efforts to use other supports, we failed to make high-performance membranes as comparable to the silica-supported ones. Besides these efforts, chapter 5 demonstrate that ultra-thin MFI

membranes fabricated using dc-5 nanosheets as seeds have high xylene isomer separation performance at industrial conditions. Chapter 6 and chapter 7 shows that these membranes are also suitable for H_2/hydrocarbons separation and ammonia/H_2/N_2 separation.

Chapter 2. Solution processable MFI nanosheets for the fabrication of low-cost MFI membranes on polymer hollow fibers

2.1. Introduction

The successful development of MFI zeolite nanosheets [49] opens up great opportunities for the preparation of ultrathin and high-performance MFI membranes [49,51]. The preparation of these nanosheets was based on a top-down exfoliation of a multilamellar MFI precursor. First, a special organic structure-directing agent was designed to template the layered structure of the MFI precursor. This OSDA was called $C_{22\text{-}6\text{-}6}$, which is a di-quaternary ammonium surfactant with a long alkyl chain (C_{22}) and two C_6 alkyl linkages [48]. With the help of this OSDA, a layered MFI precursor was synthesized. It consisted of ~3 nm-thick MFI layers stacked along their *b*-axis [48]. Single-layer MFI zeolite nanosheets can be generated from this multilamellar precursor by using a polymer-melt-blending exfoliation method [49]. In this method, the polymer (polystyrene) was melted in a polymer microcompounder and the multilamellar MFI precursor was added and co-rotated by a twin-screw extruder. The polymer chains can penetrate the space between the MFI layers and with the help of shearing, single layers of MFI nanosheets can be obtained. The polymer material introduced in the melt-blending step was roughly removed by washing in toluene and excessive polystyrene was removed by a density gradient centrifugation across chlorobenzene. Rate-zonal centrifugation in a multilayered density gradient was then employed to remove unexfoliated particles, obtaining high purity MFI nanosheets which could be dispersed in *n*-octanol and toluene [50]. ***Figure 2.1*** illustrates the entire process from multilamellar MFI precursor to dispersed MFI nanosheets.

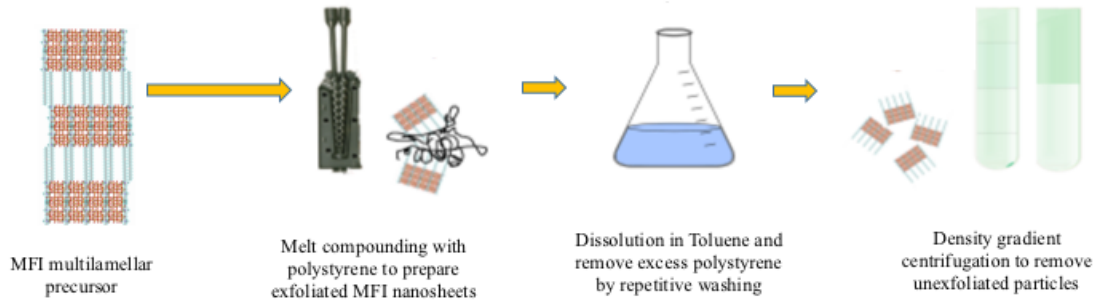

Figure 2.1: Preparation of MFI zeolite nanosheets: from multilamellar MFI precursor to dispersed MFI nanosheets. Pictures adapted from [49,51].

These nanosheets were successfully applied to prepare ultrathin MFI zeolite membranes by first coating the nanosheets on sintered silica fiber supports followed by a gel-less secondary growth. The resulted membranes were *b*-oriented, about 100 nm thick, with a butane isomer separation factor of ~60 and an *n*-butane permeance of ~5×10^{-7} mol/(m^2-s-Pa), representing the current state of art membranes for butane isomer separation [51]. After this report, simulation work was carried out to assess the potential of MFI membranes for industrial butane isomers separation [42]. It was found that a hybrid membrane-distillation process is energy efficient and economically attractive; but with the current state-of-art membrane performance, the required membrane area is about 3000 square meters with the unit price of ~5000 dollars, which is prohibitively expensive. To make it industrially viable, new membranes should be developed by either reducing the cost or improving the permeance. It was concluded that a payback period of ~3 years can be achieved if the membrane unit cost is reduced to $500 with the current state of art *n*-butane permeance of 5×10^{-7} mol/(m^2-s-Pa) and a separation factor of ~10. To cut down the manufacturing cost, it is desirable that low-cost polymer substrates can be used to

replace the high-cost inorganic supports. Previously, high-cost inorganic supports were used because the zeolite micropores were blocked by the OSDA. High-temperature calcination was needed to activate the membranes. This required the supports for the zeolite membranes to be thermally robust. To find a suitable substitute for the inorganic supports, we must work on high-temperature stable polymer materials. PBI has the ability to sustain such a high-temperature treatment. It is well-known for its outstanding heat stability and chemical resistance. It has a high glass transition temperature of about 425 °C, and its decomposition temperature is more than 500 °C. For the membrane configuration, hollow fiber membrane modules are self-supporting and have a much higher surface area to volume ratio, thus it is more compact and cost-effective. Therefore, we want to work on PBI hollow fibers as substrates for the preparation of MFI nanosheet based membranes. In parts 2.2 and 2.3, the preparation and characterization of PBI hollow fibers are discussed. During this time, a piranha treatment method [53] was found to be effective in removing the OSDA of the MFI nanosheets. Open-pore, aqueous dispersions of MFI nanosheets can be obtained using this method without the need for thermal treatment. This allows us to have more options for identifying a suitable polymeric hollow fiber support for membrane fabrication. Part 2.4 describes the preparation of various common polymer hollow fiber supports and their use to prepare membranes. PES does not swell in aqueous conditions and uniform MFI coatings can be obtained on PES hollow fibers. This result shows the promise of MFI nanosheet coating on PES hollow fibers as membranes for gas separation.

2.2 PBI hollow fiber substrate preparation

Polybenzimidazoles (PBIs) form a large family of aromatic heterocylic polymers containing benzimidazole units. PBIs, due to their impressive thermal stability and excellent chemical resistance, have been explored for various separation purposes especially at elevated temperatures and in harsh environments. As is mentioned previously,

Table 2.1: Recipe for PBI hollow fiber spinning

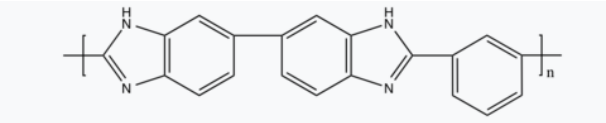

Dope Solution					Bore fluid	
PBI	DMAc	PEG400	n-Propanol	H_2O	DMAc	H_2O
16.8%	76.5%	4.2%	2.1%	0.4%	86%	14%

PBI was chosen as our first option because, at that time, open-pore MFI nanosheets could not be achieved without high-temperature calcination. PBI has the ability to sustain such a high-temperature treatment. However, a method to form porous PBI hollow fibers suitable for use as membrane substrates could not be found in the literature. Han Zhang, a member of the Tsapatsis/Macosko group, laid the groundwork of finding a processing method (see ***Table 2.1***) for porous, low defect PBI hollow fiber spinning. This coincided with my arrival to the group.

Polymer hollow fibers are usually prepared by a well-established dry-wet spinning technique based on the non-solvent induced phase inversion method. ***Figure 2.2a*** shows the schematic of this dry-wet hollow fiber spinning process. This process generally

involves the following four steps: solution preparing (dope solution and bore fluid); extrusion through spinneret; coagulation and treatment of coagulated hollow fiber. First, a dope solution, which is a mixture of several components comprising polymer, solvent, non-solvent, and additives, and a bore fluid, which contributes to the formation of the core of the nascent hollow fiber, are prepared and homogeneously mixed separately. Then, these two solutions are co-extruded through the spinneret (see the cross-section view of the structure of the spinneret in ***Figure 2.2b***. Bore liquid is extruded through the inner capillary and dope solution is extruded through the outer shell, forming a core-shell morphology.) to form a nascent hollow fiber. The nascent hollow fiber is continuously spun into the air and a subsequent coagulation water bath. An asymmetric hollow fiber

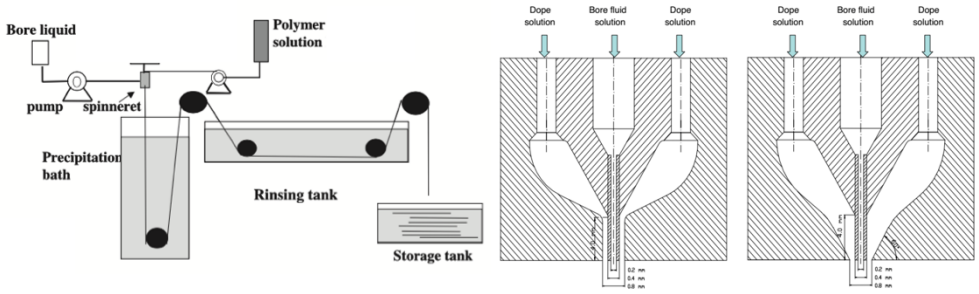

Figure 2.2. a) Dry-wet hollow fiber spinning process; b) cross section of the structure of the spinneret with different flow angles (90° and 60°, respectively). Adapted from [60].

with a dense skin layer (formed from the evaporation of the volatile solvent in the air gap) and a porous support layer (formed from the non-solvent (in this case water) induced phase inversion in the coagulation bath) is successfully obtained. Next, the asymmetric hollow fiber is guided and collected in a storage tank. Then, the fiber is cut into ~30cm pieces and immersed in a water bath for 36 hours and solvent exchanged in a methanol bath for 36 hours followed by a solvent exchange in a hexane bath for 36 hours. During the soaking

process, solvents are refreshed every 12 hours. The solvent exchange process minimizes surface pore collapse during the following drying process. Finally, the hollow fibers are dried in ambient environment overnight and thermal treated at 300 °C with an air flow of 110 mL/min for 8 hours to rigidify the hollow fiber and preserve the pore structure.

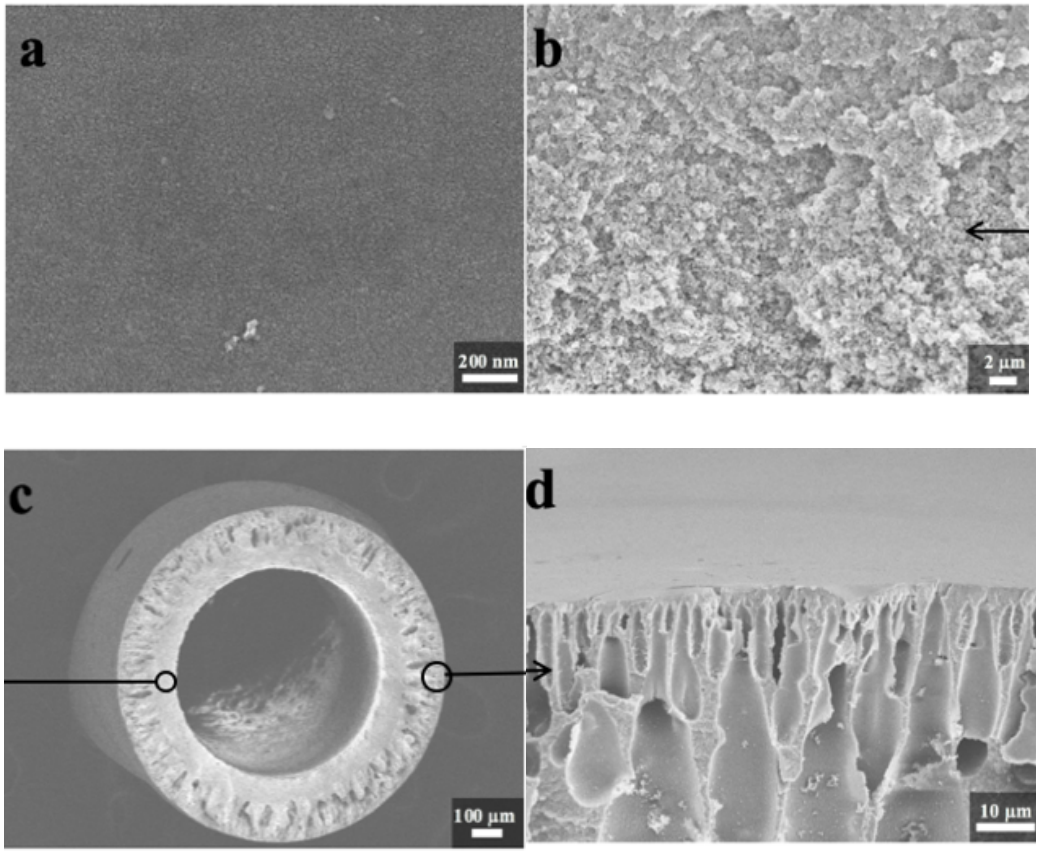

Figure 2.3: SEM images of the fabricated PBI hollow fibers: a) outer surface; b) cross section near the inner surface; c) whole view of cross section; d) cross section near the outer surface.

Typical SEM images of the fabricated PBI hollow fibers using the recipe in ***Table 2.1*** are shown in ***Figure 2.3***. As we can see from the images, the hollow fiber was in round shape, with finger type pores near the outer surface and sponge type pores near the inner surface. The main problem for this hollow fiber membrane was that the surface pores of

the PBI hollow fiber were too small (cannot be observed by SEM imaging at high magnification (×60,000)) (***Figure 2.3a***). It was found that modifying the spinning condition by increasing the coagulation bath temperature can effectively enlarge the surface pores.

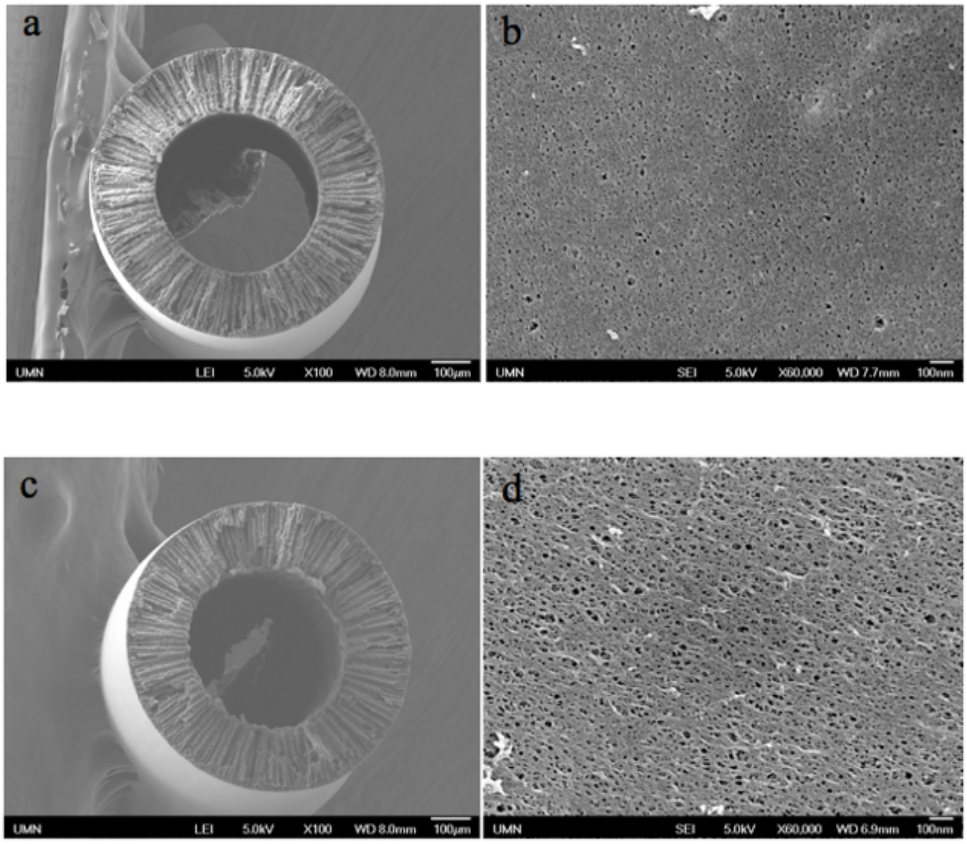

Figure 2.4. Typical SEM images of the fabricated PBI hollow fiber under the coagulation bath temperature of 60 °C (denoted as PBI-60) : a) cross section; b) outer surface and 80 °C (denoted as PBI-80): c) cross sectin; d) outer surface.

Figure 2.4 shows the typical SEM images of the fabricated PBI hollow fiber under the coagulation bath temperature of 60 °C and 80 °C. As we can see from ***Figure 2.4b***, when the coagulation bath temperature was increased to 60 °C, surface pores were observable under SEM imaging (magnification: $\times 60{,}000$). When the temperature was further increased to 80 °C, the surface pores were further enlarged (~10 nm) (***Figure 2.4d***). These large-surface-pore hollow fibers can be used as ultrafiltration membranes and are suitable to be employed as the substrates for MFI zeolite nanosheet coating.

2.3 Characterization of PBI hollow fibers by water permeation and solute rejection

The large pore size PBI hollow fibers (PBI-60 (the fabricated PBI hollow fibers under the coagulation bath temperature of 60 °C) and PBI-80(the fabricated PBI hollow fibers under the coagulation bath temperature of 80 °C)) were characterized by water permeation and solute rejection test following a commonly used approach [61]. Polyethylene glycols (PEGs) and polyethylene oxides (PEOs) of different molecular weights were used as the tracing molecules. The schematic of the testing set-up was illustrated in ***Figure 2.5***.

The flux and rejection data for the PBI-60 and PBI-80 hollow fiber samples is shown in ***Table 2.2*** and ***Table 2.3***, respectively. Here the solute rejection, R, is defined as:

$$R=(1-\frac{cp}{cf}) \quad (1)$$

where C_p and C_f are the solute concentrations in the permeate and feed solutions. The concentrations were determined by TOC (Total Organic Carbon) analyzer.

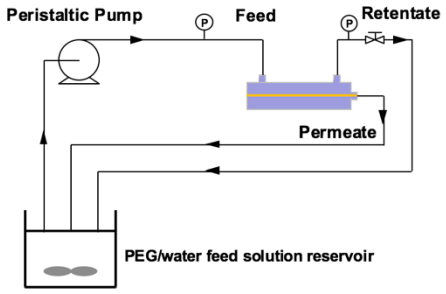

Figure 2.5: Schematic of the set-up for water permeation and solute rejection test

In a typical experiment, a piece of ~20 cm hollow fiber was introduced into a membrane module (the schematic of the hollow fiber membrane module is shown in ***Figure 2.5***). Then, epoxy was used to seal the module with one end of the fiber fully blocked and the other end encapsulated. Pure water permeation test was carried out using the set-up shown in ***Figure 2.5*** with the feed reservoir being DI water. The transmembrane pressure was regulated by the needle valve and maintained at 25 psi. Then, the amount of permeate was weighted by a balance, recorded as a function of time and further used to calculate the pure water permeance by using equation (2):

$$Permeance = \frac{J}{\Delta P A} = \frac{J}{\Delta P \pi D l} \quad (2)$$

where J is the permeation flux (L/h), ΔP is the transmembrane pressure (bar), A is the effective membrane surface area (m^2), D is the outer diameter of the hollow fiber membrane (m) and l is the effective fiber length inside the membrane module (m).

Before the solute rejection test, the DI water in the system was drained out and the feed reservoir was replaced by PEG or PEO aqueous solution (200 ppm). Then, the system was kept running at a constant pressure of 25 psi for 2 hours to stabilize. Next, a total amount of ~10 g permeate was collected and its weight was recorded as a function of time. The

recorded data was used to calculate the PEG/PEO solution permeance by using equation (2). The collected permeate and ~10 g feed solution were used as samples for TOC analysis. It is worth noting that since the samples' concentrations were broad (varying from ~1 mg C/L to ~120 mg C/L), it is non-trivial to get a good calibration curve for TOC measurement. Initially, standard stock of 200 ppm PEG solution was used to do the calibration. The lower end of the calibration curve (<10 mg C/L) failed to behave reproducibly. This may be attributed to the instrument error when doing calibration across a broad range of concentrations. To solve this problem, two separate standard stocks with different concentrations (200ppm and 20 ppm, respectively) were prepared and tested to get two calibration curves. The two calibration curves were combined, which gave us a good calibration from 1 mg C/L to 120 mg C/L with good linearity and reproducibility. After obtaining a good calibration, TOC measurements were carried out to determine C_p and C_f, and the solute rejection can be calculated by using equation (1).

The data analysis is based on the finding that the rejection coefficients of ultrafiltration membranes to the solute size of the tracing molecules remarkably fit into a log-normal probability distribution curve [62]. Having this in mind, we can draw the solute rejection (R) vs. solute diameter (*ds*) on a log-normal probability paper. This will yield a straight line. From the fitted straight line, the MWCO (molecular weight cut-off), based on its definition, can be calculated from the solute diameter (*ds*) corresponding to solute separation=90%. And according to the definition and property of log-normal distribution, the mean solute size (μ_s) is the solute diameter value corresponding to solute separation=50%. The geometric standard deviation about the mean diameter (σ_g) is the

ratio of *ds* at solute separation=84.13% and at 50%. Then the mean pore size (μ_p) and the geometric standard deviation (σ_p) of the membrane can be considered to be approximately the same as of solute mean size (μ_s) and solute geometric standard deviation (σ_g).

Table 2.2: Fluxes and rejection data for the PBI-60

	PEG 6,000			PEG 20,000		PEO 40,000			PEO 100,000	
Pure water permeance (PWP) (L/(bar-h-m²))	104.7	86.6	102.4	213.9	236.6	155.6	174.0	187.2	134.5	235.6
	Average: 97.9			**Average: 225.3**		**Average: 172.3**			**Average: 185.0**	
PEG solution permeance (PEGP) (L/(bar-h-m²))	31.5	22.4	22.5	34.5	41.4	14.7	18.7	24.3	12.7	13.1
	Average: 25.5			**Average: 38.0**		**Average: 19.2**			**Average: 12.9**	
Ratio between PEGP to PWP (%)	30.1	25.9	22.0	16.1	17.5	9.5	10.7	13.0	9.4	5.6
	Average: 26.0			**Average: 16.8**		**Average: 11.0**			**Average: 7.5**	
Rejection (%)	9.9	19.6	18.4	37.4	29.1	71.4	85.2	62.7	99.3	95.8
	Average: 16.0			**Average: 33.3**		**Average: 73.1**			**Average: 97.6**	

Table 2.3: Fluxes and rejection data for the PBI-80

	PEG 20,000		PEO 40,000		PEO 100,000		PEO 300,000	
Pure water permeance (PWP) (L/(bar-h-m²))	228.3	273.1	314.5	284.2	255.4	284.9	252.1	239.0
	Average: 250.7		**Average: 300.4**		**Average: 270.2**		**Average: 245.6**	
PEG solution permeance (PEGP) (L/(bar-h-m²))	87.3	58.9	45.9	40.1	13.8	12.8	8.2	9.1
	Average: 73.1		**Average: 43.0**		**Average: 13.3**		**Average: 8.6**	
Ratio between PEGP to PWP (%)	38.3	21.6	14.6	14.1	5.4	4.5	3.2	3.8
	Average: 30.0		**Average: 14.4**		**Average: 4.6**		**Average: 3.5**	
Rejection (%)	2.9	3.6	17.7	19.5	93.3	88.6	98.7	97.8
	Average: 3.3		**Average: 18.6**		**Average: 91.0**		**Average: 98.3**	

The next question is how we get solute diameters from the molecular weights of the solutes. On the one hand, Stokes-Einstein equation relates the Stokes radius of a macromolecule and its diffusivity:

$$D(diffusivity)=\frac{kT}{6\pi\eta a},$$

where k is Boltzmann's constant, η is the solvent viscosity and a is the Stokes radius.

On the other hand, experimental results [63-64] showed that for flexible polymers in dilute solution, the diffusivity can be calculated as follows:

$$D=\frac{2.5\times10^{6}kT}{\{\eta(M[\eta])^{1/3}\}}$$

where M is the molecular weight and $[\eta]$ is the intrinsic viscosity of the polymer, respectively.

From these two equations, we can obtain the solute radius as the following:

$$a=2.122\times10^{-8}(M[\eta])^{1/3}$$

where a is in cm, M is in g/mol and $[\eta]$ is in dL/g.

Next, rheology data from literature can be used to determine the intrinsic viscosity parameter:

For PEG [65],

$$[\eta]=4.9\times10^{-4}M^{0.672}$$

For PEO [66],

$$[\eta]=1.192\times10^{-4}M^{0.76}$$

By combining these equations, we can get the Stokes radius vs. solute molecular weight relationship as follows:

For PEG,

$$a=16.73\times10^{-10}M^{0.557}$$

For PEO,

$$a=10.44\times10^{-10}M^{0.587}$$

Finally, the Stokes diameter is obtained by multiply Stokes radius by a factor of 2:

For PEG:

$$d=33.46\times10^{-10}M^{0.557}$$

For PEO:

$$d=20.88\times10^{-10}M^{0.587}$$

After doing the calculation and data fitting, we can finally obtain the molecular weight cut-off (MWCO), the mean pore size and standard deviation of the PBI samples.

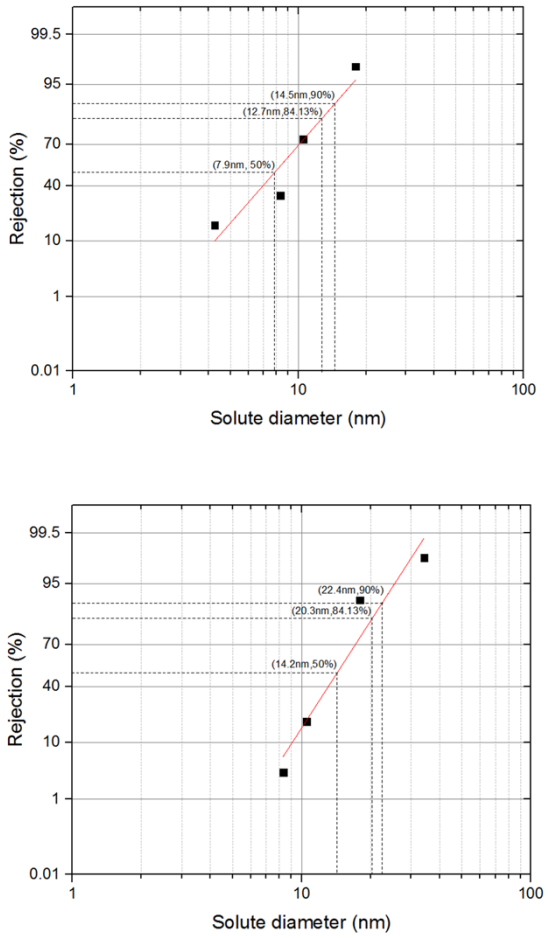

Figure 2.6: Lognornal plot of the solute rejection vs. solute diameter and the fitted straight line: a) PBI-60; b) PBI-80.

Table 2.4: The MWCO, mean pore size and standard deviation for PBI-60 and PBI-80

Membrane	**MWCO (kDa)**	**Mean pore size μ_p (nm)**	**Standard deviation σ_p (nm)**
PBI-60	70.0	7.9	1.6
PBI-80	145.5	14.2	1.4

Then, the pore size distribution plots can be generated from the mean pore size and standard deviation data.

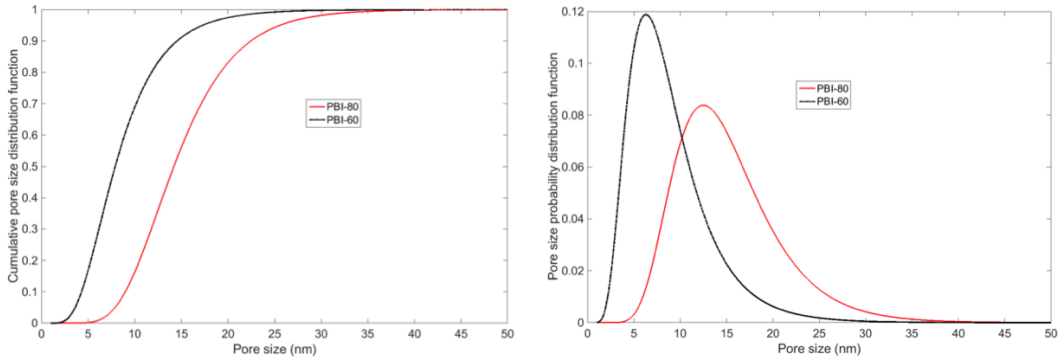

Figure 2.7: Cumulative pore size distribution and pore size probability for PBI-60 and PBI-80

The PBI-60 sample have a MWCO value of 70.0 KDa and a mean pore size of 7.9 nm. While the PBI-80 sample have a MWCO value of 145.5 KDa and a mean pore size of 14.2 nm. These membranes are good for using as a porous substrate for nanosheets coating.

2.4 Preparation of MFI nanosheet suspension

Aqueous suspension of MFI nanosheets was prepared as reported in the literature [53]. First, OSDA was prepared by two consecutive alkylation reactions. Di-quaternary ammonium-type surfactant $[C_{22}H_{45}–N^{+}(CH_3)_2–C_6H_{12}–N^{+}(CH_3)_2\text{-}C_6H_{13}](Br_2)$ ($C_{22\text{-}6\text{-}6}Br_2$) was used as OSDA. It was synthesized by a first alkylation reaction of *N,N,N',N'*-tetramethyl-1,6-diaminohexane with 1-bromodocosane at 65 °C overnight followed by a second alkylation reaction of the resultant product by 1-bromohexane at 85 °C overnight. The multi-lamellar MFI zeolite precursor was synthesized using a gel composition of 100 SiO_2: 7.5 SDA: 24 NaOH: 18 Na_2SO_4: 400 EtOH: 4000 H_2O and reacting at 150 °C for 7

days with rotation. Tetraethyl orthosilicate (TEOS) was used as the silica source. ***Figure 2.8*** shows typical SEM image of the prepared multi-lamellar MFI precursors.

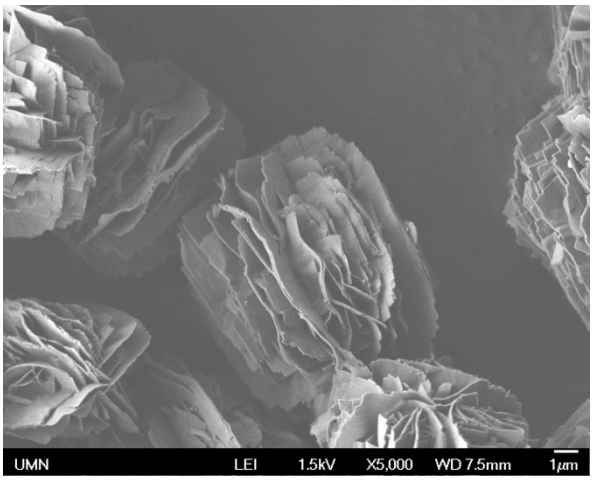

Figure 2.8: SEM image of the prepared multi-lamellar MFI precursors.

Next, the obtained multi-lamellar MFI precursor was exfoliated in a polymer melt compounder. Typically, 0.6 g of ML-MFI was mixed with 14.4 g of polystyrene (PS) in the microcompounder at 95 °C and 250 rpm for 1 hour. Single layer MFI nanosheets were generated by this exfoliation process. Now the nanosheets were embedded in the polystyrene matrix. To obtain nanosheet suspension, 3 g of the extruded nanocomposite was dissolved in 45 mL of filtered toluene and centrifuged at 40,000 *g* for 3 h. The washing process was repeated three times to remove most of the polystyrene. Finally, excessive polystyrene was removed by a density gradient centrifugation across chlorobenzene. The cake was dissolved in 20 mL toluene and the suspension was added on top of 25 mL chlorobenzene in a centrifuge tube carefully. After centrifugation at 40,000 *g* for 3 h, MFI zeolite will be collected at the bottom of the centrifuge tube while polystyrene remained dissolved in the solvent.

To activate the MFI nanosheet, the cake obtained above was washed with ethanol three times at 40,000 *g* for 3 h. Then, piranha treatment was applied to the obtained MFI cake. Typically, 6 mL of concentrated H_2SO_4 was added into the centrifuge tube and sonicated for 2 min to fully disperse the cake. Then, 2 mL of H_2O_2 (30%) was slowly added into the H_2SO_4 solution drop by drop with effective mixing by shaking. The solution was stirred at ambient temperature for 1 h and then transferred into a capped glass bottle and placed in a preheated oven at 80 °C overnight. Next, after the bottle was fully cooled down to ambient temperature, the solution was transferred into a centrifuge tube and diluted to 45 mL with DI water. The suspension was centrifuged at 40,000 *g* for 6 h. After this, the MFI cake was obtained at the bottom of the centrifuge tube. This piranha solution treatment was repeated for three more times. The cake was then washed with fresh DI water for five times at 40,000 *g* for 3 h and finally dispersed in 45 mL of DI water.

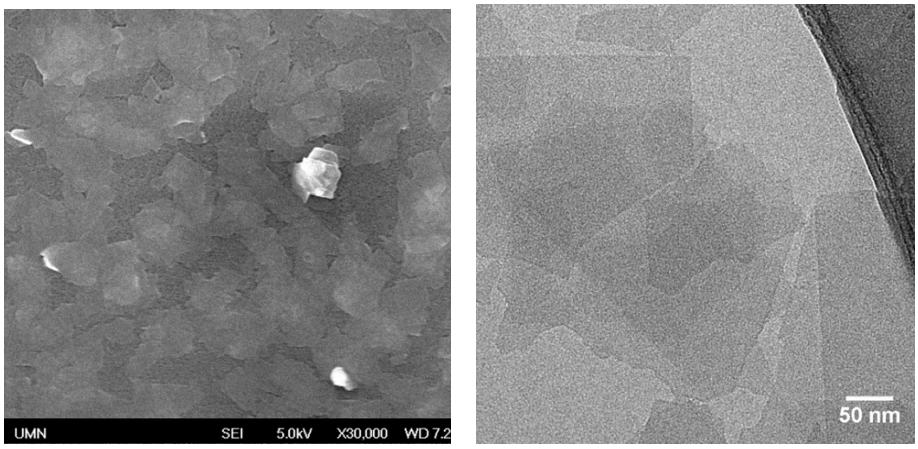

Figure 2.9: SEM image of the prepared MFI nanosheets deposited on support TEM image of the nanosheet deposited on silicon wafer.

Now, MFI nanosheets were activated and dispersed in water, but a lot of unexfoliated MFI particles were also presented in the suspension. A final centrifuge step was applied to the suspension at 5,000 g for 10 min. The top half of the suspension was collected after centrifugation and can be used for preparing membranes. Typical morphology of the prepared nanosheets is shown in ***Figure 2.9***.

2.5 Nanosheet coating on hollow fibers

2.5.1 Nanosheet coating on PBI hollow fibers

As mentioned in section 2.1, using a polymer as the membrane support is desirable because polymer materials are much cheaper and much easier to process than inorganic support. The availability of dispersible and open-pore zeolite nanosheets aqueous solutions makes this approach feasible. Deposition of these zeolite nanosheets on flat porous polymer substrates by simple filtration (without secondary growth or other treatment) yield membranes that exhibit moderate selectivity (~5.4) of *n*-butane over *iso*-butane with a high *n*-butane permeance (~3.5×10^{-7} mol/(m^2-Pa-s)) [54]. Based on this work, we attempt to extend the research on flat sheet polymer substrate to polymer hollow fiber substrate, which is self-supporting, more cost-effective and can be assembled into more compact membrane modules.

A pressurized continuous flow filtration set-up was used (see ***Figure 2.10***). In a typical coating process, 30 mL of the obtained MFI nanosheet suspension was diluted to 300 mL. The diluted suspension was fed to the hollow fiber module using a high pressure syringe pump at 2.5 mL/min. At the retentate side, a needle valve was used to regulate the pressure

inside the membrane module. A pressure of 10psi was used for the coating.

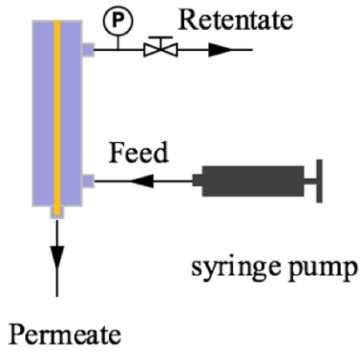

Figure 2.10: Schematic of the set-up for nanosheets coating on polymer hollow fibers

Figure 2.10 shows typical SEM images of the obtained MFI coating layer on PBI hollow fiber. Due to the dimensional change induced by swelling of the PBI substrate in the aqueous suspension, many wrinkles were induced after drying (***Figure 2.11***). In some cases, the presence of wrinkles was associated with the formation of cracks that can be detected by SEM and are unwanted since they will compromise membrane selectivity. The ideal selectivity of *n*-butane/*iso*-butane for this nanosheet coated PBI hollow fiber membrane was 1, indicating the presence of wrinkles are detrimental to membrane performance.

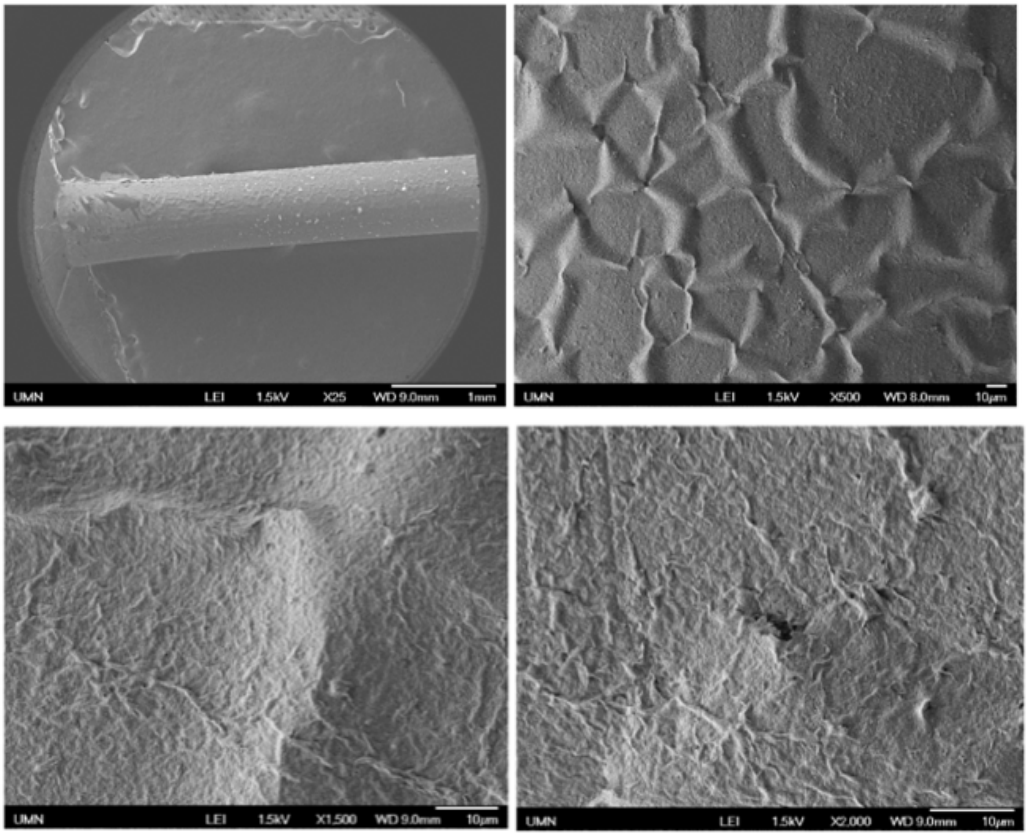

Figure 2.11: Typical SEM images of nanosheets coating on PES hollow fibers.

2.5.2 Nanosheet coating on other types of hollow fibers

Since piranha treatment can be used to effectively remove the OSDA in the micropores of the zeolite nanosheets now, high temperature calcination was not needed. This gives us the flexibility to work on other polymer hollow fibers that do not swell significantly in aqueous solution. Several common polymer hollow fibers (PVDF, PI, PES) were tried. (PVDF hollow fibers were kindly provided by Dow Chemical Company; PI and PES hollow fibers were spun in our lab following literature recipes and procedures [67,68]. The recipes for PI and PES hollow fiber spinning are summarized in ***Table 2.5*** and ***Table 2.6***, respectively. Typical cross-section and surface morphologies of the prepared PI and PES hollow fibers are shown in ***Figure 2.13*** and ***Figure 2.14***, respectively).

PES hollow fiber turned out to have negligible swelling, as can be seen from the photographs in ***Figure 2.12***. All the polymer fibers were fully stretched in the membrane module in a dry state. After wetting with water, all fibers except PES swelled and became curled. Only the PES fiber did not swell macroscopically in water. This indicated that PES is a good candidate to be used as the substrate for nanosheet coating.

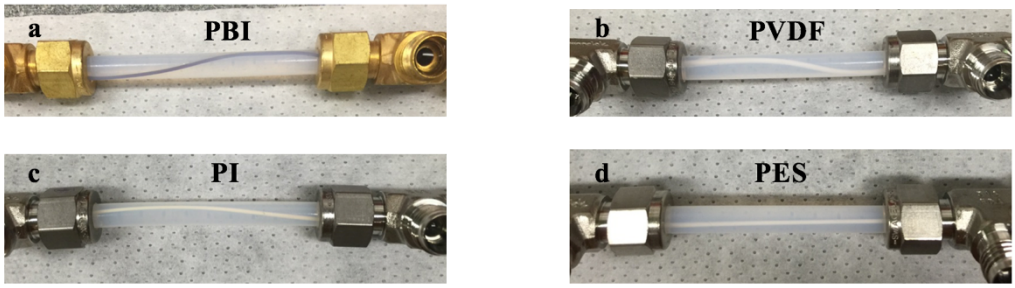

Figure 2.12: Swelling of different hollow fibers in water: a) PBI; b) PVDF; c) PI; d) PES

Table 2.5: Recipe for PI spinning [68]

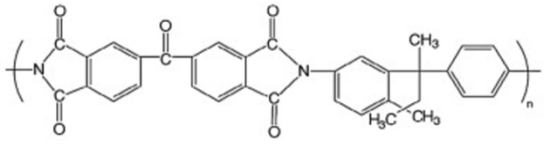

Dope Solution			Bore fluid	
PI	NMP	PEG400	NMP	H_2O
18%	64%	18%	90%	10%

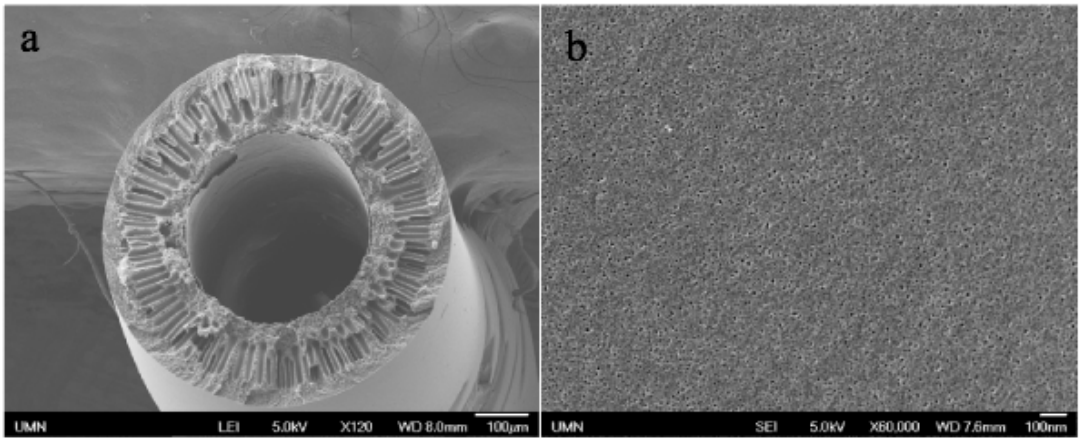

Figure 2.13: Typical SEM images of the fabricated PI hollow fiber: a) cross section; b) outer surface.

Table 2.6: Recipe for PES spinning [69]

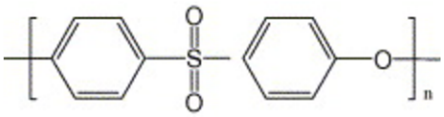

Dope Solution				Bore fluid	
PES	NMP	PEG400	H_2O	NMP	H_2O
18%	36.5%	38.5%	7%	80%	20%

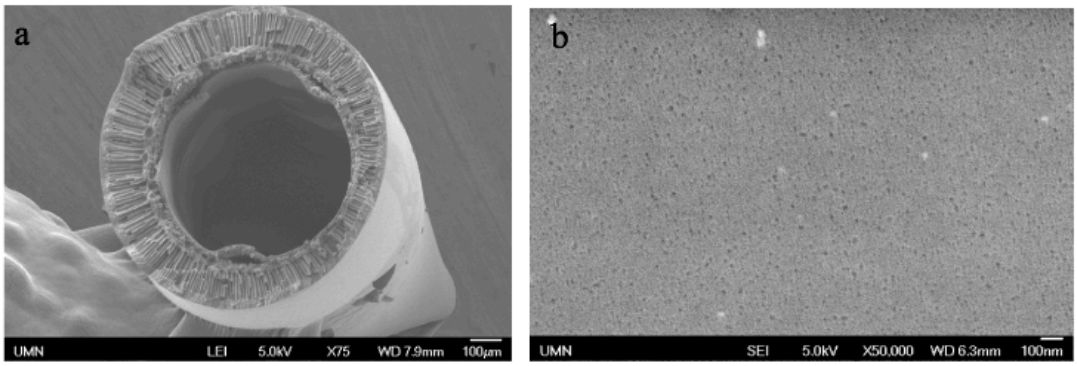

Figure 2.14: Typical SEM images of the fabricated PES hollow fiber: a) cross section; b) outer surface.

Trials on PES hollow fiber coating using the pressurized continuous flow coating process resulted in very uniform nanosheet coating layers. Before coating the PES hollow fiber, a crucial step was to remove the glycerol that was used to prevent the collapse of the porous structure of PES hollow fibers (glycerol was not used in the case of PBI hollow fibers). Glycerol can be effectively removed by immersing the hollow fiber in isopropanol overnight followed by compaction at a transmembrane pressure of ~50 psi for 3 hours (using the water permeation set-up as is shown in ***Figure 2.4***).

Typical SEM images (different magnification) of nanosheet coating on PES hollow fiber are shown in ***Figure 2.15***. Compared with the nanosheet coating on PBI hollow fiber, the coating layer is more smooth without the formation of wrinkles. However, some small scale ripples are present. These ripples are hard to prevent because even nanosheet coating on flat sheet support (either organic [53] or inorganic [51]) and GO nanosheet coating on inorganic hollow fibers [69] have this kind of rippled structure. This rippled morphology is acceptable because no observable defect was induced.

The ideal selectivity of *n*-butane/*iso*-butane for this nanosheets coated PES hollow fiber membrane was 2.1 with a *n*-butane permeance of ~3.2×10^{-7} mol/(m^2-Pa-s). This result showed promise for MFI nanosheet coating on PES hollow fibers as membranes for *n*-butane/*iso*-butane separation.

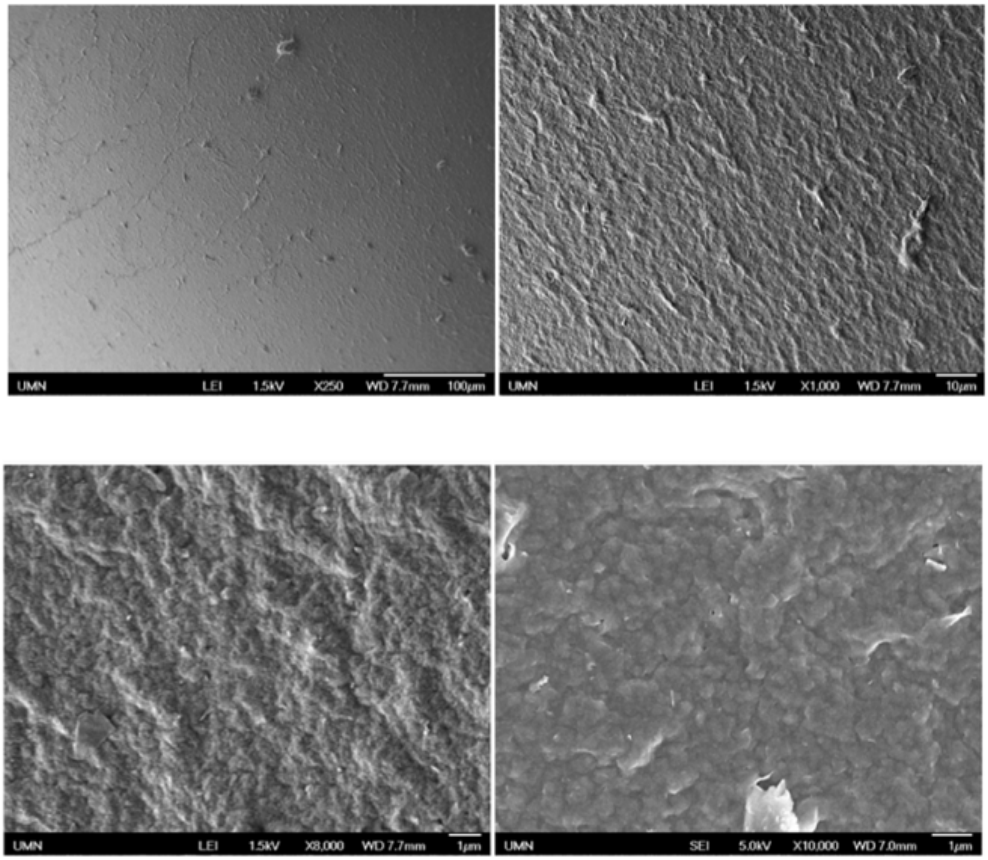

Figure 2.15: Typical SEM images of nanosheets coating on PES hollow fibers.

2.6. Conclusion

Polymer hollow fibers were prepared as substrates for the fabrication of MFI membranes. First, PBI hollow fibers were studied because of their high thermal resistance, with the hope that it can sustain high temperature calcination. The development of the piranha treatment method gives us the flexibility to work on other polymer hollow fibers. PES was identified as a suitable hollow fiber substrate for the membrane preparation. The coating of open-pore MFI nanosheet on PES hollow fiber resulted in a uniform and continuous MFI layer. The ideal selectivity of *n*-butane/*iso*-butane for this nanosheets coated PES hollow fiber membrane was 2.1 with an *n*-butane permeance of ~3.2×10^{-7} mol/(m^2-Pa-s). This result showed promise for MFI nanosheet coating on PES hollow fibers as membranes for *n*-butane/*iso*-butane separation. Despite the high permeance, the selectivity is considerably lower than the membranes made on silica supports. Further work can be done by applying a thin and highly permeable polymer layer (such as PDMS) on top of the coating to seal membrane defects and increase membrane selectivity without compromising the high permeance.

Chapter 3. Preparation of MFI membranes on low-cost alumina supports

3.1. Introduction

MFI nanosheet membranes can be prepared on silica supports with unprecedented separation performance for butane isomers separation [51] and xylene isomers separation [56]. However, these membranes require the careful preparation of very smooth and defect-less silica supports. These supports are not commercially available and are very expensive to produce. In the meanwhile, the supports are not mechanically strong enough for challenging separation tasks. It is desired to fabricate MFI nanosheet-based membranes on simpler, cheaper, and more robust supports. α-alumina supports are widely used to fabricate zeolite membranes and are cheap and commercially available. Zeolite NaA membranes made on α-alumina tubes have achieved commercial success for alcohol/water pervaporation applications [70]. Therefore, α-alumina support was selected as a substitute for the specially made silica support for the fabrication of MFI nanosheet type membranes. Changing the membrane support would change the membrane fabrication process. When silica supports were used, a gel-free secondary growth method [47] was adapted. In this method, a top 50 nm Stöber silica layer was rubbed on the surface of the silica support and it served as a sacrificial silica source to form continuous and inter-grown MFI membranes. This method was not applicable to non-silica supports. Thus, a new secondary growth process must be developed. It was reported that the use of tetraethylammonium-hydroxide (TEAOH) based silica sols can achieve homoepitaxial

growth on exfoliated MFI nanosheets [71,72] as well as dC5-MFI nanosheets [73]. Oriented films on silicon wafers were prepared using TEAOH based silica sols. In this chapter, we discuss the use of TEAOH based silica sols for the preparation of MFI membranes on α-alumina supports.

3.2. Experimental section

3.2.1. Porous α-alumina support preparation

A colloidal processing method was adapted for the fabrication of α-alumina supports [50]. First, α-Al_2O_3 powder was added to water to make an alumina suspension. The suspension was electrostatically stabilized at pH 2.2 by adding HNO_3. In a typical experiment, for one batch of support preparation (9 supports), 18 g DI water was added into a clean glass bottle, then, ~120 µL of 1M Nitric acid solution was added into water to make pH=2.2. A short time of bath sonication was applied after adding the acid solution. After this, 18 g CR-6 (Baikowski, average particle size of 400 nm) α-Al_2O_3 powder was added to the solution. The suspension was mixed by stirring using a spatula and a short period of bath sonication. Next, horn sonication (~3 min) was applied to the alumina suspension to break big aggregates and lumps. After horn sonication, the suspension was filtered through a coarse filter paper (VWR_Filter Paper 415) supported on a 1 μm stainless steel mesh to remove any remaining large agglomerates and contaminations. The microbubbles in the suspension were suppressed by the addition of ~100 μL *n*-octanol to the suspension, followed by degassing of the suspension in the bath sonicator. Now the alumina suspension was ready to be cast. 2.4 mL alumina suspension was carefully

transferred into a home-made casting mold (***Figure 3.1***) which was supported on a 0.2 μm nylon membrane and a 1 μm stainless steel mesh. The backside of the nylon membrane was kept under partial vacuum (−14 kPa) to allow the formation of alumina compact disk. After ~90 min, the vacuum pump was stopped and the alumina compacts were dried overnight in the molds before further processing. After drying, the alumina compacts were removed from the mold and sintered under airflow (150 mL/min) at 1050˚C for 3 hours with heating and cooling rates of 2 ˚C/min. After sintering, the supports became very rigid. The top surface of the alumina support was polished by using SiC grinding papers MicroCut™ (1200 grit/P2500) with water flow and the debris after polishing was removed from the support by using a sonication. In this step, the polished support was placed in a plastic container filled with ~20 mL DI water followed by sonication for 60 sec. The support was then rinsed with DI water. The process was repeated twice. After sonication, the support was dried at 60 °C and stored in a clean environment for further use.

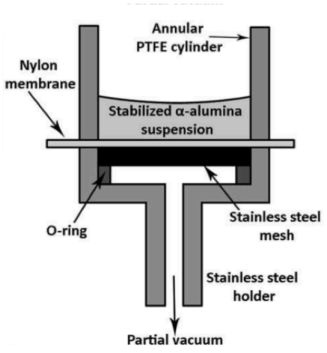

Figure 3.1. Filtration setup for making alumina supports. Adapted from [50].

3.2.2. Meso-silica sol preparation and support modification

A meso-silica layer was deposited on the α-alumina support surface. It smoothens the support surface and prevents leaching of aluminum from the underlying alumina support

during secondary growth [41]. It was prepared by hydrolyzing TEOS (60 mL) in a mixture of ethanol (63 mL) and DI water (4.87 g). The pH of the mixture was adjusted to 4 by adding 0.2 mL 0.07 M HCl. Then, cetyltrimethylammonium bromide (CTAB) (4 g) was added to 40 mL of the sol as a surfactant and the pH of the mixture was further adjusted to 2 by adding 7 mL 0.07 M HCl. The sol was aged at 50 ℃ for 2.5 days. The meso-silica layer was deposited on the support by a slip casting process. In this process, the sol was diluted 250 times by adding EtOH to it. The diluted sol was transferred to a petri dish and the α-alumina support surface was brought in to contact with the sol for 30 s and then detached gently from the suspension surface on a pendulum's trajectory move. Finally, the slip coated supports were calcined by heating at 480 °C for 4 h (heating and cooling rate: 1 °C /min). ***Figure 3.2*** shows the typical SEM surface image of the polished α-Al_2O_3 support before meso-silica coating (left) and after meso-silica coating (right).

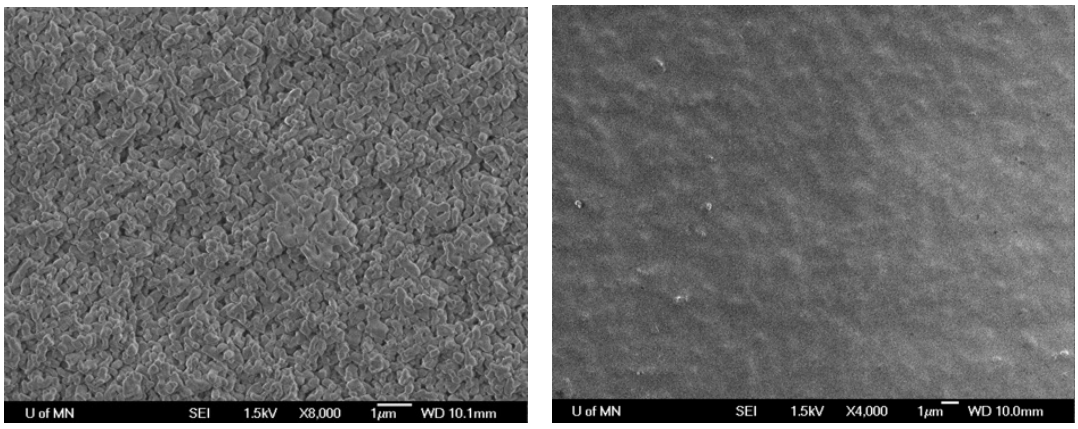

Figure 3.2: Typical SEM surface image of the polished α-Al_2O_3 support before meso-silica coating (left) and after meso-silica coating (right).

3.2.3. MFI seed crystal synthesis

Coffin-shaped crystals were synthesized following the procedures reported in [74]. Briefly, 10.1 g of TEOS (Sigma Aldrich, >99%) was added to a solution of 3.69 g TPAOH (Alfa Aesar, 40 wt%) in 87.8 g DI water and stirred for 24 h. The clear solution was filtered through a 2 μm syringe filter and then autoclaved at 150 °C under rotation for 12 h. The product after synthesis was washed with water and centrifuged repetitively until pH=7. After washing, the cake was vacuum freeze-dried and stored for further use. The morphology of prepared MFI crystals is shown in ***Figure 3.3***. The crystals were very uniform with a lateral size of about 2 μm and a thickness of about 0.5 μm.

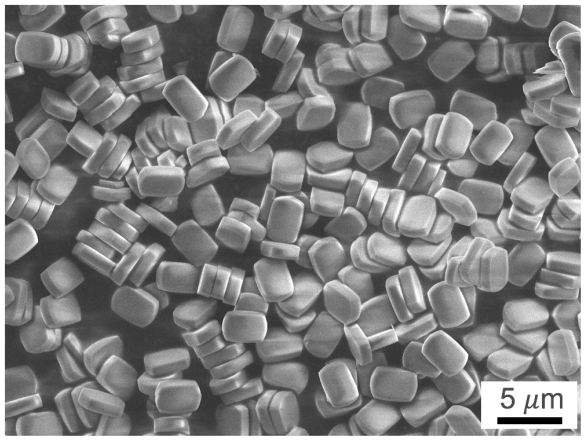

Figure 3.3: SEM image of the prepared coffin shape MFI crystals.

3.2.4. dc5 nanosheet synthesis

The dc5 nanosheets were synthesized using the same method reported in [55]. dC5 was first synthesized by exhaustive alkylation of 1,5-diaminopentane with 1-iodopropane. It was used as OSDA for templating MFI nanosheets. In parallel, MFI nanocrystals were prepared as seeds for the growth of nanosheets, using a sol composition of $10SiO_2$:2.4TPAOH:0.87NaOH:$114H_2O$. A precursor sol with a composition of

80TEOS:3.75dC5:20 KOH:9500 H_2O was then hydrolyzed and mixed with the MFI nanocrystals suspension at 1000:1 silica molar ratio of precursor sol to nanocrystal suspension. The mixture was then transferred into a Teflon-lined stainless steel autoclave and hydrothermally treated at 140 °C for 4 days. After synthesis, a nanosheet dispersion can be obtained by first centrifuging at 10,000 g for 30s (taking the upper half after centrifugation) to remove large particles and then washing at 14,500 g for 1min (collecting the bottom cake after centrifugation) for 4 times. ***Figure 3.4*** shows the TEM image of the prepared MFI nanosheets.

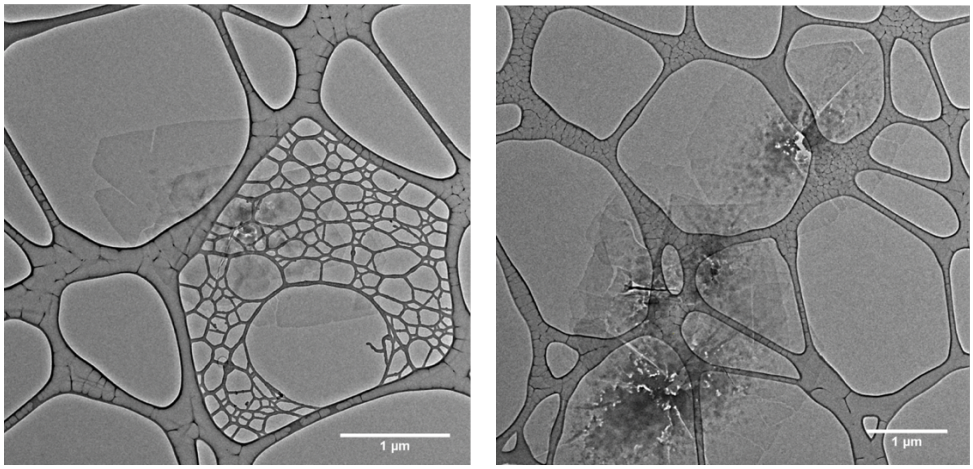

Figure 3.4: TEM image of the prepared dc5 MFI nanosheets.

3.2.5. Seeding the support

When using coffin-shaped crystals as seeds, seeds were deposited on the alumina supports by manual rubbing. To rub seeds on the supports, a polymeric intermediate layer (polyacrylic acid) was required in order to add adhesion between the seeds and the supports. A polyacrylic acid solution was prepared by dissolving 10 g polyacrylic acid (Sigma-Aldrich, Mw 1800) in 10 g DI water. Then, the solution was sonicated for 1 hour and 2 mL ethylene glycol was added to the solution. The solution was degassed by

sonication for 20 min before spin coating. Next, the polyacrylic acid solution was deposited on an alumina support by spin coating at 4,000 rpm for 15 s. The spinning process was repeated once to ensure full coverage. After spin coating, the support was pressed against the MFI powder and excess powder on the surface was rubbed by hand using powder-free gloves. The seeded support was dried at 150 ℃ for 1 min, and 50 nm Stöber silica spheres were rubbed by hand very gently on the seeded support. Finally, the seeded support was calcined at 550 ℃ to decompose the polymeric layer and fix the seeds on the support. The morphology of seeded support is shown in ***Figure 3.5***.

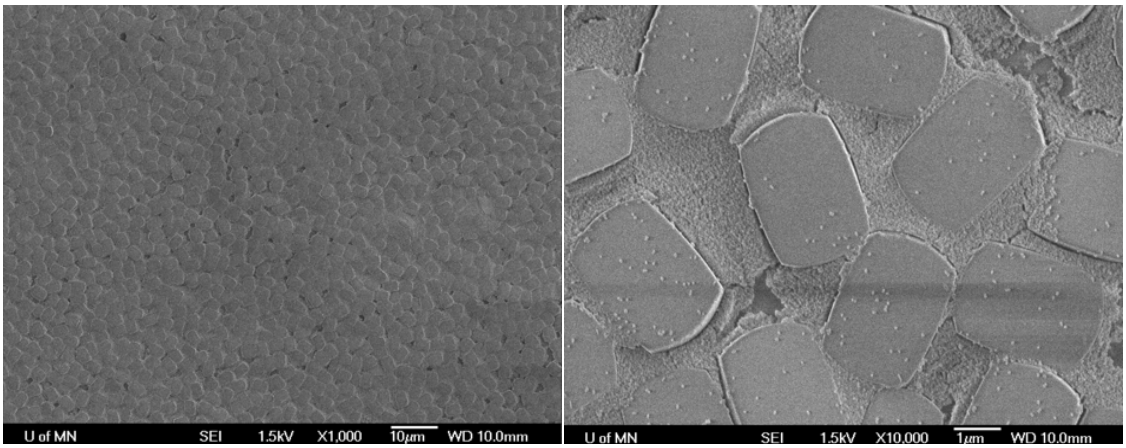

Figure 3.5: SEM image of the prepared seeded support.

When using dc5 nanosheets as seeds, seeds were deposited on the alumina supports by a vacuum-assisted filtration method [51,55]. First, the nanosheet cake obtained after washing was dispersed in 40 mL DI water. The suspension was sonicated for 2 min to fully disperse the nanosheets. Alumina supports were assembled in a home-made coating cell. The cell was connected to a vacuum pump. 1 mL of nanosheet suspension was added to the cell and the backside of the cell was maintained at ~ -10 psi. Nanosheets would slowly deposit on the support surface under the pressure difference. The filtration was typically finished

within 2 h and kept under vacuum overnight for complete drying. After coating, The MFI nanosheets were fixed on supports by calcination at 400 °C for 6 h at a heating and cooling rate of 1 °C /min under 100 mL/min of air. This filtration process was repeated 3-4 times to ensure full coverage. The typical morphology of coated support is shown in ***Figure 3.6***.

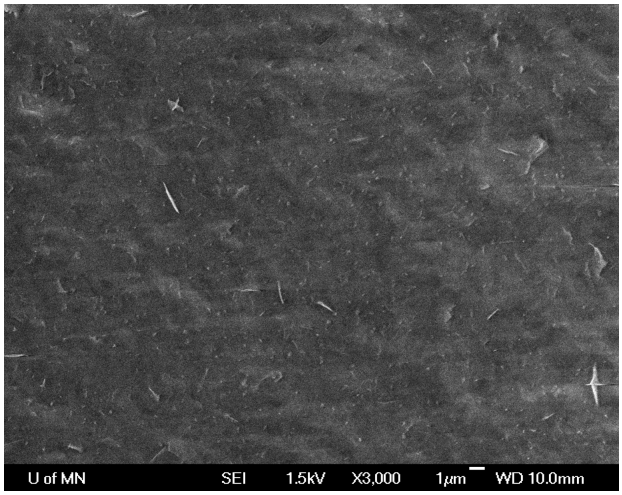

Figure 3.6: SEM image of the nanosheet coated alumina support.

3.2.6. Secondary growth of the seed coating

The seeded supports were made intergrown by using TEAOH based silica sol. A sol composition with 0.198 TEAOH:0.002 TPAOH:1 TEOS:100 H_2O was found to be a suitable recipe to accomplish homoepitaxial secondary growth to ensure *b*-orientation and intergrowth. The silica sol was prepared by adding 1.23 g TEAOH (35% in water), 0.03 g 1M TPAOH, 3.07 g TEOS and 25.68 g DI water sequentially. The solution was hydrolyzed under stirring for 24 hours. After hydrolysis, the solution was filtered through a 2 μm syringe filter to remove any aggregates. The seeded support was mounted on a home-made Teflon holder vertically and the holder, together with the support, was

inserted in a Teflon liner. Finally, ~30 mL of the synthesis gel was added to the Teflon liner and the liner was autoclaved at a desired temperature for a desired duration of time. After secondary growth, the membrane was removed from the autoclave, washed with DI water and dried at 70 °C for 2 h.

3.3. Results and discussion

Initial experiments were performed using coffin-shaped MFI crystals as seeds in order to find a suitable recipe for secondary growth. Using the same gel-less growth conditions (series #1 in ***Table 3.1***) as silica-supported membranes resulted in seeds and silica source dissolution, as shown in ***Figure 3.7 (left)***. Then, a TEAOH sol with composition 0.2 TEAOH: 1 TEOS: 100 H_2O (series #2 in ***Table 3.1***) was tried. The seeded supports had essentially no intergrowth, as shown in ***Figure 3.7 (right)***. It was reported in the literature that adding a small amount of TPAOH would facilitate the secondary growth [72]. Homoepitaxial growth of MFI nanosheets on silicon wafers using a sol composition of 0.198 TEAOH:0.002 TPAOH:1 TEOS:100 H_2O was successful [72, 73]. In our experiment, the sol composition was adapted (series #3 in ***Table 3.1***), and as a comparison, a sol composition of 0.190 TEAOH:0.010 TPAOH:1 TEOS:100 H_2O was also tried (series #4 in ***Table 3.1***). In the case of TEAOH+1%TPAOH, when growing at 120 °C for 3 days, we can clearly see the membrane was intergrown without twinning (***Figure 3.8***). For the TEAOH+5%TPAOH case, some twin crystals start to form on the surface (***Figure 3.9***). Small pinhole defects could be observed from the SEM images in these 2 cases, indicating

insufficient growth. When growing for a longer time (series #5 in ***Table 3.1***), membranes became well intergrown (***Figure 3.10***). The high quality of the membrane was also indicated by the very low N_2 permeance before calcination. Sufficient intergrowth can also be accomplished by growing at higher temperatures (series #6, #7 and #8 in ***Table 3.1***). Growing at 160 °C for 3 days resulted in membranes (***Figure 3.11***) that had a very low N_2 permeance before calcination, which indicated essentially no pinhole defects.

Table 3.1. Experiments on secondary growth of seeded supports using coffin-shaped MFI crystals at different secondary conditions

#	Structure directing agent	Growth time	Growth temperature	Resulting morphology	N_2 permeance before calcination [mol/(m^2-s-Pa)]
1	TPAOH gelless growth	1 day	180 ℃	Seeds and silica source dissolution	N/A
2	TEAOH sol growth	3 days	120 ℃	No intergrowth	N/A
3	TEAOH+1%TPAOH	3 days	120 ℃	intergrowth	5.1×10^{-7}
4	TEAOH+5%TPAOH	3 days	120 ℃	Intergrowth but too much twin growth	1.7×10^{-7}
5	TEAOH+1%TPAOH	6 days	120 ℃	Well intergrown	1.1×10^{-10}
6	TEAOH+1%TPAOH	3 days	140 ℃	Intergrowth but not defect free	4.5×10^{-8}
7	TEAOH+1%TPAOH	3 days	160 ℃	Well intergrown	5.0×10^{-11}
8	TEAOH+1%TPAOH	2 days	160 ℃	Intergrowth but not defect free	6.0×10^{-8}

TPAOH sol : 0.025M in water; Molar composition of TEAOH-based sol: 0.2 TEAOH: 1 TEOS: 100 H_2O; Molar composition of TEAOH+1%TPAOH-based sol: 0.198 TEAOH: 0.002 TPAOH: 1 TEOS: 100 H_2O; Molar composition of TEAOH+5%TPAOH-based sol: 0.190 TEAOH: 0.010 TPAOH: 1 TEOS: 100 H_2O.

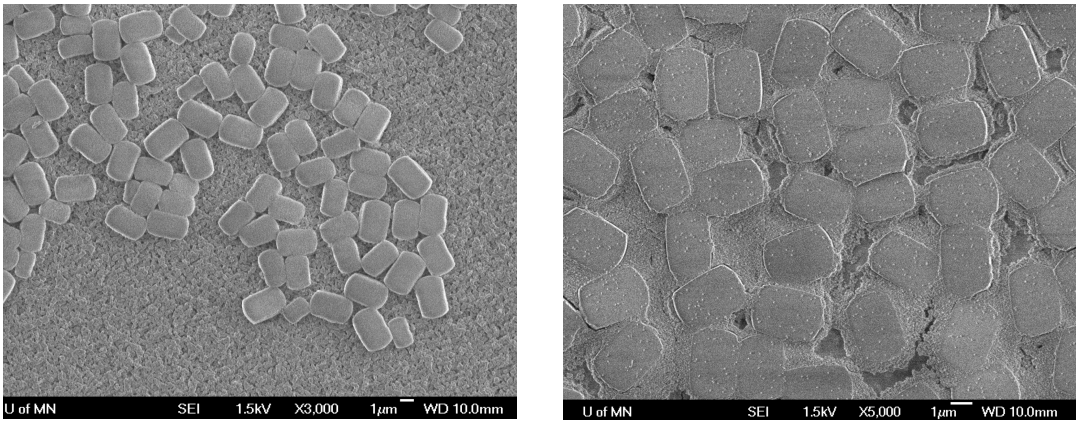

Figure 3.7: SEM images of seeded supports after secondary growth using TPAOH based gelless method (left) or TEAOH based silica sol (right). Using gelless secondary growth resulted in seeds and Stöber silica dissolution while using TEAOH based sol had essentially no intergrowth.

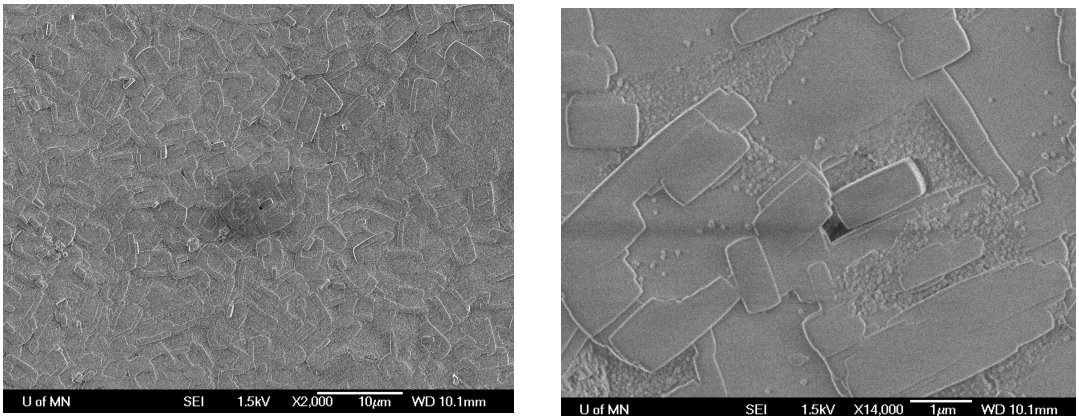

Figure 3.8: SEM images of seeded supports after secondary growth using TEAOH+1%TPAOH based silica sol at 120 °C for 3 days. Continuous membrane was formed with b-orientation. Pinhole defects were observed.

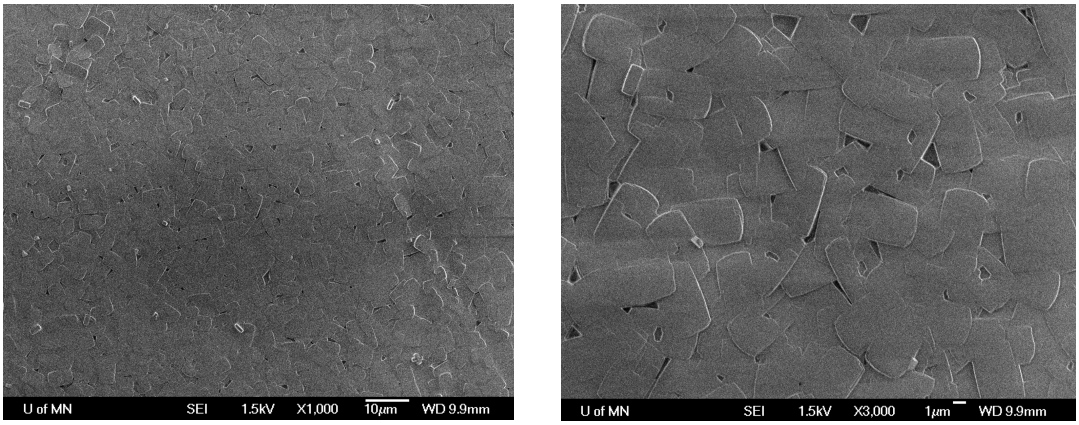

Figure 3.9: SEM images of seeded supports after secondary growth using TEAOH+5%TPAOH based silica sol at 120 °C for 3 days. The surface was less uniform compared to the case of using TEAOH+1%TPAOH based silica sol.

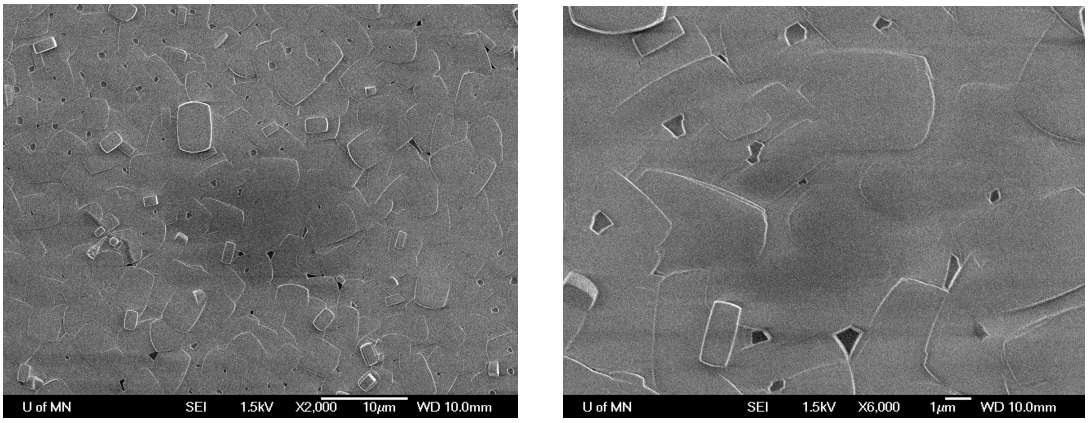

Figure 3.10: SEM images of seeded supports after secondary growth using TEAOH+1%TPAOH based silica sol at 120 °C for 6 days. The membrane was well intergrown with no defects observed.

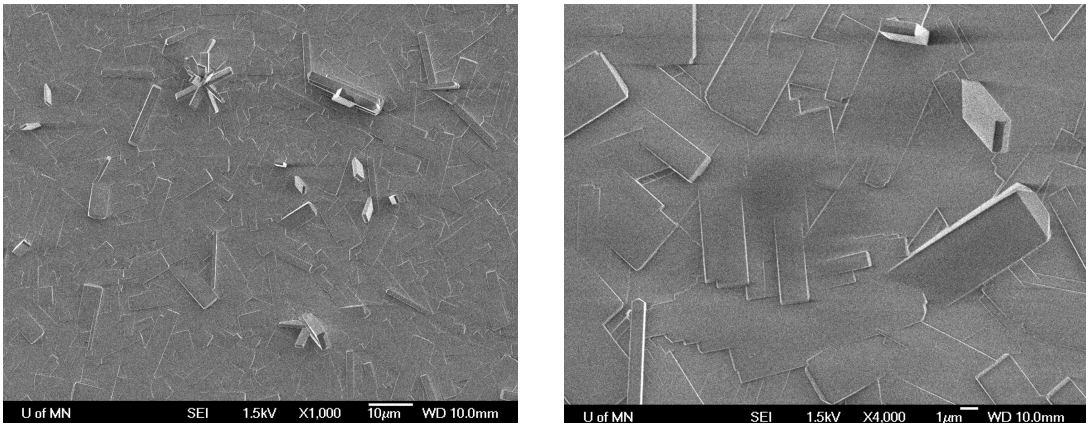

Figure 3.11: SEM images of seeded supports after secondary growth using TEAOH+1%TPAOH based silica sol at 160 °C for 3 days. The membrane was well intergrown with no defects observed. Some twinning was observed at this condition.

Activation is a concern for alumina supported MFI membranes because the alumina support has a different thermal expansion coefficient than the all silica MFI layer. When calcining at high temperature, the mismatch in thermal expansion would result in cracking. This was observed when calcining membranes at 450 °C. As is shown in ***Figure 3.12***, cracks were formed after calcination. This was detrimental to the membrane separation performance. We tried to calcine membranes at lower temperatures. ***Figure 3.13*** shows the plot of the membrane permeance and selectivity with regards to different calcining temperatures. With increasing calcining temperature, the membrane selectivity continues to decrease, indicating the formation of defects during calcination. On the other hand, the permeance increases with increasing calcining temperature. This is reasonable because more occlude SDAs would be removed at higher temperatures. In order to activate the membranes without inducing defects, other calcination method should be used, such as UV/ozone treatment [75-77] or rapid thermal processing [78-80] as reported in the literature.

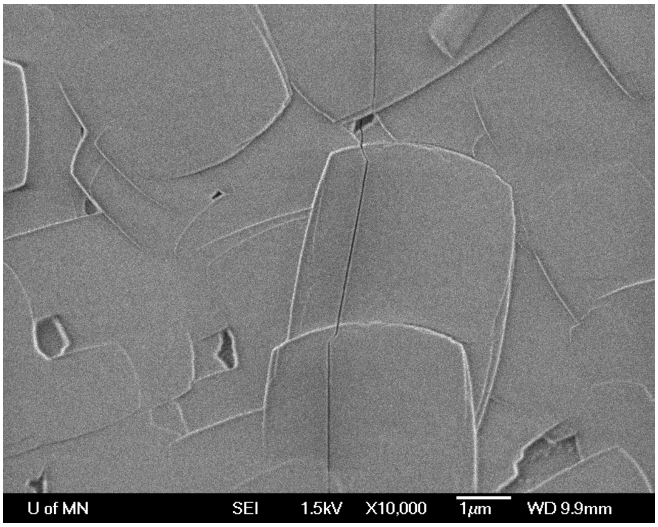

Figure 3.12: SEM image the α-alumina supported membrane (synthesized using TEAOH+1%TPAOH based silica sol at 120 °C for 6 days) after calcining at 450 °C. Cracks were induced after this calcination.

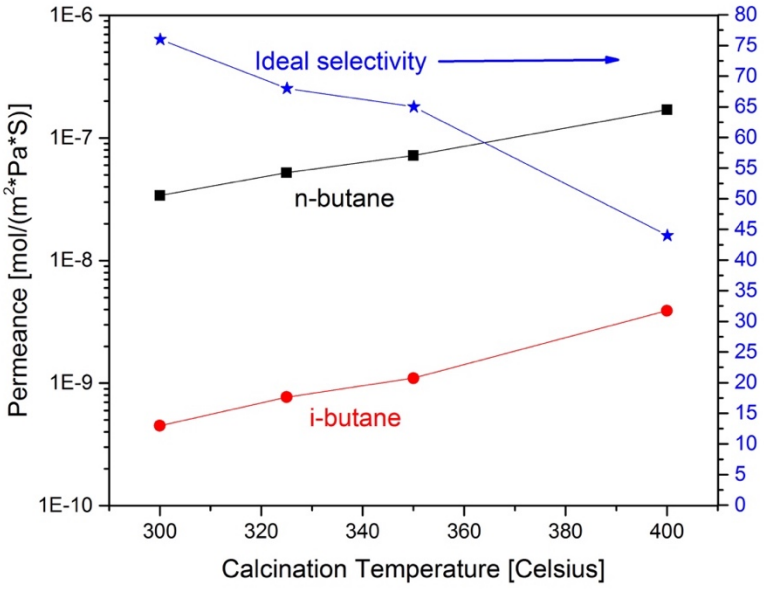

Figure 3.13: A plot of butane isomer membrane permeance and selectivity with regards to different calcining temperature. The membrane permeance increases with increasing calcining temperature while membrane selectivity decreases.

When preparing membranes using MFI nanosheets as seeds, the secondary growth conditions are different. We first tried to use the same recipe for secondary growth as the coffin-seed ones (TEAOH+1%TPAOH based silica sol at 160 °C for 3 days). It did not result in oriented membranes. Instead, the membrane was highly misoriented, as is shown in ***Figure 3.14***.

Table 3.2. Experiments on secondary growth of nanosheets seeded alumina supports using different recipes

#	Structure directing agent	Growth time	Growth temperature [℃]	Resulting morphology	N_2 permeance before calcination [mol/(m^2-s-Pa)]
M50	TEAOH+1%TPAOH	3 days	160	Highly misoriented	N/A
M53	TEAOH+1%TPAOH	3 days	120	More oriented	6.2×10^{-8}
M56	TEAOH+1%TPAOH	3 days	110	Oriented, with slightly misoriented grains	2.3×10^{-10}
M52	TEAOH+1%TPAOH	3 days	100	Oriented and well intergrown	3.0×10^{-10}
M54	TEAOH+1%TPAOH	2 days	100	Not enough intergrown	N/A
M59	TEAOH+1%TPAOH	2 days	90	No intergrowth	N/A

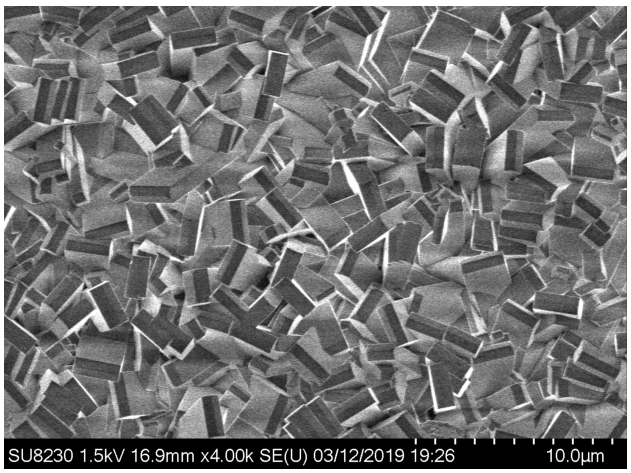

Figure 3.14: SEM image the MFI nanosheets seeded supported after secondary growth using TEAOH+1%TPAOH based silica sol at 160 °C for 3 days. The membrane was highly misoriented.

Trying to reduce the temperature for secondary growth resulted in more oriented membranes, which is shown in ***Figure 3.15***. A membrane grown at 100 ℃ for 3 days has an oriented and well intergrown surface morphology and a low N_2 permeance before calcination (***Table 3.2, M52***). Further reducing the growth temperature would result in growth inhibition, as illustrated by the SEM image of the membrane grown under 90 ℃ for 2 days.

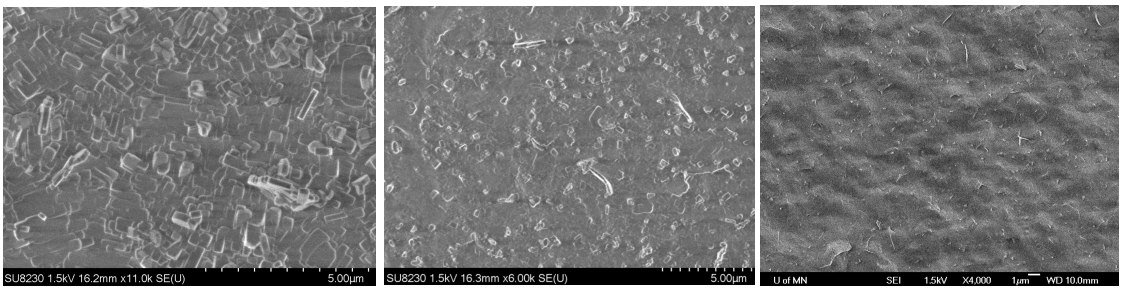

Figure 3.15: SEM image the MFI nanosheets seeded supported after secondary growth using TEAOH+1%TPAOH based silica sol at 110 °C for 3 days (left); 100 °C for 3 days (middle); and 90 °C for 2 days (right). A membrane grown at 100 °C for 3 days had a uniform and oriented surface morphology compared to other cases.

Membrane M52 and M56 was calcined at 350 ℃ for 10 hours with ramping and cooling rate of 1 ℃/min. Single gas butane isomer permeation tests were conducted. Membrane M52 showed an *n*-butane permeance of 1.5×10^{-7} mol/(m^2-s-Pa) and *n*-butane/*iso*-butane ideal selectivity of 15. Membrane M56 showed an *n*-butane permeance of 1.3×10^{-7} mol/(m^2-s-Pa) and *n*-butane/*iso*-butane ideal selectivity of 31. Further work could be done by using other detemplation methods such as plasma treatment, UV/zone treatment or rapid thermal processing method to reduce defect formation during membrane activation.

3.4. Conclusion

Methods for preparing oriented MFI membranes on alumina supports were found. The key is using TEAOH based silica sols for membrane secondary growth to inhibit twinning. Both conventional type MFI membranes and nanosheet type MFI membranes were successfully prepared using a sol composition of 0.198 TEAOH:0.002 TPAOH:1 TEOS:100 H_2O. The reaction temperature was different for the case of the conventional type and the nanosheet type. Both types of membranes exhibiting a low N_2 permeance before calcination, indicating that the membranes were defectless. High-temperature calcination would create defects due to the mismatch in the thermal expansion coefficient between the MFI layer and the underlying alumina support. Future work could be done by studying other detemplation methods such as plasma treatment, UV/ozone treatment or rapid thermal processing method.

Chapter 4. Xylene separation performance of MFI nanosheet membranes at industrially relevant conditions

4.1 Introduction

para-xylene is an important feedstock for the large scale synthesis of teraphthalic acid (TPA), which is a petrochemical intermediate component for the production of polyethylene terephthalate (PET) via the polycondensation of TPA with ethylene glycol. PET is an important downstream product which is used as polyester fiber, film, and resin for a variety of applications [44]. The demand for *para*-xylene is growing annually in the range of 6-8% per year [44]. Statistics showed that annual demand of *para*-xylene in the world was about 18 million tonnes in 2003 [45] and increased to more than 30 million tonnes in 2010 [44]. In industrial production, *para*-xylene is produced along with other isomers and is recovered using adsorption and/or crystallization processes. The current state-of-the-art commercial separation technology is an adsorptive process based on the simulated moving bed (SMB) technology. This process can produce 99.9 wt. % pure *para*-xylene, but still, it is a very energy-intensive process. Membrane technology, especially a suitable membrane reactor, if integrated with the *para*-xylene production, would largely increase *para*-xylene productivity and reduce process cost by eliminating this energy-intensive separation process. This concept is highly dependent on the success in fabricating high-performance membranes. MFI membranes have been extensively studied for this application. In early reports [81-83], membranes were prepared by in-situ crystallization with little control over membrane microstructure. Relatively thick

membranes were obtained with random crystal orientation. As a result, both membrane permeances and selectivities were quite low. Keizer et al. [84] reported binary *para*-xylene/*ortho*-xylene permeation at dilute feed conditions (0.31 kPa *p*-xylene/0.26 kPa *o*-xylene). At 200 °C, the *para*-xylene permeance was about 1×10^{-8} mol/(m^2-s-Pa) and *para*-xylene/*ortho*-xylene separation factor was about 30 for this kind of membranes.

A secondary growth method was introduced in the subsequent reports. c-oriented MFI membranes made by secondary growth method [85-87] were reported to have a *para*-xylene permeance of about $2\text{-}3\times10^{-8}$ mol/(m^2-s-Pa) at 100-150 °C under dilute feed conditions, but the *para*-xylene/*ortho*-xylene separation factor was quite low (<5). Membranes having preferred orientation in (101) direction [87] had higher performance. *para*-xylene permeances of $(2\text{-}5)\times10^{-8}$ mol/(m^2-s-Pa) and *para*-xylene/*ortho*-xylene separation factors of 60-300 were achieved with some post-modification by surfactant-templated silica sol. Later in 2003, a breakthrough was achieved by Lai et al. [25]. They reported that by using a trimer-TPAOH instead of monomer-TPAOH as a structure-directing agent, nearly defect free MFI membranes could be obtained with their b axis perpendicular to the support. A *para*-xylene permeance of $\sim10^{-7}$ mol/(m^2-s-Pa) and a *para*-xylene/*ortho*-xylene S.F. of 400-500 was achieved. The achievements came from the control of membrane defects and membrane orientation. A new secondary growth technique was reported by Pham et al. [47]. They fabricated MFI membranes on Stöber silica supports with a gel-free method. *b*-oriented membranes were also obtained, with a *para*-xylene permeance of 1.2×10^{-7} mol/(m^2-s-Pa) and a S.F. of ca. 1000. The developments of MFI nanosheet type membranes in our group [55,56] have achieved another breakthrough in terms of both the

membrane permeance (up to 5×10^{-7} mol/(m^2-s-Pa)) and selectivity (up to 10,000) under dilute feed conditions. Although this was a very exciting achievement, the ultimate success of commercialization is still elusive. A major problem presented is that all the above permeation tests were done at low temperatures (<200 °C) and very low xylene pressures (~500 Pa partial pressure or less). A solid demonstration of the separation performance at industrial conditions (high temperature and pressure) is needed. In the literature, only two reports have demonstrated MFI membrane separation performance at high temperatures and pressures. Hedlund et al. [88] reported a *para*-xylene flux of about 2.5×10^{-3} mol/(m^2-s) *and para*-xylene/*meta*-xylene mixture separation factor of 13 at 400 °C using a hydrocarbon feed diluted with hydrogen (*para*-xylene, *meta*-xylene, ethyl-benzene, 1,3,5-trimethyl-benzene and hydrogen partial pressures of 25, 65, 5, 5 and 100 kPa, respectively). At even higher feed pressure (*para*-xylene, *meta*-xylene, ethyl-benzene, 1,3,5-trimethyl-benzene and hydrogen partial pressures of 125, 325, 25, 25 and 1300 kPa, respectively), *para*-xylene flux was about 3.4×10^{-3} mol/(m^2-s) *and para*-xylene/*meta*-xylene mixture separation factor of 5 at 400 °C. In comparison, our group [89] reported a *para*-xylene flux of 0.47×10^{-3} mol/(m^2-s) and *para*-xylene/*ortho*-xylene mixture separation factor of 60 at 300 °C under feed condition of 47.5 kPa *para*-xylene, 47.5 kPa *ortho*-xylene and 5 kPa 1,3,5-trimethyl-benzene. At higher pressures (95 kPa *para*-xylene, 95 kPa *ortho*-xylene and 10 kPa 1,3,5-trimethyl-benzene), the separation factor dropped to 19.3 and *para*-xylene flux dropped to 0.24×10^{-3} mol/(m^2-s). The separation factors in Hedlund's report are not satisfactory while the fluxes in our previous report are not high enough. In this chapter, the ultra-selective MFI membranes made from dc-5 nanosheets

(as compared to exfoliated nanosheets in ref. [89]) as seeds were prepared and more tests were performed at industrially relevant conditions. The results showed record-high fluxes and separation factors for xylene isomer separation. This demonstrated the high potential of high-performance MFI membranes for xylene isomer separation in industrial practice.

4.2. Experimental section

4.2.1. Direct Synthesis of MFI nanosheets

The MFI nanosheets were prepared by a synthesis procedure reported previously [55]. The procedures were briefly described in section 3.2.4.

4.2.2. Preparation of porous sintered silica fiber (SSF) supports

Sintered silica fiber (SSF) supports were prepared as substrates for the fabrication of all-silica MFI membranes by following the same procedures reported in the literature [55,56]. The supports were specially engineered so they are smooth enough to make defect-free membranes. It was made by first crushing and then pressing commercially available silica fibers, referred to as quartz fibers, followed by sintering and polishing. First, commercially available silica fibers were crushed and pressed in a die to make silica fiber disks. The disks were sintered and polished with grinding papers to make it flat. To further smoothen the support surface, 500 nm Stöber silica spheres were rubbed manually on the top surface followed by sintering. The rubbing and sintering process was repeated several times until the surface was fully covered by the Stöber silica spheres. Finally, a top 50 nm Stöber silica layer was rubbed on the surface and fixed on the surface by sintering. It served as the silica source to form continuous and inter-grown films by the gel-free

secondary growth method. ***Figure 4.1 left*** shows the SEM image of polished sintered silica fiber support. ***Figure 4.2*** shows the SEM image of 500 nm Stöber silica modified surface of the support. ***Figure 4.2*** shows the support surface after the 50 nm Stöber silica modification.

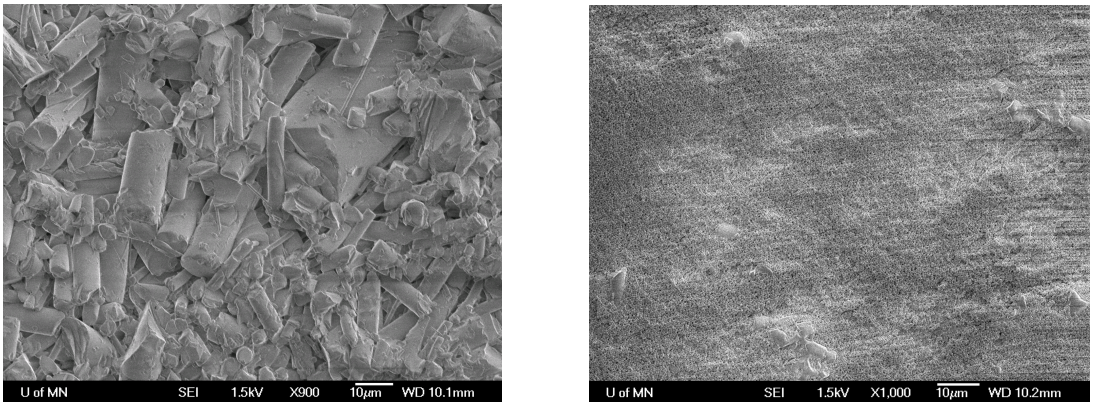

Figure 4.1: SEM image the polished sintered silica fiber support showing the big quartz fibers sintered together (left) and SEM image of 500 nm Stöber silica modified surface after 4 times of manual rubbing, showing smoother surface but quartz fibers were not fully covered (right).

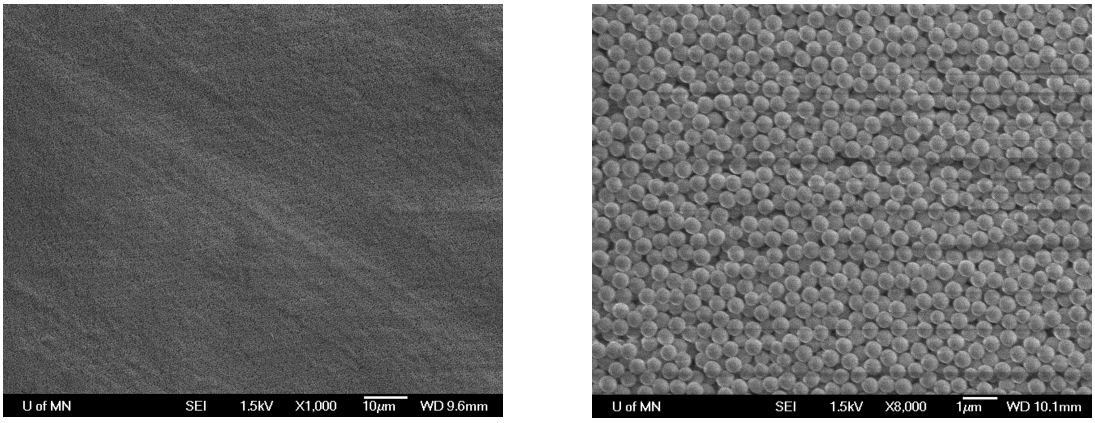

Figure 4.2: SEM images of 500 nm Stöber silica modified surface after 6-8 times of manual rubbing, showing smoother surface fully covered by the Stöber silica particles.

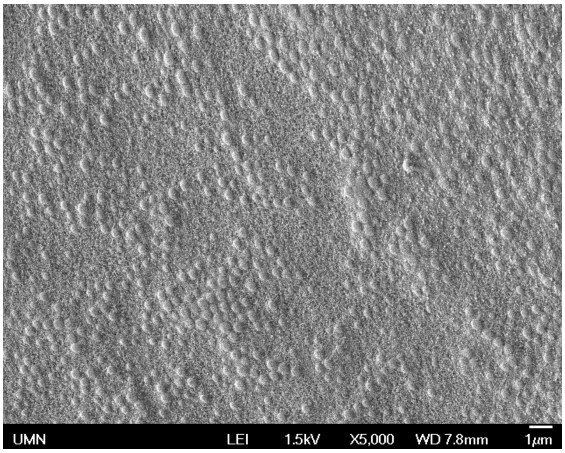

Figure 4.3: SEM images of the thin layer of 50 nm Stöber silica rubbed manually on the modified sintered silica support.

4.2.3. Fabrication of MFI membranes

Membrane fabrication was performed following the same procedures as reported earlier [56]. Briefly, the synthesized MFI nanosheets were first purified using centrifugation and dispersed in DI water containing 5 vol% ethanol. To form a thin layer of nanosheet coating on the porous SSF support as seeds, a floating particle method was used. The support was placed in a home-made Teflon™ trough. After filling the trough with DI water, the suspension was carefully transferred on the air-water interface using a micropipette, forming a uniform single layer of MFI nanosheets. When lowering the water level below the support, the MFI nanosheets layer was deposited on the support surface, obtaining a uniform layer of nanosheet coating. The coating was immobilized on the support surface by a heat treatment at 400 °C. These coating processes were repeated twice to improve the surface coverage of the nanosheets. Finally, the seeded support was treated by the gel-free secondary growth at 180 °C for 4 days using an impregnating solution with composition 0.025M TPAOH to achieve a well-intergrown and defect-free membrane.

4.3 Results and discussion

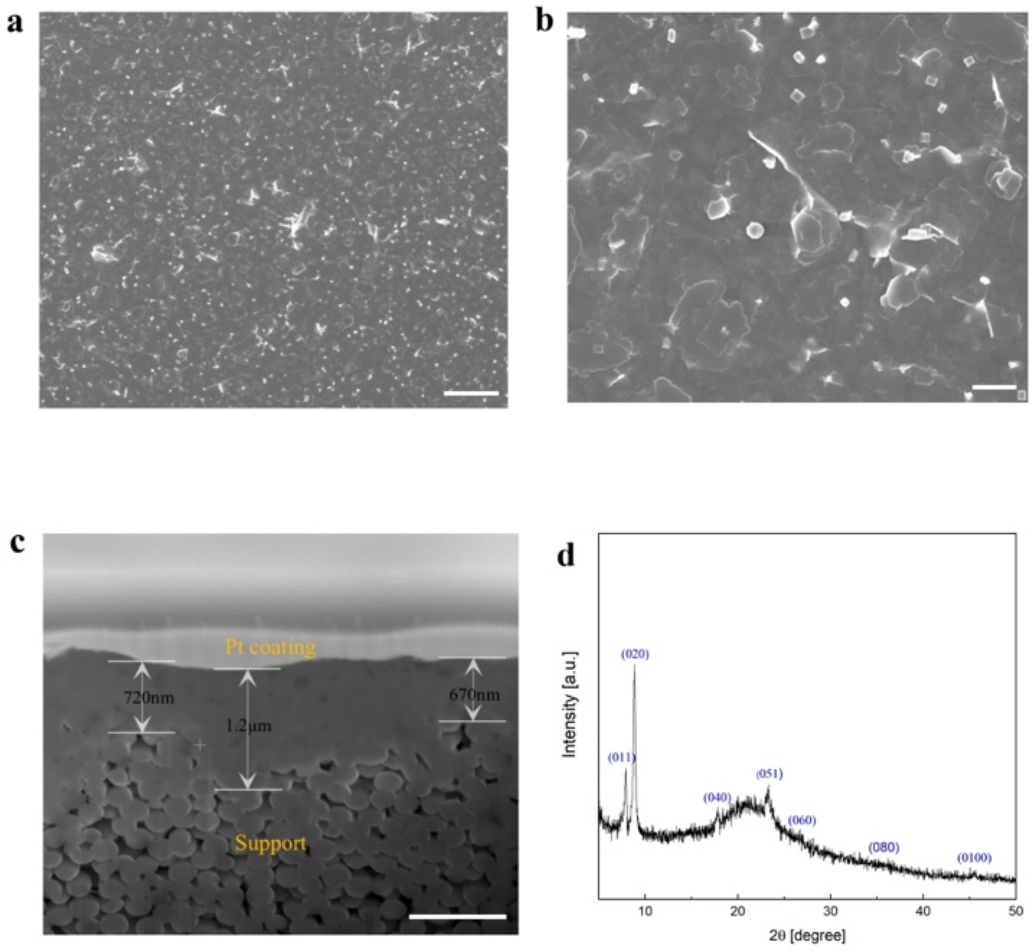

Figure 4.4. a),b) surface morphology and c) cross-secional FIB-SEM image of the MFI membrane fabricated from MFI nanosheet seed layer; d) Out-of-plane XRD pattern of the fabricated MFI membrane which is supported on amorphous silica support, indicating the preservation of b-out-of-plane orientation after secondary growth. Scale bars are a) 5μm, b) 1μm, and c) 1μm.

Figure 4.4a,b shows the typical SEM images of the obtained MFI membrane. The membrane was flat and well inter-grown. The brighter parts on the surface were thicker MFI crystals which were attributed to the secondary growth of the seed crystals presented in the center of the nanosheets [55]. The membrane was considered to be defect-free as

evidenced by the very low N_2 permeance (c.a. 1.0×10^{-11} mol/(m^2-s-Pa)) before the removal of SDA. ***Figure 4.4c*** shows the FIB-SEM image of the membrane cross-section. The membrane thickness was between 0.5-1.5 μm. The thickness variation originated from the unevenness of the underlying silica support and the non-uniform distribution of the 50 nm sacrificial silica source used to grow the MFI nanosheet coating into the defect-free membrane. XRD pattern confirmed (***Figure 4.4d***) that the membrane was zeolite MFI and it was *b*-oriented, with the most intense peak appeared at 8.8 of 2theta (which is attributed to the (020) reflection of the MFI crystals).

Permeation tests were first carried out using dilute feed conditions as described in [51,55,56]. These tests were performed in the Wicke–Kallenbach mode. A membrane was sealed in a home-made permeation cell using high temperature resistant o-rings (G75H Perlast perfluoroelastomer *o*-rings). The permeation cell was connected to the system. The feed helium gas (70 mL/min) flowed through a 50/50 *para*-xylene/*ortho*-xylene mixture using a bubbler. About 0.5 kPa *para*-xylene and 0.5 kPa o-xylene were carried out by the helium gas. The feed mixture gas was introduced into the feed side of the home-made module. The permeate side of the module was purged with helium as sweep gas (30 mL/min). Both the feed side and permeate side were kept at atmospheric pressure. After maintaining the membrane for ~20 hours to ensure the permeation reach a steady state, the concentrations of feed and permeate streams were analyzed by GC with a flame ionization detector (FID), equipped with a capillary column (DB-WAXetr, Chrometech). At each permeation condition, the analysis was repeated at least three times. The membrane separation performance is typically assessed with the membrane permeance

and membrane separation factor. The permeance is the flux normalized by the partial pressure gradient across the membrane. The separation factor is defined as the composition ratio of components A and B in the permeate mixture relative to the composition ratio of A and B in the retentate mixture, i.e., $SF(AB) = [X_A/ X_B]_{permeate} / [X_A/ X_B]_{retentate}$.

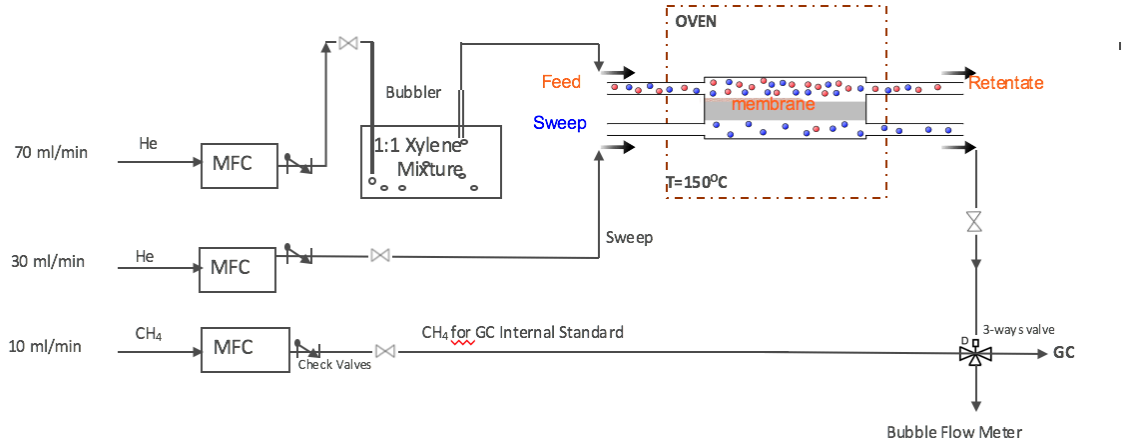

Figure 4.5: Schematic of the xylene permeation system operated at dilute feed conditions in the Wicke–Kallenbach mode.

Table 4.1: Membrane permeation results using the Wicke–Kallenbach mode under dilute feed conditions

Membrane Code	Temperature [°C]	feed ratio [p-x:o-x]	permeance [mol·m^{-2}·s^{-1}·Pa^{-1}]	Flux [mol·m^{-2}·s^{-1}]	S.F
D18	150	1:1	1.67×10^{-7}	0.0000709	184
D31	150	1:1	2.07×10^{-7}	0.0000869	112
D35	150	1:1	1.90×10^{-7}	0.0000811	640

High-pressure xylene permeation tests were performed at ExxonMobil. The system was described in ref. [90]. ***Figure 4.6***. shows the configuration of the permeation system taken

from ref. [90]. This setup can either run in dilute feed conditions through the 5-3-6 pathway, or high-pressure feed conditions through the 1-2-4-6 pathway. For high-pressure measurements, a syringe pump (ISCO, model number 500D) (2) was used to inject a liquid xylene mixture (1) (usually 50% *para*-xylene, 50% *ortho*-xylene) into a preheater (6). The preheater would vaporize the feed mixture and the superheated vapor could be sent to the membrane cell. The feed pressure was varied and controlled through the syringe pump. Hydrogen could be used as a co-feed to the membrane. At the permeate side, either non-sweep or sweep conditions could be used. The permeate pressure could be either atmospheric or vacuum. The retentate and permeate compositions were analyzed by an online GC system. The flux was determined by weighing the permeate, which was collected in a series of condensers, over a known period of time.

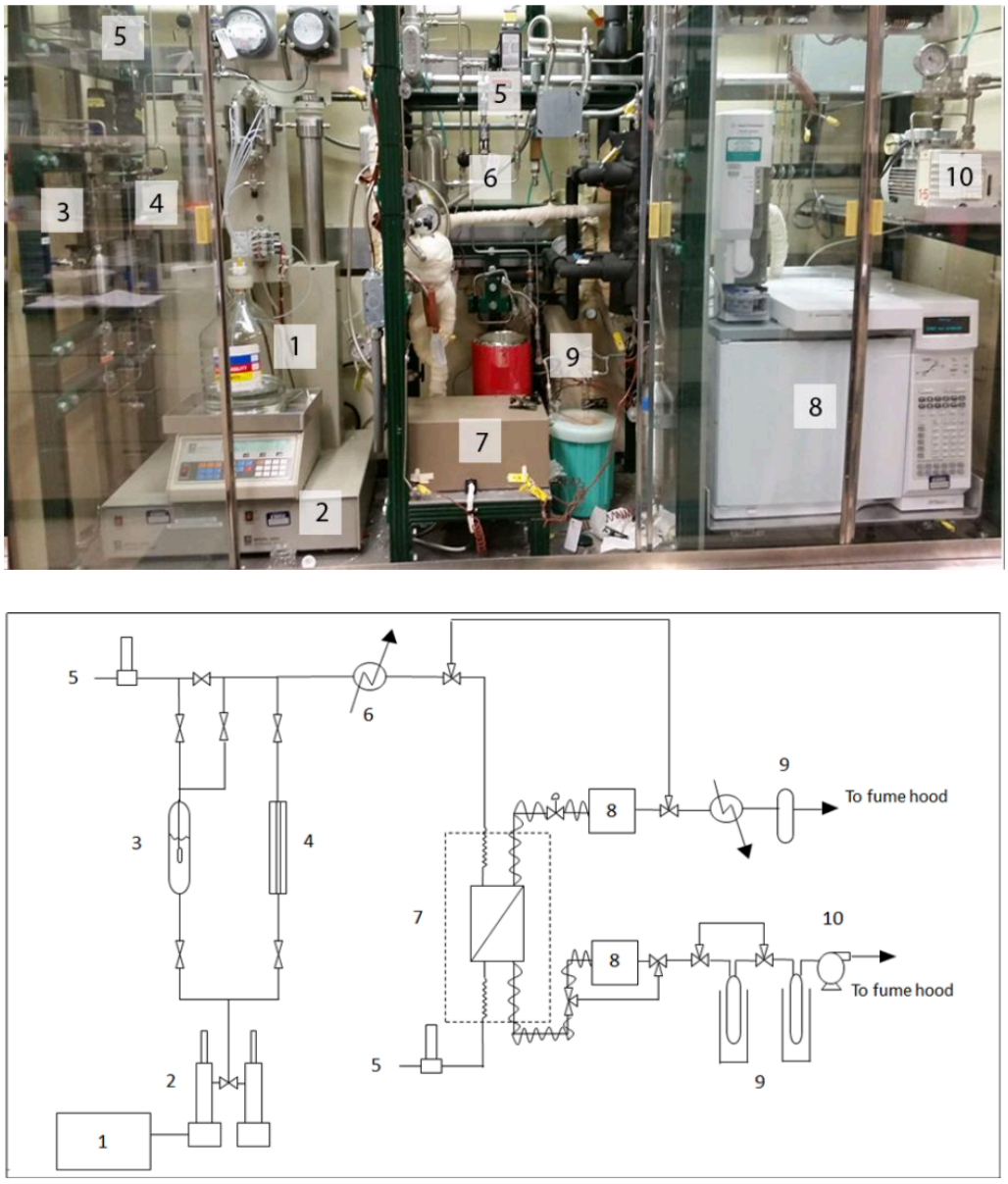

Figure 4.6: High temperature, high pressure xylene testing system at ExxonMobil. Picture of system (top) and schematic (bottom). Legend: 1 – Liquid xylene mixture, 2 – ISCO pumps for feed delivery, 3 – Sparger for dilute vapor delivery, 4 – Sight- glass 5 – MFCs and gas handling for dilute vapor, 6 – Feed preheat for saturated/superheated vapor testing, 7 – Heated membrane oven, 8 – Automated online GC analysis of feed, permeate and retentate, 9 – Liquid product collection (retentate and permeate), 10 – Vacuum pump. The schematic of this system is taken from [90].

Table 4.2: Membrane permeation results tested at ExxonMobil at high pressures and high temperature (300 °C)

Membrane Code	Temp. (°C)	Feed pressure (bar)	Feed p-x partial pressure (bar)	Feed H_2 partial pressure (bar)	H_2 sweep flow rate (sccm)	Permeate pressure (bar)	Flux [mol/(m^2-s)]	SF (p-x/ o-x)
D31	300	1	0.24	0.5	0	0.11	1.99E-03	10
D31	300	3	0.43	2.1	0	0.11	2.05E-03	75
D35	300	2	0.48	1	36	0.21	8.68E-04	51
D35	300	3	0.71	1.5	50	0.23	2.54E-03	57
D35	300	4	0.95	2	50	0.23	3.80E-03	53

Table 4.2 listed the permeation results at high pressures and high temperature. These results showed record-high fluxes and separation factors for xylene isomer separation. The results also provide us with industrially relevant data for process design and economic analysis. With these high-performance data, we are optimistic about the final industrial application of MFI membranes for xylene isomer separation.

4.4. Conclusion

In this chapter, major progress in xylene isomer separation using MFI membranes was reviewed. The lack of industrially relevant data at high feed pressure and temperature makes the ultimate success of commercialization elusive. We fabricated high-performance MFI membranes, and measurements at high pressures were performed. Results showed record-high fluxes and separation factors for xylene isomer separation at industrial conditions. This demonstrated the high potential of high-performance MFI membranes for xylene isomer separation in industrial practice.

Chapter 5. High-performance MFI membranes for H_2/Hydrocarbons separation

*Part of this work was submitted for publication.

5.1. Introduction

Refinery waste gases typically contain a low concentration of H_2 (usually 20-40 mole%) along with various concentrations of light hydrocarbons (C_1-C_4, saturated and unsaturated)[91]. These gases are generally burned to make use of their heating values. A lot of hidden values are wasted. It would be of great value if the H_2 and hydrocarbons are separated and recycled in an economical and efficient way. Pressure swing adsorption and polymeric membrane separation are two commercial methods used to separate H_2 from hydrocarbons for H_2 recovery. However, pressure swing adsorption (PSA) would require a higher H_2 concentration to be economical. Typical feed gas to the pressure swing adsorption (PSA) system contains 60–90 mole% hydrogen[92]. Recovery of the H_2 using polymeric membranes is not practical either. The gas stream has a relatively low to moderate pressure, therefore using H_2 permeable polymeric membranes to recover the H_2 would require the gas stream to be compressed first, which adds additional processing cost, making it non-profitable. In the 1990s, Air Products developed a new type of membrane[93-95] (SSF (selective surface flow) membrane) which can selectively absorb larger and more polar hydrocarbon molecules. The adsorbed hydrocarbons can hinder or completely block the flow of non-adsorbed components. This membrane was proven to be efficient in recovering H_2 from the refinery waste gases. It has been scaled-up and tested in the modular form under industrial conditions, showing good performance and long term

(continuously operated for 6 months) stability in real-world application[96]. Although its potential has been demonstrated, the commercialization has not been realized, probably due to its low hydrocarbon flux since the selective carbon layer remains thick (2-3 μm average). Zeolite membranes also have been reported to have a similar adsorption selectivity for hydrocarbons over H_2. Zeolite membranes have better thermal and chemical stability and are much easier to regenerate if fouled. In 1999, L. J. P. van denBroeke[57] reported permeation of binary gaseous mixtures through a silicalite-1 membrane. It was shown that at room temperature, the *n*-butane flux was $\sim 5 \times 10^{-3}$ mol/(m^2-s) with a separation factor ~40. Later in 2000, J. Dong et al.[58] showed that all-silica MFI membranes can separate multicomponent hydrogen/hydrocarbon mixtures in wide temperature and feed pressure ranges. At room temperature and atmospheric pressure on both feed and permeate sides, the total hydrocarbon permeation rate was measured to be $2\text{-}4 \times 10^{-4}$ mol/(m^2-s). Similar adsorptive selectivity has been shown for olefin/nitrogen separation[97] and the removal of C_{3+} from methane[98-101]. In Ref.[97], ultra-thin MFI zeolite membranes (0.5 μm) were used to separate propylene or ethylene from binary olefin/nitrogen mixtures at different temperatures. At room temperature, the permeance of propylene was 22×10^{-7} mol/(m^2-s-Pa) and the separation factor was 43. For the case of ethylene/nitrogen mixture, the maximum separation factor was 6 at 277 K with an ethylene permeance of 57×10^{-7} mol/(m^2-s-Pa). Arruebo, et al.[98] showed that silicalite-1 membranes can effectively separate hydrocarbons from methane, the highest *n*-butane/methane selectivity of 31.5 was achieved at 25 °C. However, the permeances for hydrocarbons were lower than 1.0×10^{-7} mol/(m^2-s-Pa). Lu, et al.[100] evaluated their ultra-

thin zeolite membranes (thickness ~400 nm) for the removal of propane and butane from natural gas. At room temperature, the *n*-butane/methane separation selectivity was 25, with an *n*-butane permeance of 31×10^{-7} mol/(m^2-s-Pa). The separation selectivities for propane/methane binary mixture was lower (~9.5) with a propane permeance as high as 54×10^{-7} mol/(m^2-s-Pa) at room temperature.

To improve the separation performance of MFI membranes, preferential secondary growth methods were developed to fabricate *b*-oriented membranes[25,47], in order to favor the transport of gases in the straight channels in the MFI framework in the b direction instead of the zig-zag channels in a or c directions. The development of ultra-thin MFI nanosheets, either by top-down exfoliation[49] or bottom-up direct synthesis[55], makes ultra-thin MFI membranes possible[51,55]. Min, et al.[101] used the directly synthesized MFI nanosheets as seeds for membrane fabrication on alumina hollow fibers. The obtained membranes were oriented and had a thickness of less than 800 nm. In *n*-butane/methane or propane/methane binary permeation measurements, the membranes exhibited exceptionally high permeances (2,000–3,000 GPU with separation factors of 35–300 for *n*-butane/methane separation and 5,000–10,000 GPU with separation factors of 10–45 for propane/methane separation). More recently, by employing the directly synthesized MFI nanosheet and a floating-particle coating method to form a dense and uniform nanosheet seeding layer on supports, ultra-selective MFI membranes were achieved after secondary growth with unprecedented permeances and separation factors for *para*-xylene/*ortho*-xylene separation[56]. The thinner and easier diffusion path in these membranes should also allow a much higher permeation rate for the H_2/hydrocarbons separation. Herein, we

evaluated the ultra-thin nanosheet based MFI membranes for the separation of H_2 and hydrocarbons mixtures. The separations were performed using different H_2 and hydrocarbon mixtures and tested at different feed pressures to evaluate the effect of pressure on the membrane separation performance.

Table 5.1: Literature reports of MFI membranes for adsorptive separation

Ref.	Membrane Thickness	Mixture	Sweep	Pressure	T.	Hydrocarbon flux/permeance	S.F.
[57] Moulijn, 1999	50-60 μm	50*n*-C_4:50H_2	Yes	1 bar	300k	5×10^{-3} mol/(m^2·s)	40
[58] Lin, 2000	3-5 μm	84.48H_2:7.59CH_4 :2.51C_2H_6:2.52C_2H_4 :0.75C_3H_8:1.45C_3H_6 :0.4*n*-C_4:0.3i-C_4	5.6-12.1 mL/min	1 bar	RT	$2\text{-}4\times10^{-4}$ mol/(m^2·s)	H_2 not detected
[97] Hedlund, 2017	0.5 μm	20C_3H_6:80N_2	No	10 bar	RT	22×10^{-7} mol/(m^2·s·Pa)	43
[97] Hedlund, 2017	0.5 μm	20C_2H_4:80N_2	No	10 bar	277k	57×10^{-7} mol/(m^2·s·Pa)	6
[99]Dragomirova, *et al, 2014*	40 μm	92CH_4:8*n*-C_4	vacuum	1 bar	298K	1.36×10^{-5} mol/(m^2·s)	39
[100] Hedlund, 2018	0.4 μm	10*n*-C4:90CH4	No	9 bar	RT	31×10^{-7} mol/(m^2·s·Pa)	25
[100] Hedlund, 2018	0.4 μm	10C3H8:90CH4	No	9 bar	297K	54×10^{-7} mol/(m^2·s·Pa)	9.5
[101]Nair, 2019	<0.8 μm	17.5*n*-C_4:82.5CH_4	Ar	1 bar	298K	8.4×10^{-7} mol/(m^2·s·Pa)	300
[101] Nair, 2019	<0.8 μm	16.5C_3H_8:83.5CH_4	Ar	1 bar	298K	16.7×10^{-7} mol/(m^2·s·Pa)	45
[101] Nair, 2019	0.3-1.2μm	76CH_4:8C_2H_6:8C_3H_8 :8 *n*-butane	Ar	9 bar	RT	*n*-butane: 460 GPU propane: 220 GPU ethane: 31 GPU	*n*-C_4/CH_4: 97 C_3H_8/CH_4: 48 C_2H_6/CH_4: 7

5.2. Experimental section

5.2.1. Direct Synthesis of MFI nanosheets and Membrane Fabrication

The MFI nanosheets were prepared by a synthesis procedure reported previously [55]. The procedures were briefly described in section 3.2.4. The membrane fabrication procedures were reported in [56] and were described in section 4.2.2 and 4.2.3.

5.2.2. Permeation test

Membranes were tested under different feed pressures. The atmospheric feed pressure tests were performed in the Wicke–Kallenbach mode. The feed gas mixture flowed into the feed side of the home-made module (70 mL/min). The permeate side of the module was purged with Ar as sweep gas (30 mL/min). Both the feed side and permeate side were kept at atmospheric pressure. For membrane tests at higher feed pressures, no sweep was used. The feed pressure was regulated by a pressure regulator and measured by a pressure gauge. The permeate side was kept at atmospheric pressure. After maintaining the membrane for ~20 hours at each condition to ensure the permeation reach a steady state, the concentrations of feed and permeate streams were analyzed by GC with a thermal

conductivity detector (GC/TCD), equipped with a packed-bed column (Chromosorb PAW, Agilent). Ar was used as the carrier gas for the GC. At each permeation condition, the analysis was repeated at least three times.

5.3. Results and discussion

Typical membrane structural properties were described in section 3.3. The fabricated MFI membrane was used to evaluate the separation of H_2 and hydrocarbons mixtures. ***Table 5.1*** listed the test conditions and experimental results.

Table 5.1: Binary permeation measurement conditions and membrane performance

ID	Temp	Feed conditions			Permeate conditions		Hydrocarbon permeance (mol/(m^2-s-Pa))	Hydrocarbon flux (mol/(m^2-s))	Hydrocarbon/H_2 S.F.
		Feed Pressure	Feed composition	Feed flow rate	Permeate pressure	Sweep or permeate flow rate			
1	RT	1 bar	30%H_2+70% *n*-butane	50 mL/min	1 bar (Ar sweep)	30 mL/min	2.17×10^{-7}	0.0135	59
2	RT	1 bar	30%H_2+70% propane	50 mL/min	1 bar (Ar sweep)	30 mL/min	2.20×10^{-7}	0.0129	39
3	RT	1 bar	30%H_2+70% ethane	50 mL/min	1 bar (Ar sweep)	30 mL/min	3.0×10^{-7}	0.0184	5.7
4	RT	6 bar	98%H_2+2% *n*-butane	100 mL/min	1 bar (no sweep)	2.9 mL/min	5.8×10^{-7}	9.2×10^{-4}	6.5
5	RT	8 bar	98%H_2+2% *n*-butane	200 mL/min	1 bar (no sweep)	3.1 mL/min	5.0×10^{-7}	1.1×10^{-3}	7.7
6	RT	10 bar	98%H_2+2% *n*-butane	200 mL/min	1 bar (no sweep)	3.2 mL/min	4.3×10^{-7}	1.4×10^{-3}	9.5
7	RT	2 bar	50%H_2+50% Propane	200 mL/min	1 bar (no sweep)	4.1 mL/min	5.3×10^{-7}	0.0103	31
8	RT	4 bar	50%H_2+50% Propane	200 mL/min	1 bar (no sweep)	20.5 mL/min	6.3×10^{-7}	0.0531	83
9	RT	6 bar	50%H_2+50% Propane	200 mL/min	1 bar (no sweep)	26.5 mL/min	5.9×10^{-7}	0.0688	81

Figure 5.1 shows the membrane separation performance of binary H_2 and various hydrocarbon (i.e. ethane, propane and *n*-butane) mixtures. The tests were done at room temperature and atmospheric pressure on both feed and permeate sides, and Ar was used

as the sweep gas in the permeate side. The results showed that the membrane can very effectively reject hydrogen in the presence of hydrocarbons. The membrane can selectively absorb hydrocarbon molecules and the adsorbed hydrocarbons can hinder the flow of the smaller H_2 molecules, making it hydrocarbon selective. The hydrocarbon permeances were very high, which is promising from an application standpoint. With decreasing hydrocarbon molecular weight, the permeance increases slightly. It also appears that *n*-butane can be adsorbed by the MFI membrane and saturate the membrane more easily than propane and ethane, since, in the presence of *n*-butane, the H_2 permeance is lower than the other 2 cases, resulting in a higher H_2/hydrocarbon separation factor (c.a. 59). When comparing the cases of H_2/propane and H_2/ethane, propane can be absorbed more easily than ethane, giving a moderate H_2/hydrocarbon separation factor (c.a.39). For smaller molecules like ethane, although they can be selectively absorbed by the membrane, it can only partially hinder the flow of H_2, resulting in a relatively low H_2/hydrocarbon separaion factor (c.a.6). This result agrees with the trend of light alkanes adsorption isotherms in silicalite-1 reported in the literature[102-104].

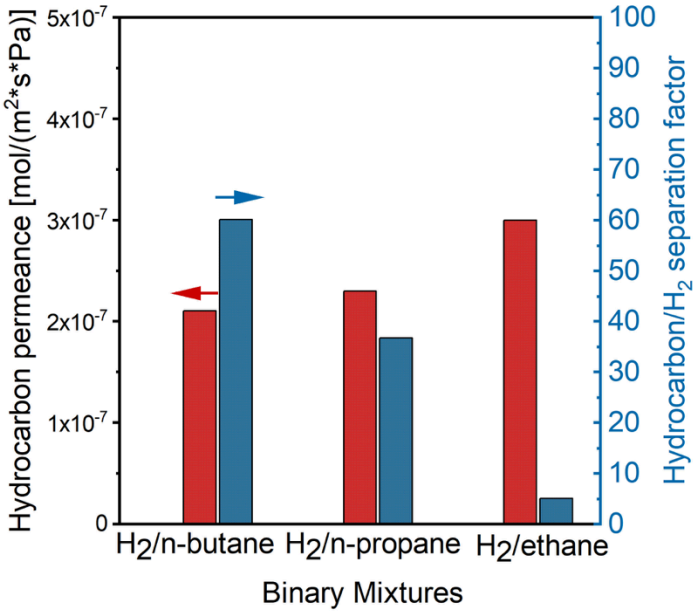

Figure 5.1: Membrane separation performance of binary H_2 and various hydrocarbon (i.e. ethane, propane and n-butane) mixtures at 1 bar feed pressure. Feed composition: 30%H_2+70% hydrocarbon; Feed flow rate: 50 mL/min; Permeate pressure: 1 bar; sweep (argon) flow rate: 30 mL/min.

We also carried out three components test to see how the membrane would behave with more components. ***Table 5.2*** listed the test conditions and experimental results.

Table 5.2: Ternary permeation measurement conditions and membrane performance

ID	Temp	Feed conditions			Permeate conditions		*n*-butane permeance (mol/(m^2-s-Pa))	Ethane or Propane permeance (mol/(m^2-s-Pa))	Hydrogen permeance (mol/(m^2-s-Pa))	*n*-butane/H_2 S.F.	Ethane or Propane/H_2 S.F.
		Feed Pressure	Feed composition	Feed flow rate	Permeate pressure	Sweep flow rate					
1	RT	1 bar	20%H_2+ 40%ethan +40% *n*-butane	50 mL/min	1 bar (Ar sweep)	30 mL/min	1.65×10^{-7}	3.2×10^{-8}	3.25×10^{-9}	42	10
2	RT	1 bar	20%H_2+ 40% propane+ 40% *n*-butane	50 mL/min	1 bar (Ar sweep)	30 mL/min	1.9×10^{-7}	1.0×10^{-7}	3.16×10^{-9}	50	29

Figure 5.2 shows the comparison between the separation performance of 20%H_2-40%ethane-40%*n*-butane and 20%H_2-40%propane-40%*n*-butane mixtures at 1 bar feed

pressure (Ar was used as the sweep gas in the permeate side). *n*-butane is the most permeable gas. The permeance of ethane or propane is smaller than that of *n*-butane. Hydrogen is the least permeable gas. In the 20%H_2-40%ethane-40%*n*-butane test (***Figure 5.2 left***), *n*-butane has a permeance of c.a. 1.65×10^{-7} mol/(m^2-s-Pa), while the hydrogen permeance is c.a. 3.2×10^{-9} mol/(m^2-s-Pa), giving a *n*-butane/H_2 separation factor of c.a. 42. Ethane has a permeance of c.a. 3.2×10^{-8} mol/(m^2-s-Pa), and the ethane/H_2 separation factor is c.a. 10. In the 20%H_2-40%propane-40%*n*-butane test (***Figure 5.2 right***), *n*-butane has a permeance of c.a. 1.9×10^{-7} mol/(m^2-s-Pa), while the hydrogen permeance is c.a. 3.2×10^{-9} mol/(m^2-s-Pa). The *n*-butane/H_2 separation factor is c.a. 50. Propane has a smaller permeance than *n*-butane (c.a. 1.0×10^{-7} mol/(m^2-s-Pa)), and the propane/H_2 separation factor is c.a. 29.

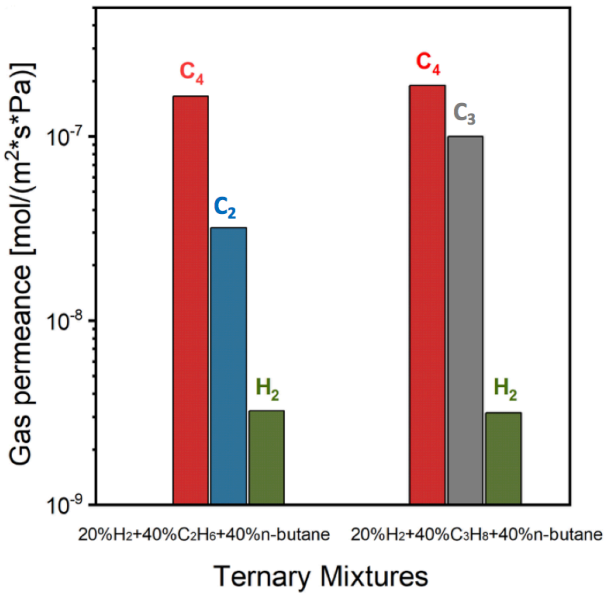

Figure 5.2: The comparison between the separation performance of 20%H_2-40%ethane-40%n-butane and 20%H_2-40%propane-40%n-butane ternary mixtures at 1 bar feed pressure; Feed flow rate: 50 mL/min; Permeate pressure: 1 bar; sweep (argon) flow rate: 30 mL/min.

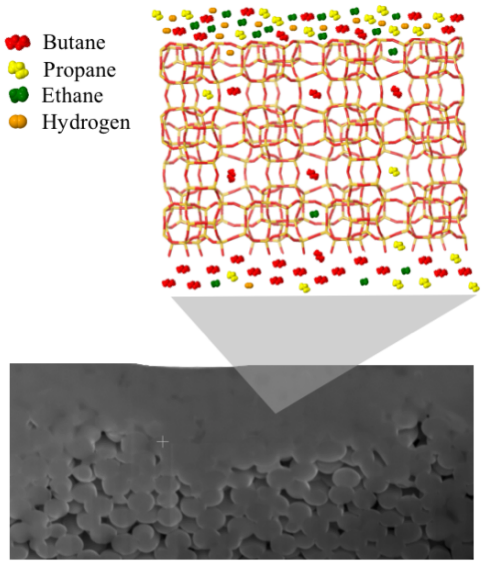

Figure 5.3: Schematic of the membrane separation process showing the competitive adsorption of hydrocarbons over hydrogen, making the membrane hydrocarbon selective.

Based on these results, we would imagine the membrane is working like a striping process. First, the *n*-butane passes more quickly than other gases. When the gas stream is depleted with *n*-butane, propane and ethane dominate the permeation, and hydrogen is the last to pass through the membrane when the membrane is not saturated by hydrocarbons. ***Figure 5.3*** shows a schematic of the adsorption dominated membrane separation process.

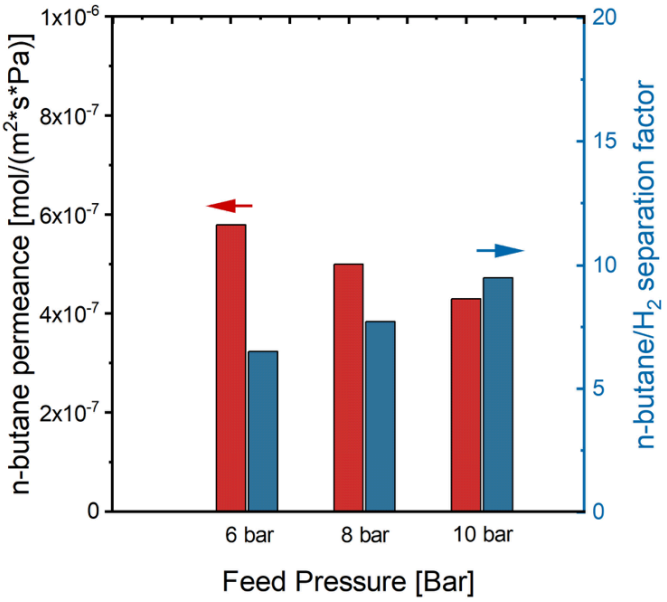

Figure 5.4: Separation test of H_2 and n-butane mixture with low n-butane concentration (2 mole%) at higher feed pressures; Feed flow rate: 200 mL/min; permeate pressure: 1 bar; no sweep was used.

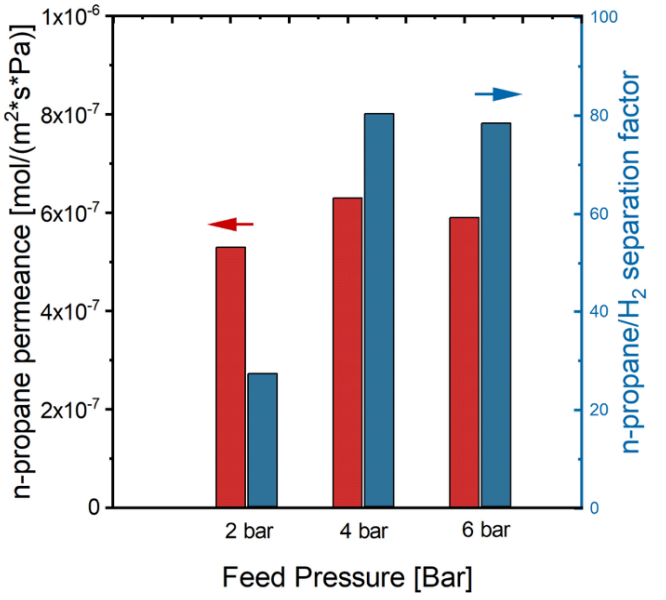

Figure 5.5: Membrane separation performance of 50-50 mole% H_2 and propane binary mixtrue at room temperature and higher feed pressures. Feed flow rate: 200 mL/min; permeate pressure: 1 bar; no sweep was used.

At atmospheric pressure, the membrane was not fully saturated for smaller molecules like propane and ethane. As a result, the H_2/hydrocarbon separation factor was lower compared to the case of H_2/*n*-butane. This problem can be solved by increasing the feed pressure. At higher feed pressures, smaller molecules can also fully saturate the membrane and completely hinder the permeation of H_2 molecules. This concept is confirmed by the experiment results shown in ***Figure 5.4*** and ***Figure 5.5***. ***Figure 5.4*** shows the results of the separation test of H_2 and *n*-butane mixture with low *n*-butane concentration (2 mol%) at higher feed pressures (permeate side is atmospheric pressure with no sweep gas). The separation factor decreased to about 6-10, meaning that the membrane is not fully saturated at lower *n*-butane partial pressures. With the increase in feed pressure, the separation factor increases. This makes sense because more *n*-butane would be absorbed and block the flow of H_2 at higher pressure. Another difference we noticed is that the *n*-butane permeances are higher than previous tests. This is because in this case, no sweep was used. In the previous test, the backflow of sweep gas would hinder the permeation of *n*-butane, which decreases the *n*-butane permeances. Further, the membrane was tested with 50%-50% H_2 and propane binary mixtrue at room temperature with higher feed pressures (permeate side is atmospheric pressure with on sweep gas). By increasing the feed pressure, the membrane showed an improved separation factor from ~30 to ~80, and the propane permeances remained high. If we convert the permeances to fluxes, the fluxes increased from ~1.0×10^{-2} mol/(m^2-s) at 2 bar feed pressure to ~6.9×10^{-2} mol/(m^2-s) when the feed pressure was increased to 6 bar. These fluxes are very high compared to the selective surface flow membranes[93-96] and the thick MFI membrane reported in the

literature[58], proving the high promise of these ultra-thin nanosheet-based MFI membranes for industrial applications.

5.4. CONCLUSION

In summary, an ultrathin MFI nanosheet membrane was fabricated and tested for hydrogen/hydrocarbons separation. It turned out to have a very high separation factor and flux compared to selective surface flow carbon membranes and other MFI membranes in the literature. Since the separation process is adsorption dominated, membrane separation performance can be improved by favoring the adsorption of hydrocarbons with the help of high pressure. With the increase in feed pressure, both fluxes and separation factors can be improved. The maximum flux achieved for H_2/propane separation at 6 bar feed pressure was c.a. 6.9×10^{-2} mol/(m^2-s) with a very high separation factor of c.a. 78. These results show that the ultra-thin MFI membranes are promising for the application of hydrogen/hydrocarbons separation. One potential application is hydrogen recovery from refinery waste gases. The membrane could be used to enrich hydrogen in the stream and the hydrogen-enriched stream can then be further processed by PSA process to produce pure hydrogen. At the permeate side of the membrane, the hydrocarbon-rich gas stream can be used as fuel or further processed to produce additional value.

Chapter 6. High-performance MFI membranes for ammonia separation

*Part of this work was submitted for publication.

6.1 Introduction

The modern industrial production of ammonia began with the discovery of the Haber–Bosch process, which converts hydrogen and nitrogen to ammonia in the presence of catalysts at high pressures (>100 bar) and temperatures (~500 °C) [105]. The reaction is limited by equilibrium at the required high temperatures since it is a strongly exothermic reaction. In industrial practice, the reactor effluent must go through refrigeration to condense ammonia, and the remaining hydrogen and nitrogen are reheated and recycled to the reactor in order to achieve a high overall conversion. An ammonia selective membrane has been envisioned to be used as a membrane reactor, which could remove the ammonia product while retaining the reactants during synthesis, thus circumventing the constraint of the reaction equilibrium [106]. This still remains a dream as no membrane that could work at such high pressures and temperatures was found. It is also beneficial to recover the ammonia from the recycled gas, which could reduce the extent of refrigeration required and improve efficiency [106,107]. To this end, different types of membranes were studied in the literature. Liquid membranes, which worked at high temperatures, were investigated by Air Products [108-110]. These membranes operate by either a mobile carrier mechanism [108-109], in which ammonia forms ammoniate complex with the molten salts, facilitating the transport of ammonia, or by the high solubility property of ammonia in ammonium salts [110]. Although they worked well at high temperatures, they failed to work at high pressures, due to the fact that the ordinary diffusion became significantly dominant

at high pressures [108-109] or even the instability of the ammonium salt membranes under high pressures [110]. Different types of polymeric membranes have also been explored for ammonia separation, including polymers containing thiocyanate [106, 110, 111] or sulfonate [112-114], cellulose acetate [115], poly(norborenylethystyrene)-b-poly(propyl-styrene-sulfonate) block copolymer [116] and poly[bis(trifluoroethoxy)phosphazene] [117]. Cussler et. al [106] studied the separation mechanism of the thiocyanate type membrane and ruled out the mobile carrier mechanism. They claimed the separation depends on the high solubility of ammonia in ammonium thiocyanate, which is produced from the reaction of ammonia and the polymer matrix. Sulfonate type membranes were claimed to be ammonia selective due to reversible reaction between ammonia and sulfate groups, and various ion-exchanged forms can facilitate the ammonia transport by the ion clusters [113], while the study carried out by Cussler [114] claimed that at lower temperature, the membranes operated by a solution-diffusion mechanism, and at higher temperatures, it was a combination of solution-diffusion and mobile carrier. The transport of ammonia, hydrogen and nitrogen through a cellulose acetate membrane was studied by Vorotyntsev et. al [115]. The selectivities and permeances were quite low. Poly(norborenylethystyrene)-b-poly(propyl styrene-sulfonate) block copolymer were designed to for the separation of ammonia [116]. The block copolymer contains two interpenetrating nanoscopic domains, one domain is ammonia selective and the other one is impermeable to gases. The impermeable phase will act as a rigid framework, which will prevent the swelling of the membrane and losing of the membrane selectivity at high pressures. More recently, the poly[bis(trifluoroethoxy)phosphazene], which has a high mechanical resistance to

pressure and good thermal and chemical resistance, was tested for ammonia separation [117]. Only single gas permeation data was presented with relatively low permeances and selectivities. Overall, polymeric membranes suffer from the decline of performance at higher pressures and temperatures, as well as the general problem of degradation, fouling, etc. Inorganic membranes can resist the high pressure and temperature required for ammonia synthesis. A screening program was carried at the University of Bath [59] to find suitable membranes for the effective recovery of ammonia. Tubular MFI zeolite membranes and silica membranes were reported to have moderate permeances but quite low selectivities. The highest selectivity obtained for ammonia/H_2 separation was 10, with an ammonia permeance of 2.1×10^{-7} mol/(m^2·s·Pa) at 80 °C. Silica membranes showed a higher permeance (7.6×10^{-7} mol/(m^2·s·Pa)) but even lower selectivity (~7). Another work reported by Kanezashi et. al [118] showed one of their silica membranes had ammonia permeance of 1.0×10^{-7} mol/(m^2·s·Pa) and ammonia/H_2 separation factor of ~30 at 50 °C. Recently, by employing the directly synthesized MFI nanosheet and a floating-particle coating method to form a dense and uniform nanosheet seeding layer on supports, ultra-selective MFI membranes were achieved after secondary growth with unprecedented permeaces and separation factors for *para*-xylene/*ortho*-xylene separation[56]. Herein, we evaluated the ultra-thin, highly selective MFI membranes for the separation of ammonia and hydrogen or nitrogen. The separations were performed at different temperatures and feed pressures to evaluate the effect of temperature and pressure on the membrane separation performance. Results showed that the membranes had very high flux and separation factor for ammonia/hydrogen and ammonia/nitrogen separations.

Table 6.1: Ammonia separation based on molten salt liquid membranes

Ref.	Material	Membrane Thickness	Feed	Sweep	T/°C	NH_3 permeability /permeance	NH_3/H_2 selectivity	NH_3/N_2 selectivity	Comments
[108] Pez, 1988 [109] Pez, 1992	Lithium Nitrate Immobilized Molten Salt Membrane		1 bar 10% NH_3	He, 1 bar	279	9900 Barrer		245	Although work well at high temperatures, they fail to be selective at high pressures
			1 bar 25% NH_3			7400 Barrer		129	
			1 bar 50% NH_3			7100 Barrer		80	
	Zinc Chloride Immobilized Molten Salt Membrane		1 bar 10% NH_3	He, 1 bar	250	100,000 Barrer		>1000	
			1 bar 20% NH_3			69,000 Barrer		>1000	
			1 bar 40% NH_3			28,000 Barrer		>1000	
			1 bar 80% NH_3			21,000 Barrer		>1000	
			1 bar 10% NH_3	He, 1 bar	300	130,000 Barrer		>1000	
			1 bar 20% NH_3			79,000 Barrer		>1000	
			1 bar 40% NH_3			44,000 Barrer		>1000	
			1 bar 60% NH_3			43,000 Barrer		>1000	
			1 bar 80% NH_3			33,000 Barrer		>1000	
			1 bar 10% NH_3	He, 1 bar	350	140,000 Barrer		>1000	
			1 bar 20% NH_3			150,000 Barrer		>1000	
			1 bar 40% NH_3			46,000 Barrer		>1000	
			1 bar single gas	He, 1 bar	311	290,000 Barrer	3200		
[110] Pez, 1988	NH_3-NH_4SCN Liquid Membrane on Nylon filter		$1NH_3$:$1N_2$ 3.6 bar	He 3.6 bar	0	2400 GPU		>1000	Cannot withstand high transmembrane pressures
					23	1900 GPU		8700	
					21	5265.5 Barrer	59.2	135	
					50	5038.6 Barrer	25.8	59.1	

Table 6.2: Ammonia separation based on polymeric membranes

Ref.	Material	Membrane Thickness	Feed	Sweep	T/°C	NH_3 permeability /permeance	NH_3/H_2 selectivity	NH_3/N_2 selectivity	Comments
[119] Brubaker, 1954	Polyethylene				15	29 Barrer	4.1	32	
[120] Browall, 1979	Ultrathin poly-etherimide	7.5 μm	Single gas, 0.33-0.79 bar	vacuum	23	48.4 Barrer	1.9	134	
[121] Brandrup, 1975	Ethyl cellulose				25	705 Barrer	8.1	84	
	Cellulose nitrate				25	57.1 Barrer	29	476	
[122] Kulprathipanja 1986	Multi-component silicone rubber/ polyethylene glycol	NA	Single gas, 50 psig	1 bar, no sweep	RT	376 GPU	78.8	1423	
					RT	164 GPU	80.7	1350	
					RT	224 GPU	78.6	1100	
[123] Pan, 1988	Polysulfone amide	NA	Single gas		23.5	118 GPU	12.5	450.4	selectivity decreasing with increasing temperature
					0	135 GPU	33.6	892.8	
					-10	520 GPU	200.8	6025	
					-16	1010 GPU	653.7	18878	
[111] Pez, 1988	Polyvinyl-ammonium chloride	80-150 μm	$3NH_3$:$1N_2$ 1 bar	He, 1 bar	17	2.9 GPU		>50	
			$3NH_3$:$1N_2$ 5 bar	He, 5 bar	17	16 GPU		>800	
			$3NH_3$:$1N_2$ 6 bar	He, 6 bar	17	50 GPU		>1000	
		~180 μm	60% NH_3 13.8 bar	He, 1 bar	25	32 GPU		2100	
			40% NH_3 20.7 bar	He, 1 bar	25	27 GPU		2500	
			30% NH_3 27.5 bar	He, 1 bar	25	24 GPU		2200	
	Polyvinyl-ammonium thiocyanate	NA	$3NH_3$:$1N_2$ 1 bar	He, 1 bar	17	98 GPU		>900	
			$3NH_3$:$1N_2$ 6 bar	He, 6 bar	17	250 GPU		>1100	
			$3NH_3$:$1N_2$ 3 bar	He, 3 bar	52	150 GPU		>1000	
			$3NH_3$:$1N_2$ 6 bar	He, 6 bar	52	220 GPU		>1100	
			$3NH_3$:$1N_2$ 3 bar	He, 3 bar	73	110 GPU		>900	
			$3NH_3$:$1N_2$ 6 bar	He, 6 bar	73	160 GPU		>1000	
		100-300 μm	38.8% NH_3 20.5 bar	He, 1 bar	26	340 GPU		1500	
			28.6% NH_3 27.8 bar	He, 1 bar	26	230 GPU		1300	
			25.4% NH_3 31.2 bar	He, 1 bar	26	210 GPU		1200	
			18.6% NH_3 42.7 bar	He, 1 bar	26	150 GPU		1100	
			13.4% NH_3 59.2 bar	He, 1 bar	26	110 GPU		970	
			12.0% NH_3 66.4 bar	He, 1 bar	26	97 GPU		890	
			13.8% NH_3 +25.9%H_2 +60.3%N_2 57.5 bar	He, 1 bar	24	54 GPU	6200	3600	
			13.8% NH_3 +25.9%H_2 +60.3%N_2 57.5 bar	He, 1 bar	60	32 GPU	1400	2000	

[110] Pez, 1988	Polyvinyl-alcohol ammonium thiocyanate	~200 μm	$1NH_3$:$1N_2$ 3.6 bar	He 3.6 bar	0	183 GPU		>3000	
					19	179 GPU		3000	
					50	180 GPU		1000	
[113] Timashev, 1991	Hydrolyzed Perfluoro-sulfonic acid polymer hollow fibers	Wall thickness 17 μm	Single gas, 2 bar	He, 1 bar	RT	7800 Barrer	> 100-1000		
[114] Bikson, 1991	Composite polysulfone hollow fiber/ sulfonated polysulfone		$NH_3/N_2/H_2$ 10/30/60 100 psig		22	132.6 GPU	33	>1000	
					9	157.3 GPU	63	>1000	
[112] Cussler, 1992	Perfluoro-sulfone (Nafion)	38 μm	5.4 bar NH_3/N_2 mixture	He	21	Flux: 14×10^{-2} mol/(m^2·s)		>3000	H^+-Nafion
						Flux: 10×10^{-2} mol/(m^2·s)		>3000	Na^+-Nafion
						Flux: 8.4×10^{-2} mol/(m^2·s)		600	Ag^+-Nafion
						Flux: 7.0×10^{-2} mol/(m^2·s)		60	NH_4^+-Nafion
						Flux: 4.0×10^{-2} mol/(m^2·s)		>3000	Zn^+-Nafion
						Flux: 3.8×10^{-2} mol/(m^2·s)		>3000	Li^+-Nafion
						Flux: 3.5×10^{-2} mol/(m^2·s)		>3000	Cu^+-Nafion
						Flux: 1.3×10^{-2} mol/(m^2·s)		>3000	K^+-Nafion
					200	Flux: 1.89×10^{-2} mol/(m^2·s)		>3000	H^+-Nafion
						Flux: 1.23×10^{-2} mol/(m^2·s)		>3000	Na^+-Nafion
						Flux: 1.71×10^{-2} mol/(m^2·s)		300	Ag^+-Nafion
						Flux: 0.87×10^{-2} mol/(m^2·s)		120	NH_4^+-Nafion
						Flux: 0.50×10^{-2} mol/(m^2·s)		60	Zn^+-Nafion
						Flux: 0.59×10^{-2} mol/(m^2·s)		>3000	Li^+-Nafion
						Flux: 0.61×10^{-2} mol/(m^2·s)		60	Cu^+-Nafion
						Flux: NA		>3000	K^+-Nafion
[115] Vorotyntsev, 2006	Cellulose acetate		Single gas, 1 bar	<4.1 kPa	RT	$980\pm44\times10^{-10}$ mol/(m^2·s·Pa)	9.3	111	
[116] Cussler, 2009	Poly-(norborenyl-ethystyrene)-b-poly(propyl styrene-sulfonate) P (N-S-S)-b-PSSP block copolymer		Single gas, 2 bar	1 bar	25	>600 Barrer		>90	selectivity retained with high pressure (~4 bar), mixed gas feeds.

[117] Makhloufi, 2012	poly[bis-(trifluoro-ethoxy)-phosphazene] (PTFEP)	NA	Single gas	Vacuum	5	5643.7 Barrer	105.3	221.3	high mechanical resistance to pressure; good thermal resistance; good chemical resistance
					21	5265.5 Barrer	59.2	135	
					50	5038.6 Barrer	25.8	59.1	

Table 6.3: Ammonia separation based on silica membranes

Ref.	Material	Membrane Thickness	Feed	Sweep	T/°C	NH_3 permeance	NH_3/H_2 selectivity	NH_3/N_2 selectivity	Comments
[59] Camus, 2006	tubular silica membranes on alumina substrates	<200 nm	16% NH_3, 3/1 H_2/N_2 10 bar	1 bar	80	7.62×10^{-7} mol/(m^2·s·Pa).	6.60	14.48	At Bath
			14% NH_3, 3/1 H_2/N_2 16.3 bar	1 bar	80	1.72×10^{-7} mol/(m^2·s·Pa).	2.74	1.59	At ECN
			14% NH_3, 3/1 H_2/N_2 21.2 bar	1 bar	80	3.71×10^{-7} mol/(m^2·s·Pa).	4.89	7.10	
			14% NH_3, 3/1 H_2/N_2 25.2 bar	1 bar	80	5.65×10^{-7} mol/(m^2·s·Pa).	4.88	10.73	
[118] Kanezashi, 2010	Si-1, average pore size 0.5-0.6 nm	<1 μm	1 bar 1/1 NH_3/H_2	1 bar	50	1.02×10^{-7} mol/(m^2·s·Pa).	28.7		
					400	1.04×10^{-7} mol/(m^2·s·Pa).	0.083		
	Si-2, average pore size 0.4-0.5 nm		1 bar 1/1 NH_3/H_2	1 bar	50	0.168×10^{-7} mol/(m^2·s·Pa).	1.02		
					400	0.117×10^{-7} mol/(m^2·s·Pa).	0.018		
	Si-3, average pore size 0.3 nm		1 bar 1/1 NH_3/H_2	1 bar	50	0.00521×10^{-7} mol/(m^2·s·Pa).	0.31		

Table 6.4: Ammonia separation based on MFI membranes

Ref.	Material	Membrane Thickness	Feed	Sweep	T/°C	NH_3 permeance	NH_3/H_2 selectivity	NH_3/N_2 selectivity	Comments
[59] Camus, 2006	MFI on alumina tube	5-15μm	16% NH_3, 3/1 H_2/N_2 10 bar	1 bar	80	2.14×10^{-7} mol/(m^2·s·Pa).	9.13	14.09	
			16% NH_3, 3/1 H_2/N_2 10 bar	1 bar	25	0.60×10^{-7} mol/(m^2·s·Pa).	2.80	3.10	
			9% NH_3, 3/1 H_2/N_2 10 bar	1 bar	25	0.64×10^{-7} mol/(m^2·s·Pa).	3.08	2.84	
			2% NH_3, 3/1 H_2/N_2 10 bar	1 bar	25	0.92×10^{-7} mol/(m^2·s·Pa).	5.00	4.61	
	MFI on fiber		16% NH_3, 3/1 H_2/N_2 10 bar	1 bar	80	0.13×10^{-7} mol/(m^2·s·Pa).	7.14	20.66	

6.2 Results and discussions

A membrane was prepared using the same method described in chapter 4. The fabricated MFI membrane was used to evaluate the performance for the separation of ammonia and hydrogen or nitrogen. ***Table 6.5*** and ***Table 6.6*** listed the test conditions and experimental results.

Table 6.5: Ammonia/hydrogen binary permeation measurement conditions and membrane performance

ID	Temp	Feed conditions			Permeate conditions		Ammonia permeance (mol/(m^2·s·Pa))	Ammonia flux (mol/(m^2·s))	Ammonia/ Hydrogen S.F.
		Feed Pressure	Feed composition	Feed flow rate	Permeate pressure	Permeate flow rate (measured)			
1	25 °C	3 bar	50%H_2+50% ammonia	400 mL/min	1 bar (no sweep)	30.0 mL/min	2.26×10^{-6}	0.090	307
2	50 °C	3 bar	50%H_2+50% ammonia	400 mL/min	1 bar (no sweep)	50.8 mL/min	3.45×10^{-6}	0.144	23.8
3	100 °C	3 bar	50%H_2+50% ammonia	400 mL/min	1 bar (no sweep)	76.6 mL/min	2.72×10^{-6}	0.173	3.8

Table 6.6: Ammonia/nitrogen binary permeation measurement conditions and membrane performance

ID	Temp	Feed conditions			Permeate conditions		Ammonia permeance (mol/(m^2·s·Pa))	Ammonia flux (mol/(m^2·s))	Ammonia /Nitrogen S.F.
		Feed Pressure	Feed composition	Feed flow rate	Permeate pressure	Permeate flow rate (measured)			
1	25 °C	3 bar	50%N_2+50 %ammonia	400 mL/min	1 bar (no sweep)	22.0 mL/min	1.10×10^{-6}	0.066	2236
2	50 °C	3 bar	50%N_2+50 %ammonia	400 mL/min	1 bar (no sweep)	44.5 mL/min	2.62×10^{-6}	0.133	191
3	50 °C	5 bar	50%N_2+50 %ammonia	400 mL/min	1 bar (no sweep)	72.5 mL/min	1.89×10^{-6}	0.216	219
4	50 °C	7 bar	50%N_2+50 %ammonia	400 mL/min	1 bar (no sweep)	87.7 mL/min	1.66×10^{-6}	0.261	221
5	100 °C	3 bar	50%N_2+50 %ammonia	400 mL/min	1 bar (no sweep)	46.8 mL/min	3.47×10^{-6}	0.131	15.8
6	100 °C	5 bar	50%N_2+50 %ammonia	400 mL/min	1 bar (no sweep)	89.4 mL/min	2.50×10^{-6}	0.248	20.0

Figure 6.1a shows the ammonia/hydrogen binary separation performance at different temperatures. Tests were done using 50%H_2 +50% ammonia at 2 bar transmembrane pressure. No sweep was used on the permeate side. The membrane had a high ammonia/hydrogen separation factor of 307 at room temperature with a very high ammonia permeance of 2.26×10^{-6} mol/(m^2·s·Pa). With increasing temperature, the selectivity dropped dramatically to 23.8 at 50 °C and 3.8 at 100 °C, respectively. A similar tendency was observed for the ammonia/nitrogen separation as is shown in ***Figure 6.1b***. The membrane had a very high ammonia/nitrogen separation factor of 2236 at room temperature with a very high ammonia permeance of 1.10×10^{-6} mol/(m^2·s·Pa). The selectivity decreased to 191 at 50 °C and 15.8 at 100 °C, however.

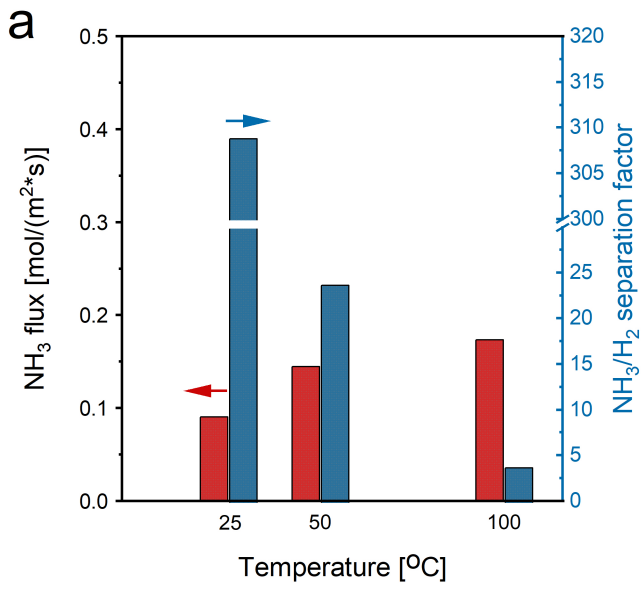

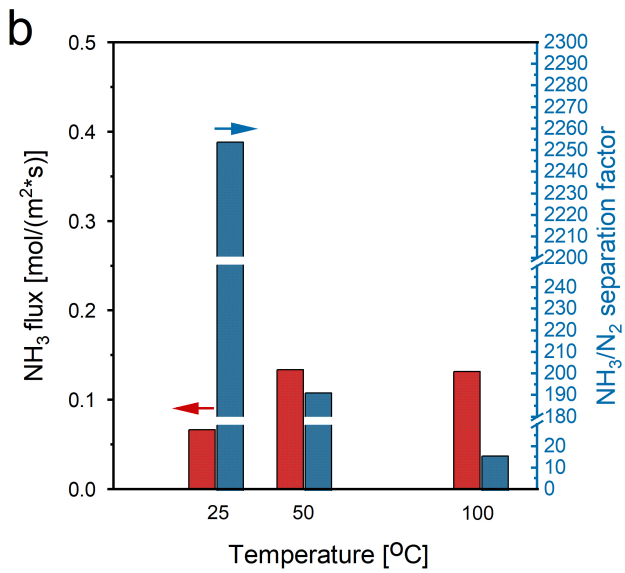

Figure 6.1: Membrane separation performance of a). 50%H_2+50% ammonia and b) 50%N_2+50% ammonia tested at 2 bar transmembrane pressure and different temperatures. Feed flow rate: 400 mL/min; Feed pressure: 3 bar; Permeate pressure: 1 bar; No sweep was used.

We also tested the effect of pressure on the membrane separation performance using an ammonia and nitrogen binary mixture. ***Figure 6.2*** shows that with the increase in feed pressure, ammonia flux increases, with a slight increase in the membrane selectivity. The increase in flux at a high feed pressure is due to the higher driving force at higher transmembrane pressure differences. The increase in membrane separation factor can be explained by the fractional loading of NH_3 in zeolite pores; at higher pressures, higher NH_3 loadings diminish the transport of nitrogen. At this time, we did not go to much higher pressures due to safety considerations. It would be interesting to see the membrane performance at much higher pressures approaching the actual pressure used during Haber–Bosch process.

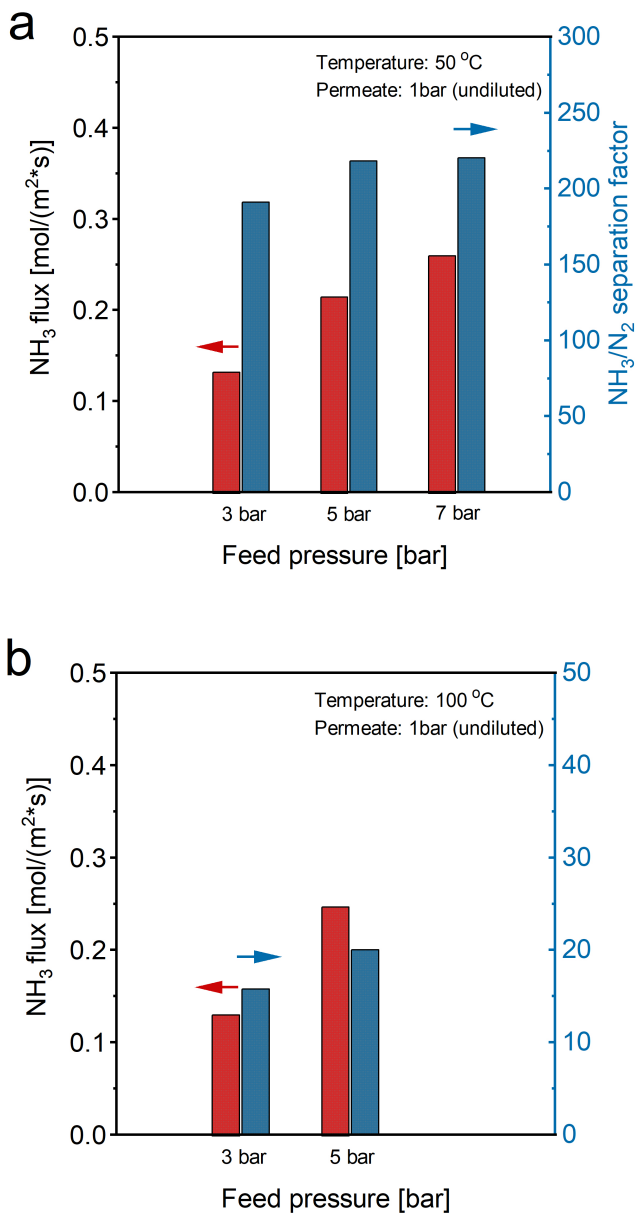

Figure 6.2: Membrane separation performance of 50-50 mole% N_2 and ammonia binary mixtrue at 50 ℃ a) and 100℃ b) and higher transmembrane pressures. Feed flow rate: 400 mL/min; permeate pressure: 1 bar; no sweep was used.

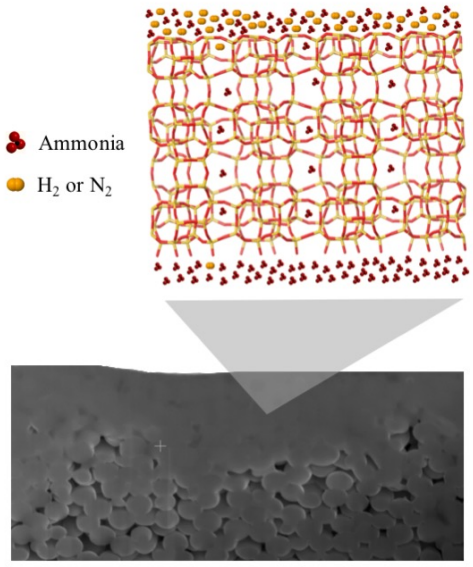

Figure 6.3: Schematic of the membrane separation process showing the preferred adsorption of ammonia over hydrogen or nitrogen, making the membrane ammonia selective.

The high membrane selectivity towards ammonia at lower temperatures is explained by the preferred adsorption of ammonia over hydrogen or nitrogen, as is schematically shown in ***Figure 6.3***. The membrane can selectively adsorb ammonia molecules and the adsorbed ammonia can hinder or block the flow of the H_2 or N_2 molecues, making it ammonia selective. This mechanism is well known for the separation of larger and heavier hydrocarbons from lighter gases like hydrogen [57,58], nitrogen [97] and methane [99-101] in literature as was described in chapter 5.

6.3 CONCLUSION

Ultra-thin, high-performance MFI membranes were fabricated and tested for ammonia/H_2, ammonia/N_2 separations. The membranes were selective towards ammonia

since it can be more easily adsorbed than hydrogen or nitrogen. The adsorbed ammonia can hinder or completely block the flow of hydrogen or nitrogen. At room temperature, the ammonia/H_2 and ammonia/N_2 separation factor can be as high as 307 and 2236, respectively, with ultra-high fluxes in the order of 10^{-1} mol/(m^2·s). With the increase in temperature, the selectivity dropped significantly. In contrast, the increase in feed pressure increased membrane selectivity. Increasing temperature and pressure can both increase gas permeation flux. These results showed the possibility of these high- performance MFI membranes for industrial ammonia/H_2/N_2 separation applications.

Chapter 7: Rate selective LTA membranes for water/air separation

7.1. Introduction

Zeolite NaA membranes are very hydrophilic and have proven to be suitable for the removal of water from organic solutions [124-130]. About 20 years ago, Mitsui Engineering and Shipbuilding Co. in Japan developed the first large scale pervaporation plant using tubular zeolite NaA membranes for the dehydration of organic solvents. After this, a lot of following up research was reported. Among these literature reports, there are two commonly used gel compositions for the preparation of LTA membranes. One is the commonly called milky gel recipe. This is the recipe that the company used for the pervaporation plant. Different types of inorganic supports and seeding techniques were used in different studies. ***Table 7.1*** lists some of the membranes made using this recipe along with their pervaporation performance. Okamoto and coworkers [124] used large seed crystals and a dip coating technique. The obtained membranes were relatively thick. Differently, Wang and coworkers [125] used smaller seed crystals and a paste rubbing technique to form a smooth seed layer. The obtained membranes were much thinner. Vacuum-assisted seeding technique has also been reported. In ref. [126], Liu et al. used vacuum-assisted coating and obtained membranes that showed a high water flux. Mullite tubes were also been used as supports for NaA membranes. Liu et al. [127] studied the influence of seeding techniques on the preparation of NaA membranes on tubular mullite supports. A combination of rubbing and dip coating gave a better seed layer. All the aforementioned membranes showed good pervaporation performance with EtOH/water separation factor larger than 10,000 and water fluxes between 2 to 7 kg/(m^2-h).

Table 7.1: Examples of Zeolite NaA membrane made by using milky gel composition (Al_2O_3:2SiO_2:2Na_2O:120H_2O)

Ref.	Support	Seeds	Reaction conditions	Membrane thickness	EtOH/Water (90%), PV, Flux	
124	α-alumina tube	Zeolite NaA (Wako Pure Chemical Co.)	100 °C, 3 h	30 μm	@75 °C, separation factor: >10,000	Flux 2.2 Kg/(m^2-h)
125	α-alumina tube	0.8 μm, seeded by paste rubbing	100 °C, 4 h	4-5 μm	@75 °C, separation factor: >10,000	Flux 3.6 Kg/(m^2-h)
126	α-alumina tube	2.8 μm, vacuum-assisted seeding	100 °C, 4 h	6 μm	@75 °C, separation factor: >17,020	Flux 7.02 Kg/(m^2-h)
127	Mullite (Al_2O_3-SiO_2)	2 μm, seeded by rubbing +dip coating	100 °C, 3.5 h	10-15 μm	@75 °C, separation factor: >15,000	Flux 3.26 Kg/(m^2-h)

Besides this milky gel recipe, another commonly used one is the so-called clear sol recipe. The sol is clear and less viscous so it is easier to make it homogenous. Different seeding techniques and reaction conditions were also studied for this recipe (See ***Table 8.2*** for some examples), and they also showed good pervaporation performance. For instance, in ref. [128], Li and coworkers used a two-time seeding technique. In the first step, they used larger crystals (2 μm) to form the first seeding layer, and in the second step, smaller crystals (0.4 μm) were used to fill in the empty spaces. They found that by using this technique the membranes were better intergrown and showed better performance. In

ref. [129], Huang and coworkers introduced a novel microwave heating technique to replace the conventional heating technique for the membrane secondary growth. This technique could considerably reduce the synthesis time. Good membranes that showed comparable pervaporation performance compared with traditional ones were successfully prepared.

Table 7.2: Examples of Zeolite NaA membrane made by using clear sol composition (Al_2O_3:5SiO_2:50Na_2O:1000H_2O)

Ref.	Support	Seeds	Reaction conditions	Membrane thickness	EtOH/Water (90%), PV, Flux	
128	α-alumina tube (Cheap and coarse)	1st seeding: 2μm, 2nd seeding: 0.4 μm	80 °C, 5 h	4 μm	@70 °C, separation factor: >10,000	Flux 2.85 Kg/(m^2-h)
129	α-alumina tube	0.5 μm, vacuum-assisted seeding	90 °C, microwave heating, 10-20 min	7.4 μm	@70 °C, separation factor: 6232.7	Flux 1.7 Kg/(m^2-h)
130	α-alumina tube	1.2 μm, vacuum-assisted seeding	60 °C, 24 h	6 μm	@70 °C, separation factor: >10,000	Flux 1.67 Kg/(m^2-h)

As for gas separations, zeolite NaA membranes were less successful. They showed poor gas separation performance due to the presence of defects. However, zeolite NaA membrane for water vapor separation is promising. In ref. [131], W. Zhu et al. showed that water permeated faster in zeolite NaA membranes than other gases due to strong adsorption and small size. The permeance of H_2O in the binary mixture was about two orders of magnitude larger than that of the permanent gases, giving a membrane separation

factor above a hundred. ***Figure 7.1 left*** shows the ideal selectivity for water vapor as a function of temperature. The room temperature single component ideal selectivities of H_2O/CO, H_2O/H_2, and H_2O/CH_4 were 16, 5 and 23 respectively, while those of a mixture of H_2O /CO, H_2O /H_2, and H_2O/CH_4 were above 200, 300, and 600 respectively (***Figure 7.1 right***). This was ascribed to the high adsorption affinity and capacity of water inside the zeolite-A cages, preventing the bypassing of the second component through the membrane.

Table 7.3: Recipe of zeolite NaA membrane for water vapor separation

Ref.	Gel composition	Support	Seeds	Reaction conditions	Membrane thickness
131	$12Al_2O_3:53SiO_2:503Na_2O:10000H_2O$	TiO_2 coated stainless steel disk	In-situ growth	80 °C, 24 h	3.5 μm

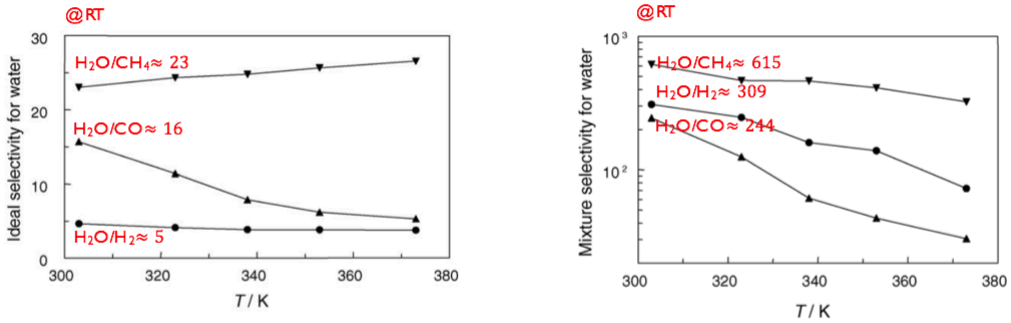

Figure 7.1: Ideal selectivity for water vapor as a function of temperature (left) and mixture permeation selectivity for water gas as a function of temperature (right). (Δ) H_2O/CO; (•) H_2O/H_2; (▽) H_2O/CH_4.

In section 7.2, we first present a facile post-synthetic treatment method for improving the permselectivity of MFI membranes. It proved that coating a thin layer of MR-2404 emulsion followed by activation can effectively improve the membrane permselectivity without significantly compromising the membrane permeance. The method was applied

to MFI membranes as a prove-of-concept, and since zeolite NaA membranes are commercially viable and are promising for water vapor separation, we propose that we can apply the current MR-2404 coating technique to zeolite NaA membranes, making higher performance membranes (surface-modified zeolite NaA membranes) towards commercialization.

7.2. Post-synthetic treatment of MFI membranes by MR-2404 emulsion

7.2.1 EXPERIMENTAL SECTION

(1) Preparation of MFI membranes using large coffin-shaped crystals as seeds:

The traditional type MFI membranes using large coffin-shaped crystals as seeds were prepared by using the same method reported in [32]. Briefly, sintered silica fiber (SSF) supports were prepared, followed by modification using 1 μm silica spheres, 350 nm Stöber silica and 50 nm Stöber silica sequentially. Coffin-shaped crystals were synthesized following the procedures reported in [74]. The procedures were briefly discussed in chapter 3. The crystals were seeded on the supports by manual rubbing with a layer of polyacrylic acid to aid the binding between the seeds and the supports. A gel-less secondary growth was performed to make the membrane continuous and well intergrown. After the membranes were obtained, a calcination step was performed to remove the occlude SDA.

(2) Preparation of MFI membranes using MFI nanosheets as seeds:

The nanosheet type MFI membranes using bottom-up synthesized MFI nanosheets as seeds were prepared, using the same method described in chapter 4.

(3) MR-2404 coating and UV/ozone treatment:

A 0.02 wt% MR-2404 coating solution was prepared by first dissolving 0.5 g MR-2404 emulsion in 50 g MeOH and sonicating for 90 min, then taking 0.5 g solution and add another 25 g MeOH to it followed by brief sonication for another 10 min. The membrane was assembled in a filtration cell and 1 g of the 0.02 wt% MR-2404 solution was added to the cell. A vacuum-assisted filtration [51,52] was performed to deposit the MR-2404 layer on top of the membrane. After coating, the membrane was carefully removed from the cell and stored in a clean environment to let it completely dry under ambient conditions. To activate the membrane, a mild UV/ozone treatment was adapted. It is reported in the literature that adding ozone in the calcination atmosphere can be effective in activating zeolite membranes at temperatures ~200 °C while suppressing crack formation [132-137]. Coupling UV radiation and in-situ ozone generation can achieve template removal at nominal room temperature. The overall process involves three overlapping photo-induced chemical reactions: dissociation of oxygen to produce ozone and atomic oxygen; excitation and/or dissociation of the organic templates; reaction between the produced ozone and atomic oxygen and the activated organic species. The UV/ozone process was successfully applied for the removal of the organic structure-directing agent in MFI membranes [75-76] and SSZ-13 membranes [77]. To perform the activation, the membrane was placed in a Jelight's UVO-Cleaner®. The UV radiation was shined on the membrane for 1 hour.

(4) Butane isomer permeation test:

Single gas permeation was tested with 1 atmospheric pressure on the feed side and vacuum on the permeate side. The membrane separation performance was assessed with the membrane permeance and membrane ideal selectivity. The membrane permeance was the butane isomer flux normalized by the pressure gradient across the membrane. The membrane ideal selectivity was calculated as the ratio of the permeance of the two butane isomers.

7.2.2 RESULTS AND DISCUSSION

We tested the effect of MR-2404 coating and UV/ozone treatment method for two types of membranes. One is the conventional *b*-oriented MFI membrane. ***Figure 7.2a*** shows the surface morphology of the prepared membrane. The as-made membrane had an *n*-butane permeance of 2.4×10^{-7} mol/(m^2-Pa-s) and an *n*-butane/*iso*-butane ideal selectivity of about 57. After applied a thin MR-2404 coating and UV/ozone treated for 1 h, the ideal selectivity increased to 238 with a very slight decrease in the *n*-butane permeance (1.0×10^{-7} mol/(m^2-Pa-s).

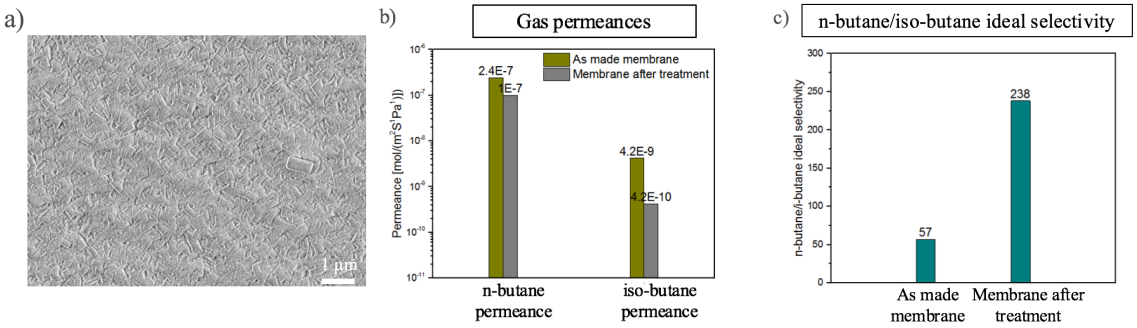

Figure 7.2: a). Surface morphology of the conventional b-oriented MFI membrane; b) and c) comparison between the separation performance of the as-made membrane and the membrane after MR-2404 coating and UV/ozone treatment.

The same behavior was also observed for the ultra-thin MFI nanosheet membrane. ***Figure 7.3a*** shows the typical surface morphology of the nanosheet type MFI membrane. Permeation results showed that the as made membrane had an *n*-butane permeance as high as 1.0×10^{-6} mol/(m^2-Pa-s) (because the membrane was much thinner) and an *n*-butane/*iso*-butane ideal selectivity of about 57. After applying a thin MR-2404 coating and UV/ozone treated for 1 h, the ideal selectivity increased to 202 with the *n*-butane permeance of 1.7×10^{-7} mol/(m^2-Pa-s). Although the *n*-butane permeance did not come back to 10^{-6} mol/(m^2-Pa-s), it was still comparable with other literature membranes with selectivity much higher than them.

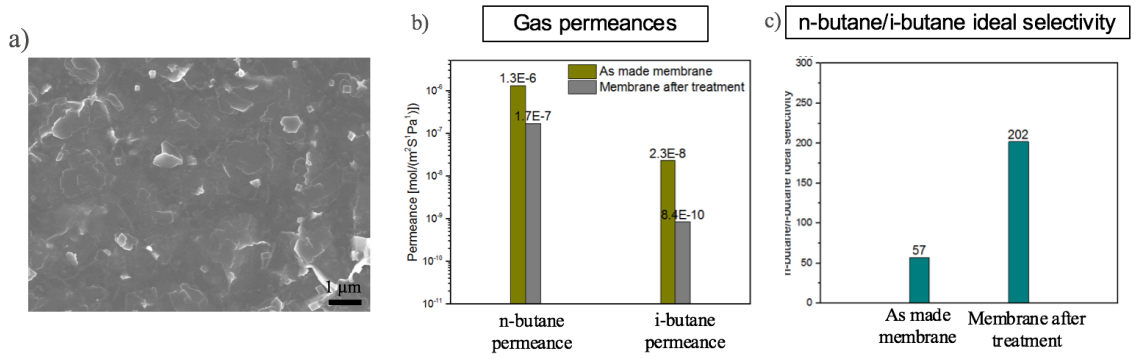

Figure 7.3: a). Surface morphology of the nanosheet type MFI membrane; b) and c) comparison between the separation performance of the as-made membrane and the membrane after MR-2404 coating and UV/ozone treatment.

Table 7.4 listed the literature reported MFI membranes for *n*-butane and *iso*-butane separation near room temperatures. Our membranes had ideal selectivities higher than the literature reported membranes. The only membrane reported in the literature that had higher permselectivity was the membrane after post-synthetic coking treatment [138]. The membrane had higher selectivity at higher temperatures. The ideal selectivity increased from 45 (before treatment) to 320 (after treatment) at 185 °C. However, the selectivity at 30 °C after the treatment was about 65.

Table 7.4: List of the literature reported MFI membranes for n-butane/iso-butane separation near room temperatures.

Ref.	Temperature (°C)	*n*-butane permeance $\times 10^7$ mol/(m^2-s)	S.F. (or ideal selectivity)
[139] Bai, 1995	27	0.59	20 (ideal selectivity)
[140] Vroon, 1996	25	0.3	52
[141] Vroon, 1998	25	0.3	100 (ideal selectivity)
[142] van de Graaf, 1998	30	0.5	25
[143] Xomeritakis, 1999	22	0.6	62
[144] Tuan, 1999	28	0.34	20 (ideal selectivity)
	28	0.13	25
[145] Piera, 1999	25	0.4	35
[146] Xomeritakis, 2000	22	0.2	71
[147] Matsufuji, 2000	27	0.01	69
[148] Gora, 2000	25	0.8	48
[149] Alfaro, 2001	25	0.35	4
[150] Gora, 2001	30	0.5	55
[151] Li, 2001	30	0.1	42
[152] Nishiyama, 2001	30	0.7	28
[153] Hedlund, 2002	25	9.8	9
[154] Bernal, 2003	25	0.35	18
[155] Jareman, 2003	25	8.7	6
[156] Gora, 2005	30	1.4	45
[157] Choi, 2006	26	0.81	47
[158] Choi, 2009	25	1.0	35
[159] Stoeger, 2011	25	0.8	25
[51] Agrawal, 2015	25	4.34	62
	25	2.34	47
	25	1-10	100-160 (ideal selectivity)
[55] Jeon, 2017	25	2.0	50
[56] Kim, 2018	22	0.97	64
	22	3.3	69
[101] Min, 2019	25	1.28	42
[160] Wu, 2019	30	1.65	37
[161] Liu, 2020	25	2.0	33
[162] Min, 2020	25	3.3	12
	25	1.4	60

In summary**,** we reported a facile post-synthetic treatment to cure membrane defects. As was demonstrated by the increase in *n*-butane/*iso*-butane ideal selectivity, the method was effective in improving the membrane permselectivity without significantly compromising the membrane permeance. In the following sections, we discuss using the same method for improving the performance of NaA membranes.

7.3. MR-2404 treatment of NaA membranes

7.3.1. Experimental Section

(1) Porous α-alumina support preparation:

The procedures for preparing $\boldsymbol{\alpha}$-alumina supports were described in chapter 3.

(2) NaA nanoseed synthesis:

NaA nanoseeds were prepared by following the exact procedure in ref. [163], using a recipe of 3.59 $(TMA)_2O$:0.1 Na_2O:0.5Al_2O_3:1SiO_2:170H_2O. In brief, 0.156 g sodium hydroxide was dissolved in 19.12 g H_2O. Then 52.36 g TMAOH was added to the solution. After stirring for ~30 min, the solution is divided into 2 equal volumes. For the first part, 4.085 g aluminum isopropoxide was added to the solution and stirred for ~30min to get a homogenous aluminate solution. For the second part, 4.005 g 30 wt% colloidal silica (LUDOX® SM 30) was added to the solution and stirred for ~30min to get a homogenous silicate solution. Then, the silicate solution was added to the aluminate solution dropwise with stirring. The solution was kept stirred for another 1 h to make sure it was well mixed. The solution was then autoclaved at 60 °C for 24 h. The product after synthesis was washed with water and centrifuged repetitively until pH=7. After washing, the cake was vacuum- freeze-dried and stored for use.

(3) NaA seeds coatings on $\boldsymbol{\alpha}$-alumina support:

For the clear sol recipe, a 0.05 wt% suspension was used. To prepare the suspension, 0.05 g nanoseed crystals were dispersed in 100 g ethanol and sonicated for 1.5 h. After sonication, the suspension was filtered through a 2 μm syringe filter to remove aggregates.

Then, the filtered suspension was transferred to a petri dish, and the **α**-alumina support surface is brought in to contact with the nanoseed suspension for 30s and then detached gently from the suspension surface on a pendulum's trajectory move. Finally, the slip coated supports are calcined by heating at 450 °C for 6 h (heating and cooling rate: 2 °C /min) to remove the SDA in the nanoseeds.

For the milky gel recipe, the only difference was using 0.1 wt% nanoseed suspension instead of 0.05 wt%.

(4) Secondary growth to make membranes:

The seeded supports were made intergrown by secondary growth. In the clear sol recipe, typically, for one batch of membranes (4 membranes), 20 g sodium hydroxide was dissolved in 86.57 g DI water. Then, the solution is divided equally into two parts. Then, 0.270 g Al powder is added to a glass bottle and one part of the NaOH solution is added to the bottle to dissolve the Al powder. The solution is preheated to 50 °C under stirring for at least 1 h. For the 2nd part, 5.007 g 30 wt% colloidal silica (LUDOX® SM 30) was added to the solution and stirred for ~30min to get a homogenous silicate solution. The 2 parts were added together at once and mix by stirring for another 1 h. Next, mount the seeded support on the home-made Teflon holder with facing down geometry and insert the holder together with the support in a Teflon liner. Finally, add ~25 mL of the synthesis gel to the Teflon liner and autoclave at 60 °C for 24 hours. After synthesis, the autoclaves were naturally cooled down and the membranes were carefully removed from the

autoclaves and washed by DI water repetitively (for at least 5 times) by soaking in DI water until pH=7 is reached. The membranes were kept in another RT water bath overnight before drying. After soaking, the membranes were dried at 60 °C and stored in a clean chamber for further tests. For the milky gel recipe, the preparation of synthesis gel was different. First, an aluminate solution was prepared by dissolving 4.0 g sodium hydroxide and 3.9 g $Al(OH)_3$ in 21 g DI water. The aluminate solution was heated at 80 °C in an oil bath with stirring. In parallel, a silicate solution was prepared by dissolving 10 g 30 wt% colloidal silica (LUDOX® SM 30) in 80 g DI water. The 2 parts were added together and mix by stirring to get a homogenous synthesis gel. The membrane preparation procedures are the same as the clear sol recipe.

7.3.2 Results and Discussion

Synthesis of zeolite NaA membranes using clear sol composition (Al_2O_3:5SiO_2:50Na_2O:1000H_2O)

(1) In-situ synthesis of zeolite NaA membranes:

Initial trials on making zeolite A membranes followed the same reaction condition in Ref. [130] (autoclaved at 60 °C for 24 h). The α-Al_2O_3 supports used in the experiments were home-made. We found that the support mounting geometry affects the membrane surface morphology. ***Figure 7.4*** shows the membrane surface morphologies using different support mounting geometries. When the membrane was mounted facing up (***Figure 7.4a***), a lot of particles deposited on the surface, making the membrane very thick and discontinuous. When the membrane was mounted in a vertical or sloped geometry

(***Figure 7.4b***), the membrane became continuous, but we can see big chunks of zeolite NaA crystals formed here and there on the surface. When the facing down geometry was used (***Figure 7.4c***), zeolite particles could not attach to the membrane side. The membrane surface became clean.

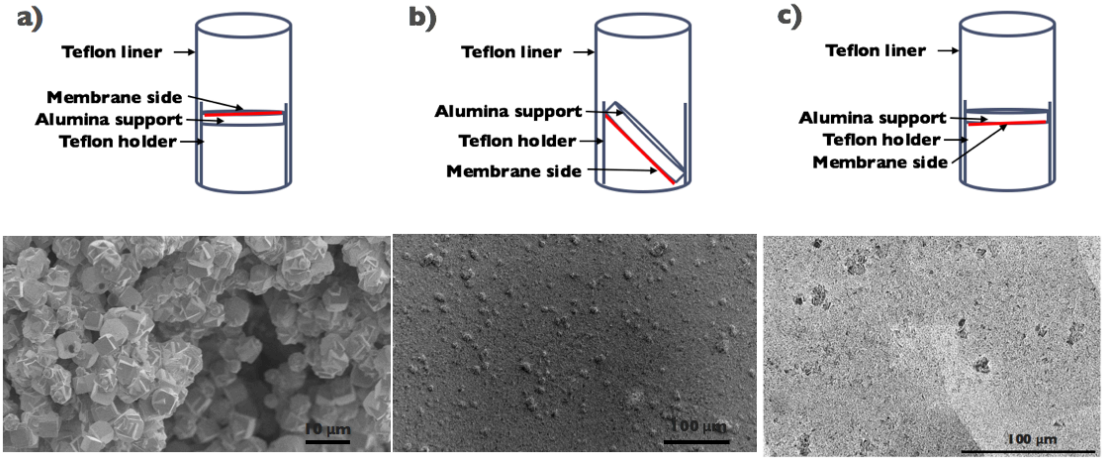

Figure 7.4: Zeolite A membrane surface morphologies using different support mounting geometry: a) facing-up geometry; b) sloped geometry and c) facing down geometry.

We also studied the effect of growth conditions on membrane surface morphology. In literature, there are 2 major reaction conditions. One is reacting at 60 °C for 24 h and the other is 80°C for 4-5 h. The second reaction condition was also tried. It was found that at 80°C, other types of zeolite particles, possibly Faujasite were easier to form (***Figure 7.5***). But at 60°C, the crystals were exclusively Zeolite NaA.

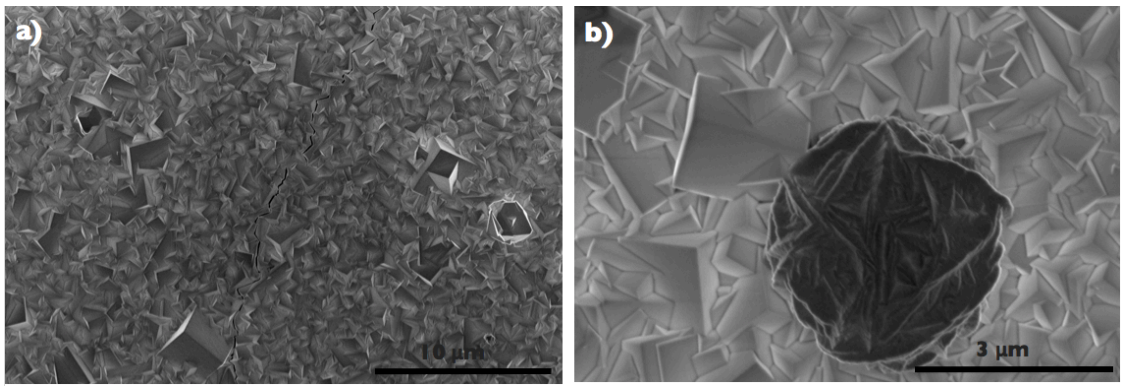

Figure 7.5: Surface morphologies of the membrane grew at 80℃ for a) 3 h; b) 5 h.

Although in-situ growth gave us membranes with clean surfaces, it failed to result in good membranes with high gas separation performance. The gas selectivities were lower or very similar to Knudsen selectivities. The seeded growth method is more preferred to get a better membrane.

(2) Seeded growth of zeolite NaA membranes:

Initial trials by using micro-sized zeolite NaA crystals (provided by Praxair) as seeds failed because it was hard to form a uniform seeding layer due to lack of attachment between large seeds and support surface. Nano-sized zeolite A particles were synthesized and used as seeds for membrane preparation. The nanoseeds had an average particle size of about 100-150 nm (***Figure 7.6***). Nanoseeds were introduced to the support by a slip casting process, followed by drying in an oven at 60 °C for 1 hour and calcination in a furnace at 450 °C for 6 h to remove the SDA in the crystals. Nanoseeds can attach firmly on the support surface after drying and calcination.

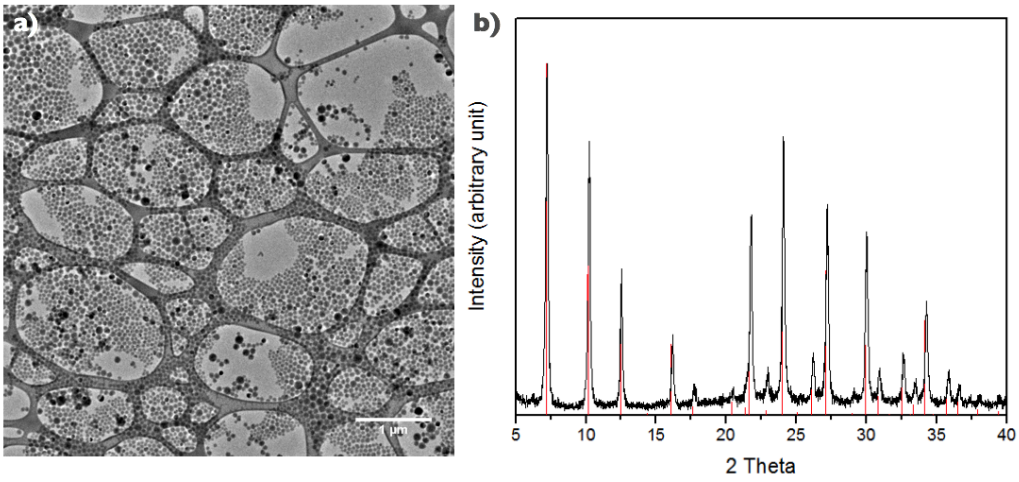

Figure 7.6: a) TEM image and b) XRD pattern of the synthesized zeolite A nanoseeds.

The effect of seed concentration on the membrane morphology and performance was studied. ***Figure 7.7*** shows the SEM images of the seeded support surface with various seed concentrations. It was found that when using a nanoseed concentration of 0.05 wt%, no crack was observed under SEM (***Figure 7.8***). The H_2 permeance was about 1.5×10^{-6} and the selectivities of H_2/CO_2, N_2 and CH_4 were 5.9, 4.5, 3.4, respectively. All these ideal selectivities were a little bit higher than Knudsen selectivity, indicating there was no large defect.

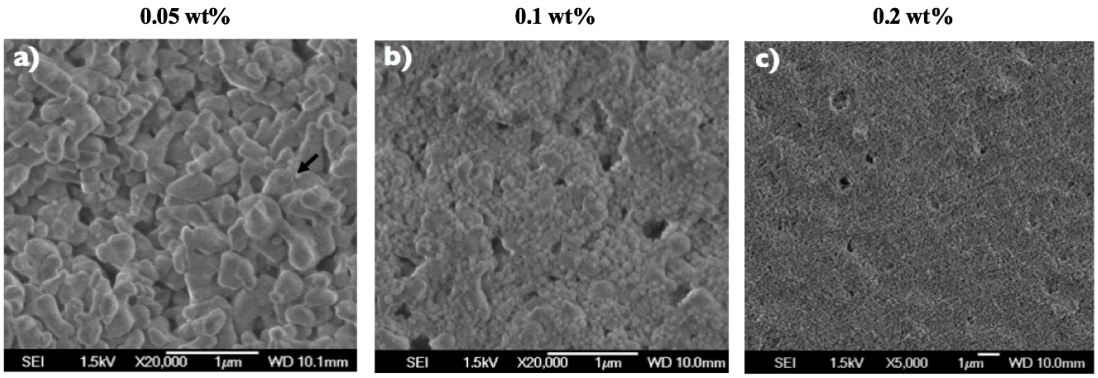

Figure 7.7: SEM images of the seeded support surface with various seed concentrations: a)0.05 wt%; b)0.1 wt%; c)0.2 wt%.

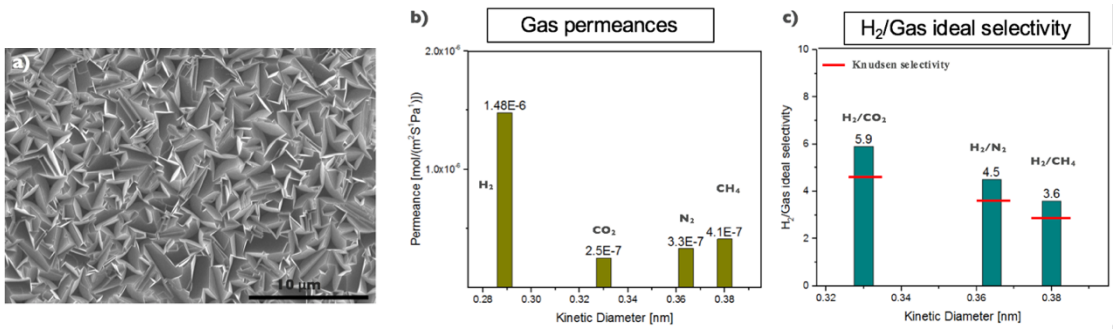

Figure 7.8: a) SEM image of the surface of the prepared membrane. No crack was observed for this membrane; b) the single gas permeance of the membrane; c) H_2/Gas ideal selectivities, Knudsen selectivity is drawn as a comparison.

Synthesis of zeolite NaA membranes using milky gel composition (Al_2O_3:2SiO_2:2Na_2O:120H_2O)

The other common gel composition was also tried for the synthesis of zeolite NaA membranes. The effect of seed concentration on the membrane morphology and performance was studied. As we can see from ***Figure 7.9***, when we used the in-situ growth,

a membrane did not form. Zeolite NaA particles were sparsely attached to the support surface. When we used a seed concentration of 0.05 wt%, more particles formed, but they were still not intergrown. When increasing the seed concentration to 0.1 wt%, a well intergrown and nicely faceted membrane was formed. ***Figure 7.10*** shows the cross-section of the membrane prepared using 0.1 wt% seeded support and its XRD pattern. XRD result confirmed that the membrane was indeed zeolite NaA. The cross-section revealed that the membrane was about 1.5-2 μm thick, which was thinner than the membranes prepared using clear sol composition (about 5 μm thick).

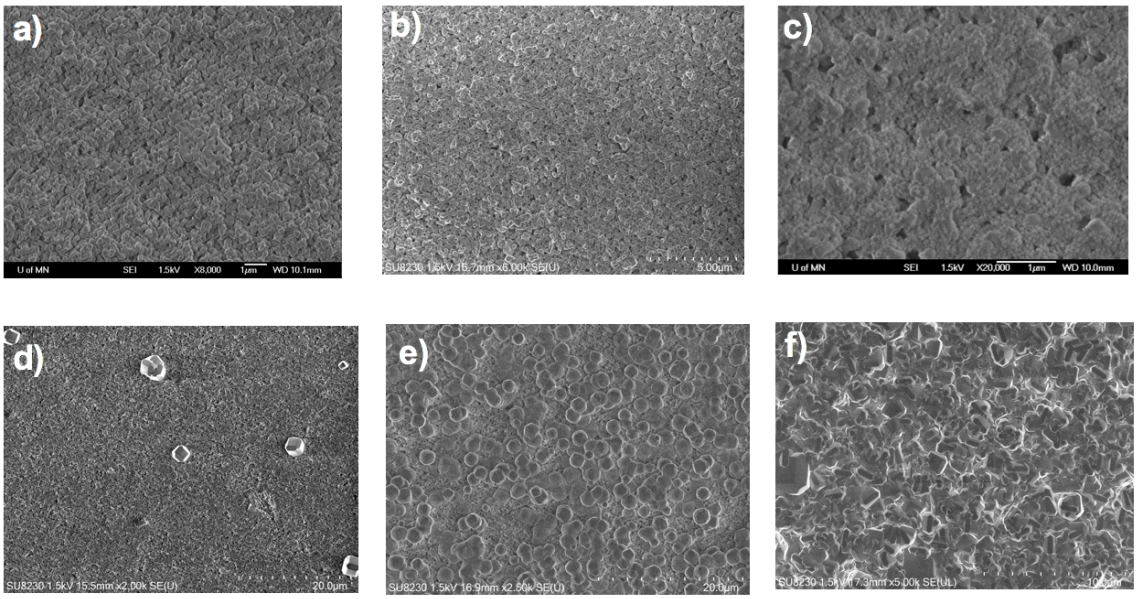

Figure 7.9: SEM images of the seeded support a) 0 wt% (no seeding); b)0.05 wt% seeding; c) 0.1 wt% seeding and the corresponding membrane surface after secondary growth, d), e), f), respectively.

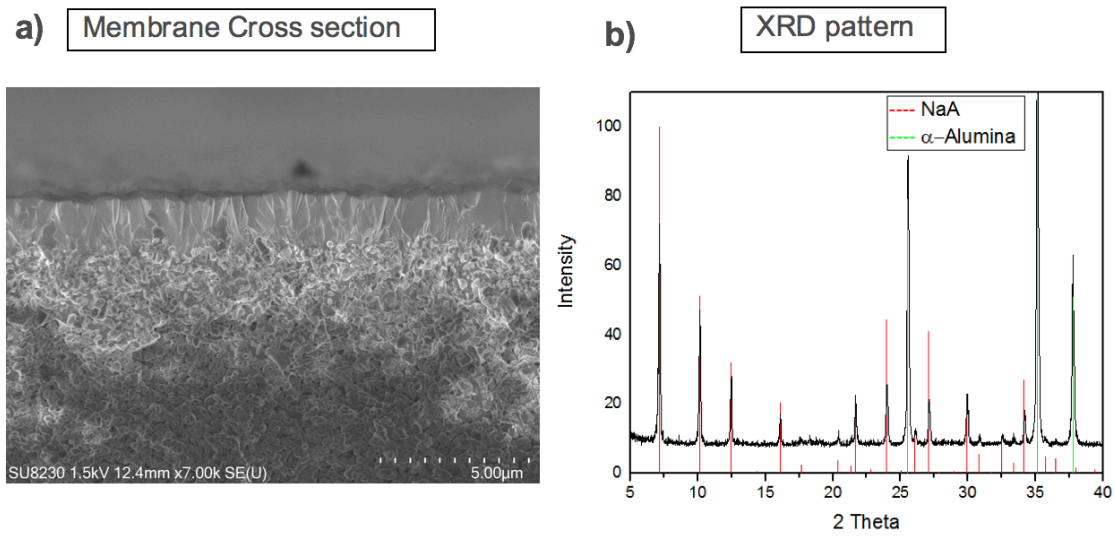

Figure 7.10: a) Cross section image and b) the XRD pattern of the membrane prepared using 0.1 wt% seeded support.

A more interesting finding was that the membrane was less defective than the previous batches as was shown by its ability to retain more *iso*-butane, which is a big molecule that cannot pass through the zeolite A pores. The *iso*-butane permeance was about 3.2×10^{-8} mol/(m^2-Pa-s), which was much smaller than that of the previous batches (about 1×10^{-7} mol/(m^2-Pa-s)).

MR-2404 treatment of the membrane

MR-2404 emulsion was coated on the membrane surface using a filtration method (***Figure 7.11***). The membrane was assembled in a membrane cell. A coating suspension (1 g 0.02 wt% of MR-2404 in MeOH) was added to the cell and the cell was connected to a vacuum pump. The pressure difference would drive the solvent to pass through the membrane and allow the MR-2404 emulsion to uniformly cover the membrane surface.

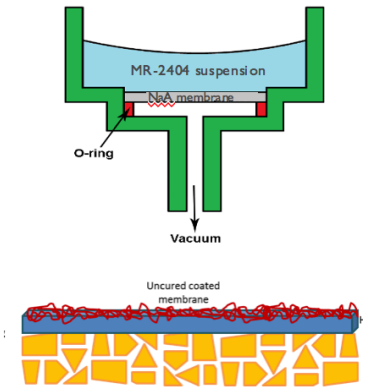

Figure 7.11: Schematic of vacuum coating of MR-2404 emulsion

To activate the coating layer, thermal calcination is not suitable because it is detrimental to the membrane. Here, we adapted the UV/Ozone treatment method. During the process, the UV lamp located on the top of the chamber generates UV irradiation with two types of wavelengths (184 and 254 nm). Each UV radiation plays a different role in the process. The 184 nm UV radiation dissociates molecular oxygen into O (^{3}P). Ozone molecules are then generated by the reaction between atomic oxygen O (^{3}P) and molecular oxygen. On the other hand, the 254 nm UV light dissociates ozone molecules into molecular oxygen and atomic oxygen O (^{3}D). Atomic oxygen O (^{3}D) is very reactive and has strong oxidation power. It can scissor organic molecular chains and remove the organics by forming volatile, simple molecules such as CO_2 and H_2O. In this way, we can remove the organics without having to go to high temperatures.

Table 7.5 lists the H_2 permeance of the membrane before and after MR-2404 coating. The H_2 permeance for the as-made membrane was 2.7×10^{-7} mol/(m^2-Pa-s). After coating treatment, the permeance significantly reduced, meaning that the membrane surface was completely covered by the emulsion. After UV/ozone treatment, the membrane was fully

activated. ***Figure 7.12*** shows the permeance of different gases before and after the treatment. For the small molecules, the permeances went back after the treatment, but this was not the case for *iso*-butane, which showed a slightly lower permeance. This means some of the defects were cured by the MR-2404 coating and UV/ozone treatment. This confirms the idea we proposed at the beginning.

Table 7.5: H_2 permeance of the membrane before and after MR-2404 coating

Gas permeance $\times 10^7$[mol/(m^2-Pa-s)]	**H_2**
As made membrane	2.7
After coating treatment	0.032

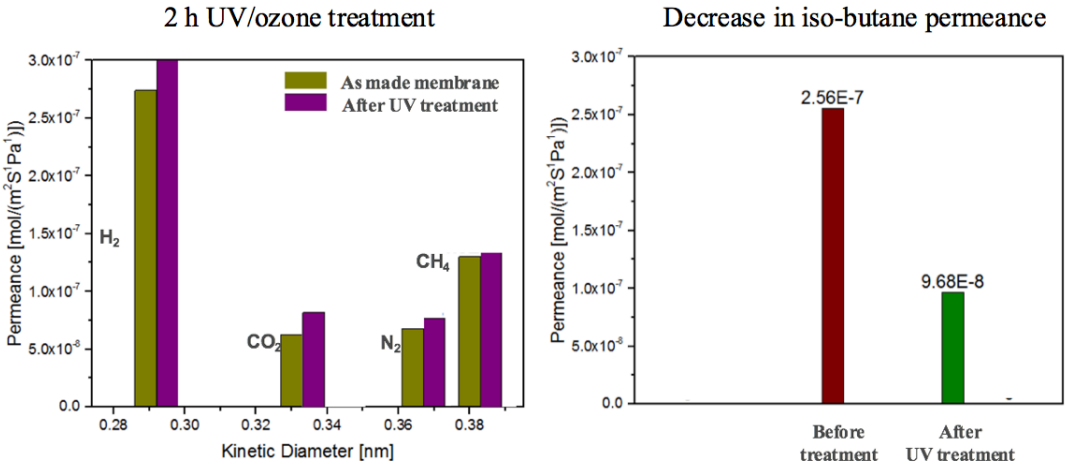

Figure 7.12: The permeance of different gases before and after the treatment.

Water/air mixture separation performance of the prepared membranes

Figure 7.13 shows a schematic of the permeation system for the water/air mixture separation test. One air stream was passed through a stainless steel bubbler, getting a water-saturated air stream. Another dry air line was added to the stream to dilute the water

concentration in order to get the desired water concentration. Then the stream was fed to the membrane at a certain pressure, and at the permeate side, N_2 was used as the sweep gas to avoid accumulation of the permeating gases. The compositions of both the feed stream and permeate stream were analyzed by a GC (for analyzing N_2 and O_2) and a water sensor (for analyzing H_2O).

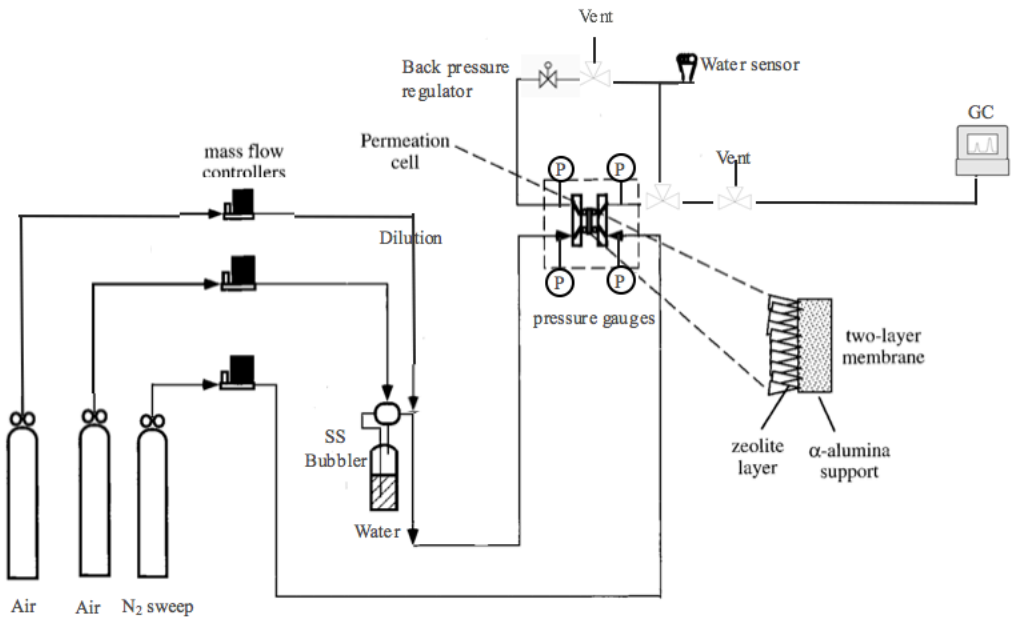

Figure 7.13: Schematic of the permeation system for the water/air mixture separation test.

Table 7.6 shows the results of the permeation tests. The MR-2404 treated membrane showed significant improvement in the separation factor. Unfortunately, the separation factor was not high enough for commercial applications.

Table 7.6: Separation performance of zeolite NaA membranes using milky gel synthesis method

Membrane	Dripping wet	Air dried	MR-2404 treated
Water Permeance mol/(m^2-Pa-s)	6.5×10^{-7}	4.5×10^{-7}	6.0×10^{-7}
Oxygen Permeance mol/(m^2-Pa-s)	3.7×10^{-8}	1.2×10^{-7}	1.5×10^{-8}
Separation Factor	13.1	3.5	32.0

7.4. Other related research

7.4.1. Preparation of Zeolite NaA membrane on silica supports

Trials were made to make zeolite NaA membranes on silica supports. First trials using clear sol composition failed to result in any membranes. The support dissolved in the synthesis gel because of the high basicity of the gel. Then, we used the milky gel composition to prepare zeolite NaA membranes on silica supports. As is shown in ***Figure 7.14***, a zeolite film was formed on the support, but it was not well-intergrown. When we carried out the synthesis for a longer time (24 h), the support also dissolved in the synthesis gel, making the gel very silica-rich. Based on the fact that the silica can dissolve in the synthesis gel and borrowing the idea of using Stöber silica as the silica source for the synthesis of MFI membranes, we tried to use the 50 nm Stöber silica as silica source and did not add any silica in the synthesis gel (other conditions were the same) for the membrane synthesis. Interestingly, a continuous zeolite NaA membrane was formed. ***Figure 7.15*** shows the SEM images of the membrane surface and cross-section. We can see the membrane was continuous and very thin (sub-micron). However, from the surface

morphology and XRD pattern, we can see the membrane was not very crystalline. There were some amorphous parts that did not completely transform to zeolite NaA. In order to make it more crystalline, we tried to synthesize the membrane for a longer time. ***Figure 7.16*** shows the membrane morphologies synthesized at 100 °C for 8 h and 12 h. A longer synthesis time (8 h) helped to increase the crystallinity. But if the time was too long (12 h), other particles start to form and attach to the membrane surface. This is a very interesting finding. Future work can be done to find the optimum gel composition and reaction condition for the synthesis of LTA membranes on silica support using this technique.

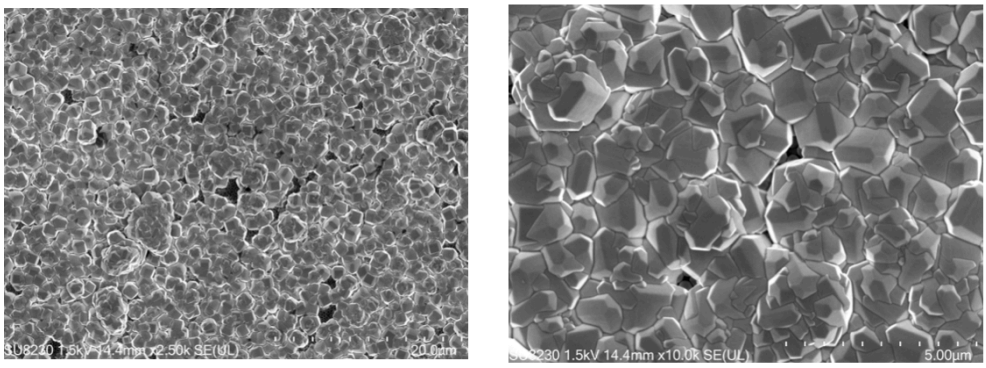

Figure 7.14: Zeolite NaA membrane on silica support using the milky gel recipe.

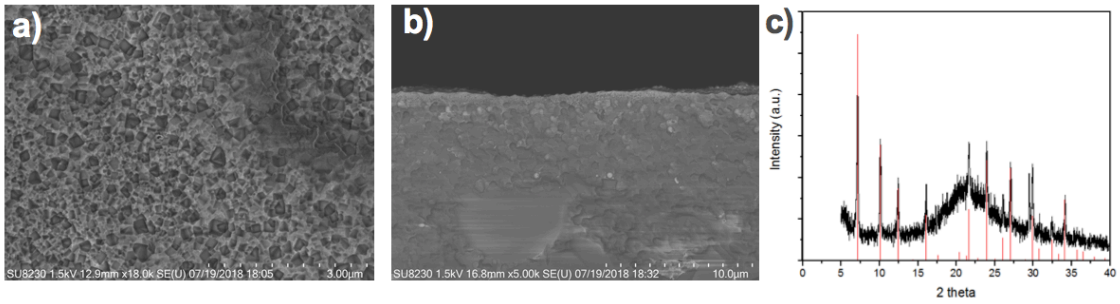

Figure 7.15: SEM images of the membrane made by using Stöber silica as silica source: a) the surface morphology; b) the cross section and the corresponding XRD pattern of the membrane c).

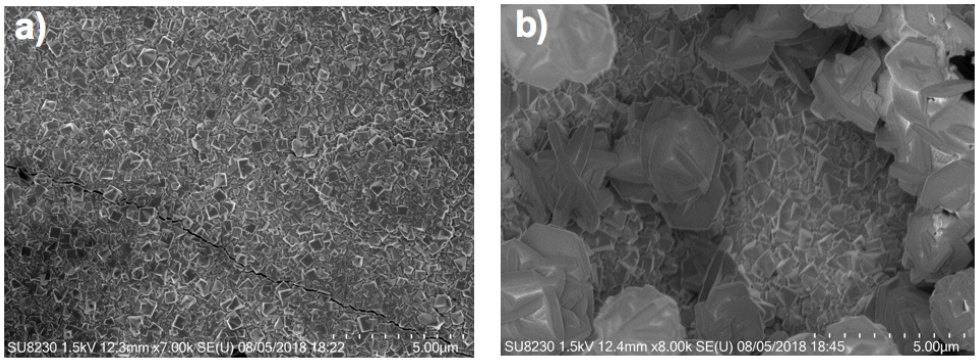

Figure 7.16: Membrane synthesized for a longer time using the new method: a) 100℃ for 8 h; b) 100℃ for 12 h.

7.4.2. Preparation of Zeolite NaA membranes on alumina hollow fibers

Zeolite A membranes were also prepared on alumina hollow fibers. The alumina hollow fibers were prepared using the same method reported in ref. [164]. In brief, an alumina dope with a composition (wt %) of 38.0 NMP: 6.8 PES: 54.7Al_2O_3: 0.5 PVP was prepared by first mixing NMP and Al_2O_3 powder, sonicating in a horn sonicator, and then heating at 60°C under vigorous stirring. Then polyvinylpyrrolidone (PVP) was added slowly into the mixture while continuing stir. Finally, poly(ether sulfone) (PES) was added and dissolved in the dope solution. The mixture was kept at 60°C and stirred for an additional

5 h to get a homogenous dope solution. Then the solution was poured into the dope chamber of our fiber spinning machine and the pressure inside the chamber was brought to vacuum overnight to remove air bubbles before spinning. The spinning was conducted with dope and bore fluid flow rates of 120 and 80 mL/h at room temperature, respectively. DI water was used as the bore fluid. The air gap was 3 cm. The alumina fiber was continuously spun into the air gap and the subsequent coagulation water bath. Then, the hollow fiber was guided and collected in a storage tank. The fiber was cut into ~30cm pieces and immersed in a water bath for 3 days to exchange the residual solvent. During the soaking process, DI water was refreshed every 24 hours. Finally, the hollow fibers were dried in ambient environment overnight and sintered at 600 °C for 2 h followed by 6 h at 1500 °C with a temperature ramping rate of 5°C /min.

The sintered fiber was used as support for membrane fabrication. First, the fiber was dip-coated by a 0.1 wt% NaA nanoseed suspension. To perform the dip coating, the coating solution was first prepared as described in section 7.3.1. The fiber was sealed by Teflon tape on both sides to prevent coating on the lumen side. Then, the sealed fiber was immersed in the suspension vertically for 30s and was lift out gently. ***Figure 7.17*** shows the SEM image of the surface of the seeded hollow fiber.

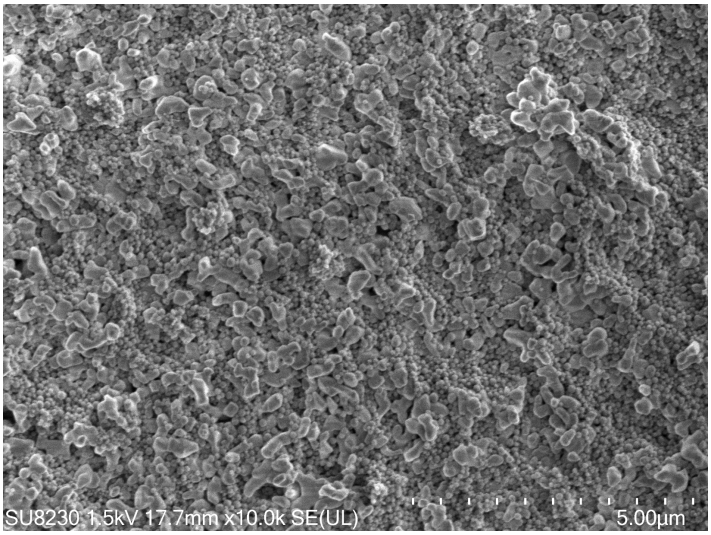

Figure 7.17: SEM image of the outer surface of alumina hollow fiber seeded by a dip coating of 0.1 wt% NaA nanoseed suspension.

After seeding, the fiber was placed vertically on a home-made Teflon holder firmly and the Teflon holder was autoclaved at 100 °C for 4 hours using the milky gel recipe for secondary growth. After secondary growth, the fiber was washed by DI water repetitively by soaking in DI water until pH=7 is reached. Finally, the fiber was dried at 60 °C and stored in a clean petri-dish for further tests. ***Figure 7.18*** shows the cross-section SEM image of the prepared NaA membrane on alumina hollow fiber. The membrane was well intergrown with a thickness of ~3 μm. The membrane was very clean and uniform. With the hollow fiber geometry, membranes can be assembled into more compact modules for separation applications.

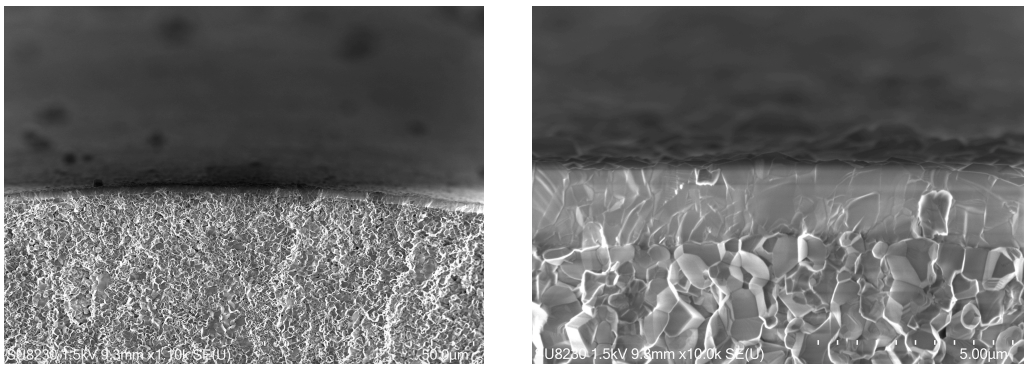

Figure 7.18: SEM images of the cross section of the fabricated NaA membrane on alumina hollow fiber support.

7.4. Conclusion

As a proof of concept, coating a thin layer of MR-2404 emulsion on MFI membranes followed by activation can effectively improve the membrane permselectivity without significantly compromising the membrane permeance. Then, thin LTA membranes with highly intergrown polycrystalline morphologies were successfully made by secondary growth using 0.05 wt% nanoseed coated α-Al_2O_3 supports for the clear sol composition and 0.1 wt% nanoseed coated α-Al_2O_3 supports for the milky gel composition. Membranes synthesized using the milky gel composition had a smoother surface morphology and better separation performance than the ones synthesized using the clear sol composition. MR-2404 coating followed by UV/ozone activation proved to be successful in curing some of the membrane defects, thus improving the gas separation performance. The MR-2404 treated membrane showed significant improvement in the separation factor compared to the as made one. Unfortunately, the separation factor was still not high enough for commercial applications.

Chapter 8: Concluding remarks

This thesis focused on several aspects of MFI membranes towards their industrial applications. My first project focused on making MFI membranes on low-cost polymer supports. Previously, the state-of-the-art MFI membrane preparation was based on MFI nanosheets seeding (to achieve ultra-thin membranes) followed by a secondary growth (to make it defect-free). Despite the high performance of the prepared membranes, the commercialization of MFI membrane has not been realized. One major problem was that the micropores of the nanosheets and the resulted MFI membrane were blocked by the organic structure-directing agent (OSDA) used to template the MFI growth. High-temperature calcination was needed to detemplate the OSDA. This requires the supports of the zeolite membranes to be thermally robust. As a result, high-cost inorganic supports are employed, which contribute to the major share of the total cost of the membranes. For my research, instead of using the secondary growth technique, a solution processing technique (filtration to achieve a thin layer of MFI coating) was used to fabricate MFI membranes on low-cost polymer supports. This would cut down the membrane cost dramatically and make MFI membranes commercially viable.

My second project was to make MFI membranes on more simple and scalable α-alumina supports. The previously mentioned state-of-the-art MFI membranes were prepared on specially made silica supports. The silica supports were carefully engineered to ensure the optimal delivery of silicate reactants during secondary growth. These supports are hard to make and not commercially available. At the same time, the supports are not mechanically strong enough for challenging separation tasks. It is desired to

fabricate MFI membranes on simpler, cheaper and more robust α-alumina supports. In my research, a fabrication protocol of making MFI membranes on α-alumina supports was established. Although we failed to make high-performance membranes as comparable to the silica-supported ones, the membrane fabrication protocols also have good implications for the scale-up and application of these MFI membranes.

Research efforts were also made on testing xylene isomer separation performance of high-performance nanosheet membranes under industrially relevant conditions. *para*-xylene is an important commodity chemical in industry. The production of *para*-xylene requires energy-intensive adsorption and/or crystallization processes for the recovery of *para*-xylene from its isomers. Membrane technology, especially a suitable membrane reactor, if integrated with the *para*-xylene production, would largely increase *para*-xylene productivity and reduce process cost by eliminating the currently employed energy-intensive separation processes. Our membranes showed record-high fluxes and separation factors for xylene isomer separation. The permeation tests provide us with industrially relevant data for process design and economic analysis. With these high-performance data, we are optimistic about the final industrial application of MFI membranes for xylene isomer separation.

We also explored the application of MFI membranes on refinery waste gas recovery and ammonia recovery. Refinery waste gases typically contain a low concentration of H_2 along with various concentrations of light hydrocarbons (C_1-C_4, saturated and unsaturated). These gases are generally burned to make use of their heating values. A lot of hidden values are wasted. MFI membranes are highly promising for enriching hydrogen

in the stream and the hydrogen-enriched stream can then be further processed by the PSA process to produce pure hydrogen. At the permeate side of the membrane, the hydrocarbon-rich gas stream can be used as fuel or further processed to produce additional value. MFI membranes are also potentially suitable for ammonia recovery which could be integrated with the traditional Haber–Bosch process. Ideally, if the membrane could work at high pressures (>100 bar) and temperatures (~500 °C), a membrane reactor could be installed, which could remove the ammonia product while retaining the reactants during the Haber–Bosch process. This would circumvent the constraint of the reaction equilibrium. Alternatively, it would also be beneficial to recover the ammonia from the recycled gas at lower temperatures to replace the currently used refrigeration process. Our membranes showed high fluxes and separation factors for the recovery of H_2 from hydrocarbons and for the separation of ammonia from H_2 and N_2. These results demonstrated the high potential of MFI membranes in these industrially important separation tasks.

With all the efforts I spend during my Ph.D. career, I hope the commercialization of MFI membranes will finally come true.

Bibliography

[1] Barrer, R. M. (1981). Zeolites and their synthesis. *Zeolites*, 1(3), 130-140.

[2] Cundy, C. S., & Cox, P. A. (2003). The hydrothermal synthesis of zeolites: history and development from the earliest days to the present time. *Chemical Reviews*, 103(3), 663-702.

[3] Van Donk, S., Janssen, A. H., Bitter, J. H., & de Jong, K. P. (2003). Generation, characterization, and impact of mesopores in zeolite catalysts. *Catalysis Reviews*, 45(2), 297-319.

[4] Rahimi, N., & Karimzadeh, R. (2011). Catalytic cracking of hydrocarbons over modified ZSM-5 zeolites to produce light olefins: A review. *Applied Catalysis A: General*, 398(1-2), 1-17.

[5] Weitkamp, J., & Puppe, L. (Eds.). (2013). *Catalysis and zeolites: fundamentals and applications*. Springer Science & Business Media.

[6] Bein, T. (1996). Synthesis and applications of molecular sieve layers and membranes. *Chemistry of Materials*, 8(8), 1636-1653.

[7] Bai, C., Jia, M. D., Falconer, J. L., & Noble, R. D. (1995). Preparation and separation properties of silicalite composite membranes. *Journal of Membrane Science*, 105(1-2), 79-87.

[8] Tavolaro, A., & Drioli, E. (1999). Zeolite membranes. *Advanced Materials*, 11(12), 975-996.

[9] Caro, J., Noack, M., Kölsch, P., & Schäfer, R. (2000). Zeolite membranes–state of their development and perspective. *Microporous and Mesoporous Materials*, 38(1), 3-24.

[10] Gascon, J., Kapteijn, F., Zornoza, B., Sebastian, V., Casado, C., & Coronas, J. (2012). Practical approach to zeolitic membranes and coatings: state of the art, opportunities, barriers, and future perspectives. *Chemistry of Materials*, 24(15), 2829-2844.

[11] Weitkamp, J., Fritz, M., & Ernst, S. (1993, January). Zeolites as media for hydrogen storage. In *Proceedings from the ninth international zeolite conference* (pp. 11-19). Butterworth-Heinemann.

[12] Menon, V. C., & Komarneni, S. (1998). Porous adsorbents for vehicular natural gas storage: a review. *Journal of Porous Materials*, 5(1), 43-58.

[13] Xu, X., Wang, J., & Long, Y. (2006). Zeolite-based materials for gas sensors. *Sensors*, 6(12), 1751-1764.

[14] Sahner, K., Hagen, G., Schönauer, D., Reiß, S., & Moos, R. (2008). Zeolites—Versatile materials for gas sensors. *Solid State Ionics*, 179(40), 2416-2423.

[15] Wang, Z. B., Mitra, A., Wang, H. T., Huang, L. M., & Yan, Y. (2001). Pure silica zeolite films as low-k dielectrics by spin-on of nanoparticle suspensions. *Advanced Materials*, 13(19), 1463-1466.

[16] Wang, Z., Wang, H., Mitra, A., Huang, L., & Yan, Y. (2001). Pure-silica zeolite low-k dielectric thin films. *Advanced Materials*, 13(10), 746-749.

[17] Li, Z., Johnson, M. C., Sun, M., Ryan, E. T., Earl, D. J., Maichen, W., ... & Deem, M. W. (2006). Mechanical and dielectric properties of pure-silica-zeolite low-k materials. *Angewandte Chemie*, 118(38), 6477-6480.

[18] Calzaferri, G., Pauchard, M., Maas, H., Huber, S., Khatyr, A., & Schaafsma, T. (2002). Photonic antenna system for light harvesting, transport and trapping. *Journal of Materials Chemistry*, 12(1), 1-13.

[19] Yan, Y., Davis, M. E., & Gavalas, G. R. (1995). Preparation of zeolite ZSM-5 membranes by in-situ crystallization on porous α-Al_2O_3. *Industrial & Engineering Chemistry Research*, 34(5), 1652-1661.

[20] Takaba, H., Koshita, R., Mizukami, K., Oumi, Y., Ito, N., Kubo, M., ... & Miyamoto, A. (1997). Molecular dynamics simulation of *iso*-and *n*-butane permeations through a ZSM-5 type silicalite membrane. *Journal of membrane science*, 134(1), 127-139.

[21] Kusakabe, K., Murata, A., Kuroda, T., & Morooka, S. (1997). Preparation of MFI-type zeolite membranes and their use in separating *n*-butane and *i*-butane. *Journal of Chemical Engineering of Japan*, 30(1), 72-78.

[22] Takaba, H., Koshita, R., Mizukami, K., Oumi, Y., Ito, N., Kubo, M., ... & Miyamoto, A. (1997). Molecular dynamics simulation of *iso*-and *n*-butane permeations through a ZSM-5 type silicalite membrane. *Journal of Membrane Science*, 134(1), 127-139.

[23] Gump, C. J., Lin, X., Falconer, J. L., & Noble, R. D. (2000). Experimental configuration and adsorption effects on the permeation of C4 isomers through ZSM-5 zeolite membranes. *Journal of Membrane Science*, 173(1), 35-52.

[24] Xomeritakis, G., & Tsapatsis, M. (1999). Permeation of aromatic isomer vapors through oriented MFI-type membranes made by secondary growth. *Chemistry of Materials*, 11(4), 875-878.

[25] Lai, Z., Bonilla, G., Diaz, I., Nery, J. G., Sujaoti, K., Amat, M. A., ... & Vlachos, D. G. (2003). Microstructural optimization of a zeolite membrane for organic vapor separation. *Science*, 300(5618), 456-460.

[26] Daramola, M. O., Burger, A. J., Pera-Titus, M., Giroir-Fendler, A., Miachon, S., Dalmon, J. A., & Lorenzen, L. (2010). Separation and isomerization of xylenes using zeolite membranes: a short overview. *Asia-Pacific Journal of Chemical Engineering*, 5(6), 815-837.

[27] Kim, D., Jeon, M. Y., Stottrup, B. L., & Tsapatsis, M. (2018). para-Xylene Ultra-selective Zeolite MFI Membranes Fabricated from Nanosheet Monolayers at the Air–Water Interface. *Angewandte Chemie*, 130(2), 489-494.

[28] Sano, T., Hasegawa, M., Kawakami, Y., & Yanagishita, H. (1995). Separation of methanolrmmethyl-tert-butyl ether mixture by pervaporation using silicalite membrane. *Journal of Membrane Science*, 107(1-2), 193-196.

[29] Liu, Q., Noble, R. D., Falconer, J. L., & Funke, H. H. (1996). Organics/water separation by pervaporation with a zeolite membrane. *Journal of Membrane Science*, 117(1-2), 163-174.

[30] Smetana, J. F., Falconer, J. L., & Noble, R. D. (1996). Separation of methyl ethyl ketone from water by pervaporation using a silicalite membrane. *Journal of Membrane Science*, 114(1), 127-130.

[31] Zhang, X. L., Zhu, M. H., Zhou, R. F., Chen, X. S., & Kita, H. (2012). Synthesis of a silicalite zeolite membrane in ultradilute solution and its highly selective separation of organic/water mixtures. *Industrial & Engineering Chemistry Research*, 51(35), 11499-11508.

[32] Elyassi, B., Jeon, M. Y., Tsapatsis, M., Narasimharao, K., Basahel, S. N., & Al-Thabaiti, S. (2016). Ethanol/water mixture pervaporation performance of b-oriented silicalite-1 membranes made by gel-free secondary growth. *AIChE Journal*, 62(2), 556-563.

[33] Zhu, B., Myat, D. T., Shin, J. W., Na, Y. H., Moon, I. S., Connor, G., ... & Duke, M. (2015). Application of robust MFI-type zeolite membrane for desalination of saline wastewater. *Journal of Membrane Science*, 475, 167-174.

[34] Li, L., Dong, J., Nenoff, T. M., & Lee, R. (2004). Desalination by reverse osmosis using MFI zeolite membranes. *Journal of Membrane Science*, 243(1-2), 401-404.

[35] Lia, L., Dong, J., Nenoff, T. M., & Lee, R. (2004). Reverse osmosis of ionic aqueous solutions on aMFI zeolite membrane. *Desalination*, 170(3), 309-316.

[36] Li, L., Dong, J., & Nenoff, T. M. (2007). Transport of water and alkali metal ions through MFI zeolite membranes during reverse osmosis. *Separation and Purification Technology*, 53(1), 42-48.

[37] Duke, M. C., O'Brien-Abraham, J., Milne, N., Zhu, B., Lin, J. Y., & da Costa, J. C. D. (2009). Seawater desalination performance of MFI type membranes made by secondary growth. *Separation and Purification Technology*, 68(3), 343-350.

[38] Kazemimoghadam, M., & Mohammadi, T. (2007). Synthesis of MFI zeolite membranes for water desalination. *Desalination*, 206(1-3), 547-553.

[39] Zhu, B., Kim, J. H., Na, Y. H., Moon, I. S., Connor, G., Maeda, S., ... & Duke, M. (2013). Temperature and pressure effects of desalination using a MFI-type zeolite membrane. *Membranes*, 3(3), 155-168.

[40] Zhu, B., Hong, Z., Milne, N., Doherty, C. M., Zou, L., Lin, Y. S., ... & Duke, M. (2014). Desalination of seawater ion complexes by MFI-type zeolite membranes: temperature and long term stability. *Journal of Membrane Science*, 453, 126-135.

[41] Lai, Z., Tsapatsis, M., & Nicolich, J. P. (2004). Siliceous ZSM-5 membranes by secondary growth of b-oriented seed layers. *Advanced Functional Materials*, 14(7), 716-729.

[42] Mittal, N., Bai, P., Kelloway, A., Siepmann, J. I., Daoutidis, P., & Tsapatsis, M. (2016). A mathematical model for zeolite membrane module performance and its use for techno-economic evaluation of improved energy efficiency hybrid membrane-distillation processes for butane isomer separations. *Journal of Membrane Science*, 520, 434-449.

[43] G. V. Research, Butane Market Analysis By Application (LPG, Petrochemicals, Refinery) And Segment Forecasts To 2020.

[44] Wantanachaisaeng, P., & O'Neil, K. (2007). Capturing opportunities for *para*-xylene production. *UOP LLC*.

[45] Daramola, M. O., Burger, A. J., Pera-Titus, M., Giroir-Fendler, A., Miachon, S., Dalmon, J. A., & Lorenzen, L. (2010). Separation and isomerization of xylenes using zeolite membranes: a short overview. *Asia-Pacific Journal of Chemical Engineering*, 5(6), 815-837.

[46] Agrawal, K. V., Topuz, B., Pham, T. C. T., Nguyen, T. H., Sauer, N., Rangnekar, N., ... & Macosko, C. W. (2015). Oriented MFI membranes by gel-less secondary growth of sub-100 nm MFI-nanosheet seed layers. *Advanced Materials*, 27(21), 3243-3249.

[47] Pham, T. C. T., Nguyen, T. H., & Yoon, K. B. (2013). Gel-free secondary growth of uniformly oriented silica MFI zeolite films and application for xylene separation. *Angewandte Chemie*, 125(33), 8855-8860.

[48] Choi, M., Na, K., Kim, J., Sakamoto, Y., Terasaki, O., & Ryoo, R. (2009). Stable single-unit-cell nanosheets of zeolite MFI as active and long-lived catalysts. *Nature*, *461*(7261), 246-249.

[49] Varoon, K., Zhang, X., Elyassi, B., Brewer, D. D., Gettel, M., Kumar, S., ... & Cococcioni, M. (2011). Dispersible exfoliated zeolite nanosheets and their application as a selective membrane. *Science*, 334(6052), 72-75.

[50] Agrawal, K. V., Topuz, B., Jiang, Z., Nguenkam, K., Elyassi, B., Francis, L. F., ... & Navarro, M. (2013). Solution-processable exfoliated zeolite nanosheets purified by density gradient centrifugation. *AIChE Journal*, 59(9), 3458-3467.

[51] Agrawal, K. V., Topuz, B., Pham, T. C. T., Nguyen, T. H., Sauer, N., Rangnekar, N., ... & Macosko, C. W. (2015). Oriented MFI membranes by gel-less secondary growth of sub-100 nm MFI-nanosheet seed layers. *Advanced Materials*, 27(21), 3243-3249.

[52] Tsapatsis, M. (2011). Toward high-throughput zeolite membranes. *Science*, 334(6057), 767-768.

[53] Zhang, H., Xiao, Q., Guo, X., Li, N., Kumar, P., Rangnekar, N., ... & Topuz, B. (2016). Open-pore two-dimensional MFI zeolite nanosheets for the fabrication of hydrocarbon-isomer-selective membranes on porous polymer supports. *Angewandte Chemie International Edition*, 55(25), 7184-7187.

[54] Golemme, G., Bruno, A., Manes, R., & Muoio, D. (2006). Preparation and properties of superglassy polymers—zeolite mixed matrix membranes. *Desalination*, 200(1-3), 440-442.

[55] Jeon, M. Y., Kim, D., Kumar, P., Lee, P. S., Rangnekar, N., Bai, P., ... & Basahel, S. N. (2017). Ultra-selective high-flux membranes from directly synthesized zeolite nanosheets. *Nature*, 543(7647), 690-694.

[56] Kim, D., Jeon, M. Y., Stottrup, B. L., & Tsapatsis, M. (2018). para-Xylene Ultra-selective Zeolite MFI Membranes Fabricated from Nanosheet Monolayers at the Air–Water Interface. *Angewandte Chemie*, 130(2), 489-494.

[57] van den Broeke, L. J., Bakker, W. J., Kapteijn, F., & Moulijn, J. A. (1999). Binary permeation through a silicalite-1 membrane. *AIChE journal*, 45(5), 976-985.

[58] Dong, J., Lin, Y. S., & Liu, W. (2000). Multicomponent hydrogen/hydrocarbon separation by MFI-type zeolite membranes. *AIChE journal*, 46(10), 1957-1966.

[59] Camus, O., Perera, S., Crittenden, B., van Delft, Y. C., Meyer, D. F., PAC Pex, P., ... & Chanaud, P. (2006). Ceramic membranes for ammonia recovery. *AIChE journal*, *52*(6), 2055-2065.

[60] Chung, T. S. N. (2008). Fabrication of hollow-fiber membranes by phase inversion. *Advanced Membrane Technology and Applications*, 821-839.

[61] Singh, S., Khulbe, K. C., Matsuura, T., & Ramamurthy, P. (1998). Membrane characterization by solute transport and atomic force microscopy. *Journal of Membrane Science*, 142(1), 111-127.

[62] Michaels, A. S. (1980). Analysis and prediction of sieving curves for ultrafiltration membranes: A universal correlation?. *Separation Science and Technology*, 15(6), 1305-1322.

[63] Mandelkern, L., & Flory, P. J. (1952). The frictional coefficient for flexible chain molecules in dilute solution. *The Journal of Chemical Physics*, 20(2), 212-214.

[64] Hsieh, F. H., Matsuura, T., & Sourirajan, S. (1979). Reverse osmosis separations of polyethylene glycols in dilute aqueous solutions using porous cellulose acetate membranes. *Journal of Applied Polymer Science*, 23(2), 561-573.

[65] Meireles, M., Bessieres, A., Rogissart, I., Aimar, P., & Sanchez, V. (1995). An appropriate molecular size parameter for porous membranes calibration. *Journal of Membrane Science*, 103(1-2), 105-115.

[66] Nabi, G. (1968). Light-scattering studies of aqueous solutions of poly (ethylene oxide). *Pakistan J. Sci.*, 20, 136-140.

[67] Ren, J., Li, Z., Wong, F. S., & Li, D. (2005). Development of asymmetric BTDA-TDI/MDI (P84) co-polyimide hollow fiber membranes for ultrafiltration: the influence of shear rate and approaching ratio on membrane morphology and performance. *Journal of Membrane Science*, 248(1-2), 177-188.

[68] Xu, Z. L., & Qusay, F. A. (2004). Polyethersulfone (PES) hollow fiber ultrafiltration membranes prepared by PES/non-solvent/NMP solution. *Journal of Membrane Science*, 233(1-2), 101-111.

[69] Goh, K., Setiawan, L., Wei, L., Si, R., Fane, A. G., Wang, R., & Chen, Y. (2015). Graphene oxide as effective selective barriers on a hollow fiber membrane for water treatment process. *Journal of Membrane Science*, 474, 244-253.

[70] Morigami, Y., Kondo, M., Abe, J., Kita, H., & Okamoto, K. (2001). The first large-scale pervaporation plant using tubular-type module with zeolite NaA membrane. *Separation and Purification Technology*, 25(1-3), 251-260.

[71] Rangnekar, N., Shete, M., Agrawal, K. V., Topuz, B., Kumar, P., Guo, Q., ... & Macosko, C. W. (2015). 2D zeolite coatings: Langmuir–Schaefer deposition of 3 nm thick MFI zeolite nanosheets. *Angewandte Chemie International Edition*, *54*(22), 6571-6575.

[72] Shete, M., Kumar, M., Kim, D., Rangnekar, N., Xu, D., Topuz, B., ... & Basahel, S. (2017). Nanoscale Control of Homoepitaxial Growth on a Two-Dimensional Zeolite. *Angewandte Chemie International Edition*, *56*(2), 535-539.

[73] Kim, D., Shete, M., & Tsapatsis, M. (2018). Large-grain, oriented, and thin zeolite MFI films from directly synthesized nanosheet coatings. *Chemistry of Materials*, *30*(10), 3545-3551.

[74] Pham, T. C. T., Kim, H. S., & Yoon, K. B. (2011). Growth of uniformly oriented silica MFI and BEA zeolite films on substrates. *Science*, 334(6062), 1533-1538.

[75] Li, Q., Amweg, M. L., Yee, C. K., Navrotsky, A., & Parikh, A. N. (2005). Photochemical template removal and spatial patterning of zeolite MFI thin films using UV/ozone treatment. *Microporous and Mesoporous Materials*, 87(1), 45-51.

[76] Zhao, J., Luo, T., Zhang, X., Lei, Y., Gong, K., & Yan, Y. (2012). Highly selective zeolite membranes as explosive preconcentrators. *Analytical Chemistry*, 84(15), 6303-6307.

[77] Yang, S., Kwon, Y. H., Koh, D. Y., Min, B., Liu, Y., & Nair, S. (2019). Highly Selective SSZ-13 Zeolite Hollow Fiber Membranes by Ultraviolet Activation at Near-Ambient Temperature. *ChemNanoMat*, 5(1), 61-67.

[78] Choi, J., Jeong, H. K., Snyder, M. A., Stoeger, J. A., Masel, R. I., & Tsapatsis, M. (2009). Grain boundary defect elimination in a zeolite membrane by rapid thermal processing. *Science*, *325*(5940), 590-593.

[79] Stoeger, J. A., Choi, J., & Tsapatsis, M. (2011). Rapid thermal processing and separation performance of columnar MFI membranes on porous stainless steel tubes. *Energy & Environmental Science*, *4*(9), 3479-3486.

[80] Chang, N., Tang, H., Bai, L., Zhang, Y., & Zeng, G. (2018). Optimized rapid thermal processing for the template removal of SAPO-34 zeolite membranes. *Journal of Membrane Science*, *552*, 13-21.

[81] Yan, Y., Davis, M. E., & Gavalas, G. R. (1995). Preparation of zeolite ZSM-5 membranes by in-situ crystallization on porous α-Al_2O_3. *Industrial & Engineering Chemistry Research*, 34(5), 1652-1661.

[82] Yan, Y., Tsapatsis, M., Gavalas, G. R., & Davis, M. E. (1995). Zeolite ZSM-5 membranes grown on porous α-Al_2O_3. Journal of the Chemical Society, *Chemical Communications*, (2), 227-228.

[83] Lai, R., & Gavalas, G. R. (1998). Surface seeding in ZSM-5 membrane preparation. *Industrial & Engineering Chemistry Research*, 37(11), 4275-4283.

[84] Keizer, K., Burggraaf, A. J., Vroon, Z. A. E. P., & Verweij, H. (1998). Two component permeation through thin zeolite MFI membranes. *Journal of Membrane Science*, *147*(2), 159-172.

[85] Xomeritakis, G., & Tsapatsis, M. (1999). Permeation of aromatic isomer vapors through oriented MFI-type membranes made by secondary growth. *Chemistry of Materials*, 11(4), 875-878.

[86] Xomeritakis, G., Nair, S., & Tsapatsis, M. (2000). Transport properties of alumina-supported MFI membranes made by secondary (seeded) growth. *Microporous and Mesoporous Materials*, 38(1), 61-73.

[87] Xomeritakis, G., Lai, Z., & Tsapatsis, M. (2001). Separation of xylene isomer vapors with oriented MFI membranes made by seeded growth. *Industrial & Engineering Chemistry Research*, *40*(2), 544-552.

[88] Hedlund, J., Sterte, J., Anthonis, M., Bons, A. J., Carstensen, B., Corcoran, N., ... & Lai, F. (2002). High-flux MFI membranes. *Microporous and Mesoporous Materials*, 52(3), 179-189.

[89] Kumar, P., Kim, D. W., Rangnekar, N., Xu, H., Fetisov, E. O., Ghosh, S., ... & Dumitrica, T. (2020). One-dimensional intergrowths in two-dimensional zeolite nanosheets and their effect on ultra-selective transport. *Nature Materials*, *19*(4), 443-449.

[90] Rangnekar, N. (2017). Ultra-thin MFI zeolite films: Synthesis, Characterization and Progress Toward Industrial Applications.

[91] Sircar, S., Rao, M. B., & Thaeron, C. M. A. (1999). Selective surface flow membrane for gas separation. *Separation Science and Technology*, 34(10), 2081-2093.

[92] Sircar, S., & Golden, T. C. (2000). Purification of hydrogen by pressure swing adsorption. *Separation Science and Technology*, 35(5), 667-687.

[93] Rao, M., & Sircar, S. (1993). Nanoporous carbon membranes for separation of gas mixtures by selective surface flow. *Journal of Membrane Science*, 85(3), 253-264.

[94] Rao, M. B., & Sircar, S. (1993). Nanoporous carbon membrane for gas separation. *Gas Separation & Purification*, 7(4), 279-284.

[95] Rao, M. B., & Sircar, S. (1996). Performance and pore characterization of nanoporous carbon membranes for gas separation. *Journal of Membrane Science*, 110(1), 109-118.

[96] Naheiri, T., Ludwig, K. A., Anand, M., Rao, M. B., & Sircar, S. (1997). Scale-up of selective surface flow membrane for gas separation. *Separation Science and Technology*, 32(9), 1589-1602.

[97] Yu, L., Grahn, M., Ye, P., & Hedlund, J. (2017). Ultra-thin MFI membranes for olefin/nitrogen separation. *Journal of Membrane Science*, 524, 428-435.

[98] Arruebo, M., Coronas, J., Menendez, M., & Santamarıa, J. (2001). Separation of hydrocarbons from natural gas using silicalite membranes. *Separation and Purification Technology*, 25(1-3), 275-286.

[99] Dragomirova, R., Stöhr, M., Hecker, C., Lubenau, U., Paschek, D., & Wohlrab, S. (2014). Desorption-controlled separation of natural gas alkanes by zeolite membranes. *RSC Advances*, 4(104), 59831-59834.

[100] Yu, L., Grahn, M., & Hedlund, J. (2018). Ultra-thin MFI membranes for removal of C_{3+} hydrocarbons from methane. *Journal of Membrane Science*, 551, 254-260.

[101] Min, B., Yang, S., Korde, A., Kwon, Y. H., Jones, C. W., & Nair, S. (2019). Continuous zeolite MFI membranes fabricated from 2D MFI nanosheets on ceramic hollow fibers. *Angewandte Chemie International Edition*, 58(24), 8201-8205.

[102] Zhu, W., Van de Graaf, J. M., Van den Broeke, L. J. P., Kapteijn, F., & Moulijn, J. A. (1998). TEOM: a unique technique for measuring adsorption properties. Light alkanes in silicalite-1. *Industrial & Engineering Chemistry Research*, 37(5), 1934-1942.

[102] Zhu, W., Kapteijn, F., & Moulijn, J. A. (2000). Equilibrium adsorption of light alkanes in silicalite-1 by the inertial microbalance technique. *Adsorption*, 6(2), 159-167.

[104] Krishna, R., & Paschek, D. (2001). Molecular simulations of adsorption and siting of light alkanes in silicalite-1. *Physical Chemistry Chemical Physics*, 3(3), 453-462.

[105] Liu, H. (2014). Ammonia synthesis catalyst 100 years: Practice, enlightenment and challenge. *Chinese Journal of Catalysis*, *35*(10), 1619-1640.

[106] Bhown, A., & Cussler, E. L. (1991). Mechanism for selective ammonia transport through poly (vinylammonium thiocyanate) membranes. *Journal of the American Chemical Society*, *113*(3), 742-749.

[107] Choe, J. S., & Kellogg Jr, L. J. (1995). *U.S. Patent No. 5,455,016*. Washington, DC: U.S. Patent and Trademark Office.

[108] Pez, G. P., Carlin, R. T., Laciak, D. V., & Sorensen, J. C. (1988). *U.S. Patent No. 4,761,164*. Washington, DC: U.S. Patent and Trademark Office.

[109] Laciak, D. V., Pez, G. P., & Burban, P. M. (1992). Molten salt facilitated transport membranes. Part 2. Separation of ammonia from nitrogen and hydrogen at high temperatures. *Journal of Membrane Science*, *65*(1-2), 31-38.

[110] Pez, G. P., & Laciak, D. V. (1988). *U.S. Patent No. 4,762,535*. Washington, DC: U.S. Patent and Trademark Office.

[111] Laciak, D. V., & Pez, G. P. (1988). *U.S. Patent No. 4,758,250*. Washington, DC: U.S. Patent and Trademark Office.

[112] He, Y., & Cussler, E. L. (1992). Ammonia permeabilities of perfluorosulfonic membranes in various ionic forms. *Journal of Membrane Science*, *68*(1-2), 43-52.

[113] Timashev, S. F., Vorobiev, A. V., Kirichenko, V. I., Popkov, Y. M., Volkov, V. I., Shifrina, R. R., ... & Bobrova, L. P. (1991). Specifics of highly selective ammonia transport through gas-separating membranes based on perfluorinated copolymer in the form of hollow fibers. *Journal of Membrane Science*, *59*(2), 117-131.

[114] Bikson, B., Nelson, J. K., & Perrin, J. E. (1991). *U.S. Patent No. 5,009,678*. Washington, DC: U.S. Patent and Trademark Office.

[115] Vorotyntsev, I. V., Drozdov, P. N., & Karyakin, N. V. (2006). Ammonia permeability of a cellulose acetate membrane. *Inorganic Materials*, *42*(3), 231-235.

[116] Phillip, W. A., Martono, E., Chen, L., Hillmyer, M. A., & Cussler, E. L. (2009). Seeking an ammonia selective membrane based on nanostructured sulfonated block copolymers. *Journal of Membrane Science*, *337*(1-2), 39-46.

[117] Makhloufi, C., Belaissaoui, B., Roizard, D., & Favre, E. (2012). Interest of poly [bis (trifluoroethoxy) phosphazene] membranes for ammonia recovery–potential application in Haber process. *Procedia Engineering*, *44*, 143-146.

[118] Kanezashi, M., Yamamoto, A., Yoshioka, T., & Tsuru, T. (2010). Characteristics of ammonia permeation through porous silica membranes. *AIChE journal*, *56*(5), 1204-1212.

[119] Brubaker, D. W., & Kammermeyer, K. (1954). Separation of gases by plastic membranes-permeation rates and extent of separation. *Industrial & Engineering Chemistry*, *46*(4), 733-739.

[120] Browall, W. R. (1979). *U.S. Patent No. 4,156,597*. Washington, DC: U.S. Patent and Trademark Office.

[121] Polymer Handbook (Eds: J. Brandrup, E. H. Immergut), 3rd ed., Wiley, New York 1989.

[122] Kulprathipanja, S., & Kulkarni, S. S. (1986). *U.S. Patent No. 4,608,060*. Washington, DC: U.S. Patent and Trademark Office.

[123] Pan, C. Y., & Hadfield, E. M. (1988). *U.S. Patent No. 4,793,829*. Washington, DC: U.S. Patent and Trademark Office.

[124] Okamoto, K. I., Kita, H., Horii, K., & Kondo, K. T. (2001). Zeolite NaA membrane: preparation, single-gas permeation, and pervaporation and vapor permeation of water/organic liquid mixtures. *Industrial & Engineering Chemistry Research*, 40(1), 163-175.

[125] Wang, Z., Ge, Q., Gao, J., Shao, J., Liu, C., & Yan, Y. (2011). High-performance zeolite membranes on inexpensive large-pore supports: highly reproducible synthesis using a seed paste. *ChemSusChem*, 4(11), 1570-1573.

[126] Liu, Y., Wang, X., Zhang, Y., He, Y., & Gu, X. (2015). Scale-up of NaA zeolite membranes on α-Al_2O_3 hollow fibers by a secondary growth method with vacuum seeding. *Chinese Journal of Chemical Engineering*, 23(7), 1114-1122.

[127] Liu, Y., Yang, Z., Yu, C., Gu, X., & Xu, N. (2011). Effect of seeding methods on growth of NaA zeolite membranes. *Microporous and Mesoporous Materials*, 143(2-3), 348-356.

[128] Li, H., Wang, J., Xu, J., Meng, X., Xu, B., Yang, J., ... & Yin, D. (2013). Synthesis of zeolite NaA membranes with high performance and high reproducibility on coarse macroporous supports. *Journal of Membrane Science*, 444, 513-522.

[129] Huang, A., Lin, Y. S., & Yang, W. (2004). Synthesis and properties of A-type zeolite membranes by secondary growth method with vacuum seeding. *Journal of Membrane Science*, 245(1-2), 41-51.

[130] Kuanchertchoo, N., Suwanpreedee, R., Kulprathipanja, S., Aungkavattana, P., Atong, D., Hemra, K., ... & Wongkasemjit, S. (2007). Effects of synthesis parameters on zeolite membrane formation and performance by microwave technique. *Applied Organometallic Chemistry*, 21(10), 841-848.

[131] Zhu, W., Gora, L., Van den Berg, A. W. C., Kapteijn, F., Jansen, J. C., & Moulijn, J. A. (2005). Water vapour separation from permanent gases by a zeolite-4A membrane. *Journal of Membrane Science*, 253(1-2), 57-66.

[132] Heng, S., Lau, P. P. S., Yeung, K. L., Djafer, M., & Schrotter, J. C. (2004). Low-temperature ozone treatment for organic template removal from zeolite membrane. *Journal of Membrane Science*, 243(1-2), 69-78.

[133] Kuhn, J., Sutanto, S., Gascon, J., Gross, J., & Kapteijn, F. (2009). Performance and stability of multi-channel MFI zeolite membranes detemplated by calcination and ozonication in ethanol/water pervaporation. *Journal of Membrane Science*, 339(1-2), 261-274.

[134] Motuzas, J., Heng, S., Lau, P. Z., Yeung, K. L., Beresnevicius, Z. J., & Julbe, A. (2007). Ultra-rapid production of MFI membranes by coupling microwave-assisted

synthesis with either ozone or calcination treatment. *Microporous and Mesoporous Materials*, 99(1-2), 197-205.

[135] Wang, L., Zhang, C., Gao, X., Peng, L., Jiang, J., & Gu, X. (2017). Preparation of defect-free DDR zeolite membranes by eliminating template with ozone at low temperature. *Journal of Membrane Science*, 539, 152-160.

[136] Wang, M., Bai, L., Li, M., Gao, L., Wang, M., Rao, P., & Zhang, Y. (2019). Ultrafast synthesis of thin all-silica DDR zeolite membranes by microwave heating. *Journal of Membrane Science*, 572, 567-579.

[137] Zhang, Y., Wang, M., Liu, S., Wang, M., Xu, N., Gao, L., & Zhang, Y. (2019). Mild template removal of SAPO-34 zeolite membranes in wet ozone environment. *Separation and Purification Technology*, 228, 115758.

[138] Yan, Y., Davis, M. E., & Gavalas, G. R. (1997). Preparation of highly selective zeolite ZSM-5 membranes by a post-synthetic coking treatment. *Journal of Membrane Science*, *123*(1), 95-103.

[139] Bai, C., Jia, M. D., Falconer, J. L., & Noble, R. D. (1995). Preparation and separation properties of silicalite composite membranes. *Journal of Membrane Science*, *105*(1-2), 79-87.

[140] Vroon, Z. A. E. P., Keizer, K., Gilde, M. J., Verweij, H., & Burggraaf, A. J. (1996). Transport properties of alkanes through ceramic thin zeolite MFI membranes. *Journal of Membrane Science*, *113*(2), 293-300.

[141] Vroon, Z. A. E. P., Keizer, K., Burggraaf, A. J., & Verweij, H. (1998). Preparation and characterization of thin zeolite MFI membranes on porous supports. *Journal of Membrane Science*, *144*(1-2), 65-76.

[142] van de Graaf, J. M., van der Bijl, E., Stol, A., Kapteijn, F., & Moulijn, J. A. (1998). Effect of operating conditions and membrane quality on the separation performance of composite silicalite-1 membranes. *Industrial & Engineering Chemistry Research*, *37*(10), 4071-4083.

[143] Xomeritakis, G., Gouzinis, A., Nair, S., Okubo, T., He, M., Overney, R. M., & Tsapatsis, M. (1999). Growth, microstructure, and permeation properties of supported zeolite (MFI) films and membranes prepared by secondary growth. *Chemical Engineering Science*, *54*(15-16), 3521-3531.

[144] Tuan, V. A., Falconer, J. L., & Noble, R. D. (1999). Alkali-free ZSM-5 membranes: preparation conditions and separation performance. *Industrial & Engineering Chemistry Research*, *38*(10), 3635-3646.

[145] Piera, E., Bernai, M. P., Salomon, M. A., Coronas, J., Menendez, M., & Santamaria, J. (1999). Preparation and permeation properties of different zeolite tubular membranes. In *Studies in Surface Science and Catalysis* (Vol. 125, pp. 189-196). Elsevier.

[146] Xomeritakis, G., Nair, S., & Tsapatsis, M. (2000). Transport properties of alumina-supported MFI membranes made by secondary (seeded) growth. *Microporous and Mesoporous Materials*, *38*(1), 61-73.

[147] Matsufuji, T., Nishiyama, N., Matsukata, M., & Ueyama, K. (2000). Separation of butane and xylene isomers with MFI-type zeolitic membrane synthesized by a vapor-phase transport method. *Journal of Membrane Science*, *178*(1-2), 25-34.

[148] Gora, L., Jansen, J. C., & Maschmeyer, T. (2000). Controlling the Performance of Silicalite-1 Membranes. *Chemistry–A European Journal*, *6*(14), 2537-2543.

[149] Alfaro, S., Arruebo, M., Coronas, J., Menéndez, M., & Santamaría, J. (2001). Preparation of MFI type tubular membranes by steam-assisted crystallization. *Microporous and Mesoporous Materials*, *50*(2-3), 195-200.

[150] Gora, L., Nishiyama, N., Jansen, J. C., Kapteijn, F., Teplyakov, V., & Maschmeyer, T. (2001). Highly reproducible high-flux silicalite-1 membranes: optimization of silicalite-1 membrane preparation. *Separation and Purification Technology*, *22*, 223-229.

[151] Li, Y., Zhang, X., & Wang, J. (2001). Preparation for ZSM-5 membranes by a two-stage varying-temperature synthesis. *Separation and Purification Technology*, *25*(1-3), 459-466.

[152] Nishiyama, N., Gora, L., Teplyakov, V., Kapteijn, F., & Moulijn, J. A. (2001). Evaluation of reproducible high flux silicalite-1 membranes: gas permeation and separation characterization. *Separation and Purification Technology*, *22*, 295-307.

[153] Hedlund, J., Sterte, J., Anthonis, M., Bons, A. J., Carstensen, B., Corcoran, N., ... & Lai, F. (2002). High-flux MFI membranes. *Microporous and Mesoporous Materials*, *52*(3), 179-189.

[154] Bernal, M. P., Coronas, J., Menendez, M., & Santamarıa, J. (2003). On the effect of morphological features on the properties of MFI zeolite membranes. *Microporous and Mesoporous Materials*, *60*(1-3), 99-110.

[155] Jareman, F., Hedlund, J., & Sterte, J. (2003). Effects of aluminum content on the separation properties of MFI membranes. Separation and Purification Technology, 32(1-3), 159-163.

[156] Gora, L., & Jansen, J. C. (2005). Hydroisomerization of C_6 with a zeolite membrane reactor. *Journal of Catalysis*, *230*(2), 269-281.

[157] Choi, J., Ghosh, S., King, L., & Tsapatsis, M. (2006). MFI zeolite membranes from a-and randomly oriented monolayers. *Adsorption*, *12*(5-6), 339-360.

[158] Choi, J., Jeong, H. K., Snyder, M. A., Stoeger, J. A., Masel, R. I., & Tsapatsis, M. (2009). Grain boundary defect elimination in a zeolite membrane by rapid thermal processing. *Science*, *325*(5940), 590-593.

[159] Stoeger, J. A., Choi, J., & Tsapatsis, M. (2011). Rapid thermal processing and separation performance of columnar MFI membranes on porous stainless steel tubes. *Energy & Environmental Science*, *4*(9), 3479-3486.

[160] Wu, A., Tang, C., Zhong, S., Wang, B., Zhou, J., & Zhou, R. (2019). Synthesis optimization of (h0h)-oriented silicalite-1 membranes for butane isomer separation. *Separation and Purification Technology*, *214*, 51-60.

[161] Liu, Y., Qiang, W., Ji, T., Zhang, M., Li, M., & Lu, J. (2020). Uniform hierarchical MFI nanosheets prepared via anisotropic etching for solution-based sub–100-nm-thick oriented MFI layer fabrication. *Science Advances*, *6*(7), eaay5993.

[162] Min, B., Yang, S., Korde, A., Jones, C. W., & Nair, S. (2020). Single-Step Scalable Fabrication of Zeolite MFI Hollow Fiber Membranes for Hydrocarbon Separations. *Advanced Materials Interfaces*, 2000926.

[163] Larlus, O., Mintova, S., & Bein, T. (2006). Environmental syntheses of nanosized zeolites with high yield and monomodal particle size distribution. *Microporous and Mesoporous Materials*, 96(1-3), 405-412.

[164] Kwon, Y. H., Min, B., Yang, S., Koh, D. Y., Bhave, R. R., & Nair, S. (2018). Ion-exchanged SAPO-34 membranes for krypton–xenon separation: control of permeation properties and fabrication of hollow fiber membranes. *ACS Applied Materials & Interfaces*, *10*(7), 6361-6368.